PIEZOELECTRIC ENERGY HARVESTING UTILIZING METALLIZED POLY-VINYLIDENE FLUORIDE (PVDF)

A Thesis Submitted to the College of

Graduate Studies and Research

in Partial Fulfillment of the Requirements

for the Degree of Masters Of Science

in the Department of Mechanical Engineering

University of Saskatchewan

Saskatoon

By

Brandon Alexander Hall

PERMISSION TO USE

In presenting this thesis in partial fulfillment of the requirements for a Master of Science degree from the University of Saskatchewan, I agree that permission for copying of this thesis in any manner, in whole or in part, for scholarly purposes may be granted by the Professors who supervised the thesis work or, in their absence, by the Head of the Department or the Dean of the College in which the thesis work was done. It is understood that any copying or publication or use of this thesis or parts thereof for financial gain shall not be allowed without the author's written permission. It is also understood that due recognition shall be given to the author and the University of Saskatchewan in any scholarly use which may be made of any material in this thesis.

Requests for permission to copy or make other use of the material in this thesis in whole or part should be addressed to:

Head of the Department of Mechanical Engineering
University of Saskatchewan
57 Campus Drive
Saskatoon, Saskatchewan, Canada
S7N 5A9

ABSTRACT

The primary objective of the enclosed thesis was to identify and develop a viable concept for an autonomous sensor system that could be implemented onto the surface of a road. This was achieved by an analysis of combinations of materials, sensing methods, power sources, microsystems, energy storage options, and wireless data transmission systems; the sub-systems required for an autonomous sensor.

Comparison of sensing methods for the application of an on-road, autonomous sensor yielded a piezoelectric material as the ideal choice. A 52μm thin film of poly-vinylidene fluoride (PVDF) was chosen and coated with Ag electrodes on both sides. This was due to many constraints imposed by the intended environment including: physical, electrical, thermal, and manufacturing characteristics.

One major hurdle in providing an autonomous sensor is the power source for the sensing, encoding, and transmission of data. Research involved determining the option best suited for providing a power source for the combination of sensors and wireless telemetry components. An energy budget of 105μJ was established to determine an estimate of energy needed to wirelessly transmit data with the selected RF transmitter. Based on these results, several candidates for power sources were investigated, and a piezoelectric energy harvesting system was identified to be the most suitable.

This is an ideal case as the sensor system was already based on a piezoelectric material as the sensing component. Thus, a harvesting circuit and the sensor can be combined into one unit, using the same material. By combining the two functions into a single component, the complexity, cost and size of the unit are effectively minimized.

In order to validate the conclusions drawn during this sensor system analysis and conceptual research, actual miniaturized systems were designed to demonstrate the ability to sense and harvest energy for the applications in mind. This secondary aspect of the research was a proof-of-concept, developing two prototype energy harvesting/sensing systems. The system designed consisted of a PVDF thin film with a footprint of 0.2032 m x 0.1397m x 52μm. This film was connected to an energy-harvesting prototype circuit consisting of a full-wave diode bridge and a storage capacitor. Two prototypes were built and tested, one with a 2.2μF capacitor, the other with a 0.1mF capacitor.

The film was first connected to an oscilloscope and impulsed in an open circuit condition to determine the sensor response to a given signal. Secondly, the energy harvesting circuits were tested in conjunction with the film to test the energy supply component of the system. Lastly, the film and both energy-harvesting systems underwent full scale testing on a road using a vehicle as the stimulus.

Both systems showed excellent rectification of the double polarity input with an evident rise in voltage across the capacitor, meaning energy was harvested. Typical results from the tests yielded 600-800mV across the 2.2μF capacitor, harvesting only a few μJ of energy. The 0.1mF capacitor system yielded approximately 4V per vehicle axle across the capacitor, harvesting 400-800μJ of energy. This equates to 4-8 times the required energy for wireless data transmission of the measurement data, which was estimated by other research groups to be on the order of 105μJ for the given system, and therefore proves the concept both, for bench-top and full-scale on-road experiments under controlled laboratory conditions.

ACKNOWLEDGEMENTS

I would like to express my gratitude to the many people who have helped me along the way with the completion of my thesis. Firstly my supervisors, Dr. Sven Achenbach and Dr. Qiaoqin Yang without their encouragement, guidance and support none of this would have been possible. Also, thanks go to my supervisory committee for their guidance and questions, which helped me develop my research throughout the course of my project.

To Randy Hanson and the engineering department of International Road Dynamics for the countless hours spent discussing this project and for their financial support over the course of my research.

I would like to thank Bob Wilson for his input and endless discussions regarding my circuits and for the construction of my prototype devices and help with testing. I would like to thank Mike Miller for use of the Hardy Lab without which I would not have completed my testing.

I would like to acknowledge the hard work and planning by Kelley Neale and the Mechanical Engineering Department over the course of my project.

For the financial support of my supervisors and the Mechanical Engineering Department I am forever grateful. Also, the financial support from the National Science and Engineering Research Council (NSERC) and International Road Dynamics through the Industrial Postgraduate Scholarship program, without this support I could not have completed this research.

To everyone that believed in my ideas and me, thank you all.

DEDICATION

I would like to dedicate this thesis to my parents whose unconditional love, support, and guidance have kept me going throughout the years.

TABLE OF CONTENTS:

List of Figures:

List of Tables:

1.0 INTRODUCTION

As current technology progresses, the need for smaller and smarter devices becomes more and more evident in design and engineering. The benefits of miniaturized devices are; smaller systems, less materials used, faster systems, better device performance and new application areas.

The need for miniaturized-systems has lead to the development of fabrication methods, which further decreased the sizes of electronic and mechanical systems. The combination of these electrical and mechanical devices into micro sized systems are known as Micro-electrical-mechanical-systems, more commonly, MEMS.

Micro-electrical-mechanical systems are micro sized devices incorporating both electrical and mechanical components integrated for the purpose of achieving a task. The development of advanced techniques has significantly decreased device size and costs.

A major component of MEMS, one that has developed slower than the fabrication technology that creates the devices, is the power supply for MEMS. Power supplies for wireless MEMS is a dramatically increasing field of research due to the significantly slower rate of progression when compared to fabrication processes. Creating MEMS for standalone use only becomes important once a viable, portable power sources become available.

The most important aspect of creating a standalone MEMS sensor is independent power. The amount of power needed for a MEMS system with actuators, sensors, and transmission is only a fraction of that needed in the macroscopic realm; this is due to the miniaturization of the device. There are several methods currently being studied to achieve self-powered sensors, which will be discussed in length in Sections 4.0-5.0.

1.1 Goals and Outline

The aim of this thesis was to identify and develop a sensing and energy harvesting approach that could be used for self-powered sensors. This thesis describes a method for harvesting energy via the piezoelectric effect utilizing a thin film poly-vinylidene fluoride (PVDF) piezoelectric polymer. Firstly, the thesis will discuss current MEMS systems and the fabrication methods involved in creating them.

The next section of the thesis covers power generation methods in general, listing all suitable methods of power generation. This section provides the benefits and drawbacks of each method for the intended purpose of a power supply for a self-powered sensor. This section will discuss in depth wireless power transfer as a method of powering a device. The three main branches of wireless power are investigated for feasibility; inductive coupling power transfer, wireless power transfer by microwave and radio frequency waves. This section continues to detail the current status of wireless power transfer, as well as experiments and results of research groups worldwide.

The piezo-electric energy generation section covers in-depth: an introduction to piezoelectricity, the theory behind it, as well as energy generation/harvesting via the piezoelectric effect. An extensive literature review of current and past harvesting systems, materials and configurations is detailed.

Since energy is being generated, a storage method and modulation circuit is needed. A comprehensive look at state of the art modulation circuits both in industry and research are investigated, with conclusions about which to use in the case of different energy storage methods. Wireless transmission of data from a MEMS devices is investigated to determine average power consumptions of wireless MEMS.

Investigation of the power generation of a polyvinylidene fluoride (PVDF) thin film for the purpose of charging a capacitor is outlined and theoretically calculated. The experimental results are investigated to determine the feasibility of using this energy to power a wireless RF transmitter for sensor data transmission.

1.2 Research Objectives

There are a few main objectives for the current research project:

- Primary Objectives:
    - To identify and develop a sensing and energy harvesting approach to produce a viable concept for autonomous sensing

    To objectively define a possible combination of sensing, power supply, energy storage and data transmission needed for a wireless sensor, based on current research and literature
- Secondary Objectives:
    - Using the conclusions drawn from the primary objective, design a possible autonomous sensing system
    - Validate the conclusions drawn from the primary objective by constructing and testing a prototype
    - Complete full scale testing of prototype using a vehicle and correlate data to current research worldwide

1.3 MICRO ELECTRO MECHANICAL SYSTEMS (MEMS)

Micro-electrical-mechanical-systems, or MEMS, are the combination of components into one micro sized system for the purpose of a specific task. These components can be electrical, mechanical, optical, or opto-electric, with a least one dimension in the micron range. An overall MEMS system is defined as an intelligent system comprising sensing, processing, and or actuating functions into a single or multi-chip hybrid. Overall system size ranges from a few microns to a few millimeters depending on the system and the number of components. These MEMS can be very complex such as a "lab-on-a-chip" or as simple as a pressure sensor. They are typically comprised of four main components; sensor, actuator, signal processing, and interface to the environment.

Many micro systems are fabricated by micro fabrication technologies initially developed for the semi-conductor industry. These and other technologies include thin film deposition, lithography, etching (wet or dry), micro machining, laser ablation, electron-beam writing and more.

1.3.1 Market and Systems

MEMS are a very unique, recently developed technology, prevalent in many industrial areas with new applications constantly being developed. A study completed by Nexus in 1998 and again in 2005 demonstrates the growth of the micro and nano market in industry with prevalent and expanding fields of applications. This report summarized that IT peripherals (hard disc drive head, inkjet nozzles, and flat panel displays) were and continue to be one of the most prominent application of MEMS devices. Following the IT peripherals were the automotive and telecommunications devices.

A second study completed by Shimoyama at the University of Tokyo demonstrated the increase in the Japanese MEMS market from 2002 to 2010. Their forecast, which was surprisingly accurate, estimated a 10 billion dollar (CAD) increase in the MEMS market in 8 years. This estimate of the Japanese market, demonstrated that information processing and communication equipment was $361,000,000 in 2010. This area includes video camera components, cell phones, copiers, dvd, and other disc drives. Following this industrial area, the second largest area was the automotive industry providing vehicle sensors and non-sensor systems. The automotive industry in Japan

alone was 387 million for 2010. A Nexus study on the US MEMS market demonstrated a total of 57 billion US dollars in 2009. The amount of money invested into MEMS recently has yielded a dramatic increase in the technology as well as the available devices and applications.

1.3.2 How Small is Micro? A Perspective Look at Micro Systems

The first major obstacle in micro systems engineering is that most people have a great difficulty putting a micro scale device into perspective. People have difficulty visualizing or imagining a micrometer (micron) ($1x10^{-6}$ m). The easiest way to put the size scale into perspective is to develop a comparison chart demonstrating living things and manmade things from the macro to the micro to the nano scale. The National Nantechnology Initiative provides an excellent comparison chart demonstrating a size comparison of man made and natural micro and nano scale objects.

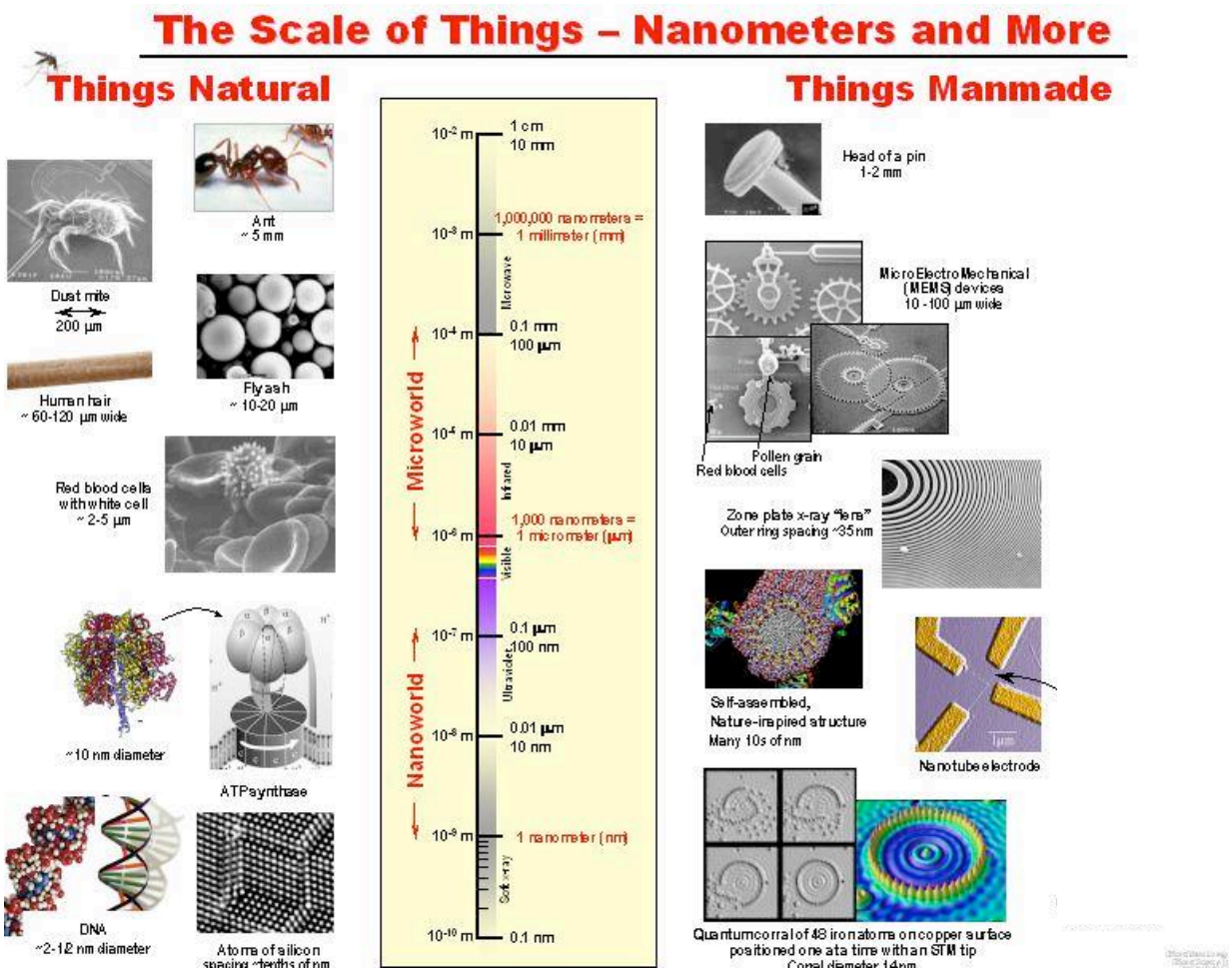

Figure 1.3.2.1: Size comparison of natural and manmade objects

(http://www.nano.gov/html/facts/The_scale_of_things.html)

Now that a size perspective has been established, a significant amount of confusion is typically experienced. How can a MEMS device be implemented into actual devices if they are so small?

This question is answered by the four components of a typical MEMS device: sensors, actuators, signal processing, and interface to the environment. The interface to the environment is rarely micro scale; a macro scale integration with the real world completes the MEMS device. This is outlined in Figure 1.3.2.2 below with a diagram showing the participation of micro systems with an overall device. The figure is created based on the participation ratio from Shimoyama's Microsystems Market Assessment.

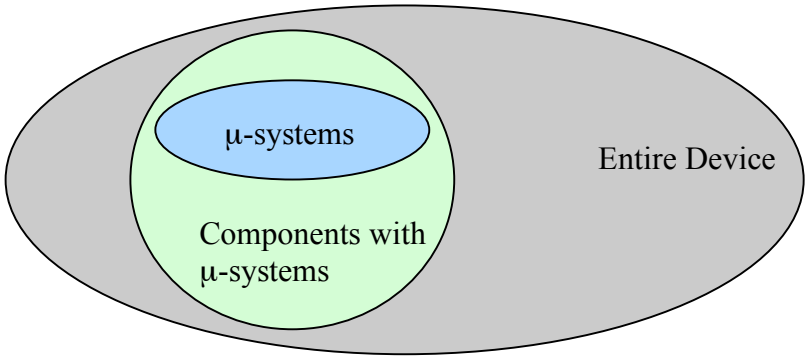

Figure 1.3.2.2: Illustration of the participation of a micro-system with a device

1.4 MICROFABRICATION

Microfabrication is a very in-depth field with dozens of processes. Each type of manufacturing process has different tolerances and accuracy therefore will yield different microsystems. When designing the fabrication process for a specific system, the overall size, minimum feature size, material and cost must all be taken into account. If only one final structure is used it may be beneficial to use a micromachining technique, while batch manufacturing will require a photolithography process. Some relevant microfabrication processes are outlined below. These techniques are described to allow for a better understanding of MEMS in general; to achieve a strong understanding of the fabrication involved with miniaturizing a device.

1.4.1 Thin Film Deposition/Coating

Thin film deposition is the deposition of thin layers of a material onto a substrate material for a specific purpose. In micro fabrication, thin film deposition is the standard technique used for creating the materials from which MEMS will be fabricated. The deposition method depends on the material to be deposited and also the substrate material. Typically, in lithographic fabrication, spin coating is used to deposit the thin film. Spin coating involves taking the substrate and rotating it while dripping or slowly pouring a viscous fluid onto it. The rotation causes an even distribution of the material and the desired depth can be controlled by spin rate and the drip rate. Once finished, the substrate and thin film are exposed to a “soft bake” process to slightly harden the material prior to exposure in the lithography process. Thin film deposition can also be completed

via the Physical Vapor Deposition process. PVD processes include: evaporation, sputtering, arc vapor deposition, and plasma and ion enhanced vapor deposition. In contrast to PVD, a chemical vapor deposition process can be used.

Thin film deposition is the first and most basic step of the micro-fabrication process.

1.4.2 Mechanical Micromachining

Mechanical micromachining is a basic micro fabrication technique that employs precision cutting of metals, alloys, polymers, and silicon. This method uses specially shaped tools made of diamond, hard metals, and ceramics. These micro machining methods are identical to milling and lathing used in regular machining but have a higher accuracy. There are some inherent problems with this type of approach as the smallest dimension achievable is a few dozen microns. The smallest groove size is limited by the tool size which is typically around 20-30 microns. The primary use of micromachining is to create prototypes and master mold inserts. Mechanical micro fabricated structures have poor quality and high roughness.

1.4.3 Lithography

Lithography, is the central patterning technique in the micro-electronics and systems technology. Lithography is defined as a technique for the transfer of patterns into a (photo) sensitive layer by means of energetic radiation by using masks or directly writing.

Lithography in itself is a multi-step process starting with coating, which is then exposed, and developed. Coating, as explained earlier, is typically done by spin coating the photosensitive layer (resist). This is then exposed to energetic radiation to polymerize the resist into the desired pattern.

The energetic radiation that is employed in lithography ranges in both the type of particle and the energy used. Typically, photons are used in the visible, ultra-violet, and x-ray wavelengths with an energy of 1eV to 20keV. When electrons are used, the energy is much higher energy of about 10keV to 100 keV. When extremely high energy is needed, ions and protons are used as the energetic medium with an energy of 1 MeV to 20MeV.

The energetic radiation impinges onto the photosensitive layer, known as the resist. This resist is sensitive to radiation but 'resists' further development steps such as etching. There are two types of resists used in lithography, positive and negative. A positive resist is a resist where the exposed areas become soluble in a developer and the unexposed areas get polymerized and harden. A negative resist is a layer in which the exposed areas get polymerized or cross-linked and harden and the unexposed areas are soluble in the developer.

The development stage in the lithography process is broken down into a few process stages; etching, development, modification.

1.4.4 Etching

Etching is a subtractive process to remove material based on either a chemical or physical reaction; wet and dry etching respectively. Wet etching is the submersion of a material into a chemical (liquid) to attack the material to be removed by a chemical reaction. This method can be anisotropic (along crystallographic planes) or isotropic depending on the material. This method cannot produce high aspect ratio structures but can be used to create free-standing structures and cantilevers by under-etching and using sacrificial layers.

Dry etching, on the other hand, is removal of a material based on a plasma gas discharge. This includes methods such as ion beam etching, reactive ion etching, plasma and barrel etching. This process can also be anisotropic or isotropic depending on the chemical selectivity. As the chemical selectivity increases the degree of anisotropy decreases.

2.0 OPTIONS TO POWER A MEMS DEVICE

Power generation is a very important aspect when designing certain systems, especially MEMS. Newer micro systems have very low power budgets and as such require low amounts of useable power. This leads to possibilities of further miniaturizing the micro system, as well as making it independent of wiring it to a power source. Without the need for wires connecting the micro system to a power source, the power required for operation must be generated within the operation of the micro system or stored in a battery or thin film super-capacitor. Further explanation of energy storage will be presented in Section 6.0.

Until recently, the usage of power generation has remained in the macro realm; from power plants, to petrol burning generators. In recent years, there has been a tremendous amount of work done to miniaturize a generator for the implementation within a self-powered micro system. There are several ways to convert or scavenge energy from the environment; thermal, photon, mechanical and chemical. The following section will explain and evaluate each method as it pertains to providing a power source for a wireless micro-electrical-mechanical-system.

2.1 Thermal to Electrical

The generation of an electrical voltage from a temperature differences is known most commonly as the thermoelectric effect. When a temperature difference is experienced across a thermoelectric device, a voltage is generated. Thermoelectricity typically deals with three prominent effects; the Seebeck effect, the Peltier effect, and the Thompson effect.

The most common type of energy scavenging device is a thermoelectric generator, which is based on the Seebeck effect. This device converts temperature differences between two different metal thermocouples into a voltage. Although in theory these devices are appealing, the efficiency is typically very low at around 5-10%. [2]

The efficiency limits the application in microsystems as well as the aspect of environment. Thermoelectric generators are typically employed in an environment that experiences rapid changes in temperature. The environment for the proposed microsystem is an outdoor environment, which, in a typical day will experience a very

slow, gradual temperature gradient rather than a rapid one. Without a rapid change in temperature, the device will yield almost no power generation for the intended device.

2.2 Photon to Electrical

The conversion of a photon to electrical or useable energy is a large area of research; photovoltaic cells, or solar cells. Solar cells are devices that convert incoming radiation from the sun into useable energy via the photovoltaic effect. The photovoltaic effect occurs when photons (sunlight) hit the solar cell material (typically Silicon) which causes electrons to become knocked loose from their atoms. These electrons are then free to move, but are constrained to one direction. This flow of electrons can then be used as a useable current. Current systems have an efficiency of 5-20% of converting incoming sunlight to useable energy. Although this efficiency is large enough to supply power to a micro system, the main drawback of a solar system is the large area of the photovoltaic panel required to harness the incoming sunlight.

There are thousands of different types and sizes of solar panels ranging from macro scale powering houses to micro scale in research. Currently, the power produced from a micro scale photocell is too small, as the impinging photons do not have a large area to hit. Micro scale photocells are not practically feasible unless arranged into a large array, which, in the current micro system is not feasible due to harsh environmental conditions on roadways. With a photovoltaic system, the micro system would still need to be wired to the photon harvesting system which could not be implemented at the same location as the micro system thereby defeating the “wireless” aspect of the harvesting device.

2.3 Chemical to Electrical

Conversion of chemical energy to useable electrical energy is one of the most common forms of energy conversion. A chemical reaction is used to create free electrons, which can be stored for use. The most common form of a chemical to electrical energy conversion is a battery. Batteries range from large to small from powering a vehicle to a watch. There are two main types of batteries; primary (disposable) and secondary (rechargeable).

Primary batteries are not feasible for long life applications as once depleted the battery needs to be replaced. Secondary batteries, may, in the future have some application for extended life applications. Although, currently, secondary battery technology is limited; the devices lose 10% of their charge within 24 hours and continue to discharge at about 10% for every month after. Although these batteries can be recharged, the length of one cycle is not long enough for an in-situ application. Replacing or recharging batteries would defeat the purpose of creating a "self-powered" device. For a micro-system, secondary batteries are not the ideal choice due to limited life cycle as well as the macro size requirements.

2.4 Mechanical to Electrical

Mechanical energy conversion is not a new field. Devices such as water wheels were evident in early civilization and now turbines are moved by water to provide useable electricity. There are several methods to convert mechanical energy to electrical energy. In the MEMS field there are only a handful of devices that utilize different methods. In the macro realm here is a magneto hydrodynamic power generator (MHD) which uses extreme temperatures and plasma to move parts in turn generating energy, but this device is not portable due to its extremely high temperature requirements [5]. The second most common type of conversion is the piezoelectric energy generator (PEG). PEG's have become a large area of interest due to the decrease in power requirements of micro-electronics. Until recently, PEG's could not generate a enough charge to power electronics, but now, the increase in generation potential and decrease in power requirements have lead to a generation method that is perfectly suited for a long-life in-situ MEMS device that is self powered via the piezoelectric effect. Section 4.0 will provide an in-depth coverage of piezoelectric energy generation theory and current devices and materials.

2.5 Wireless Power Transfer

Wireless power transfer is the process of electrical energy transfer between devices without the need for wires. To utilize this technology a macro scale transmitter could be used to transmit power to a micro scale device. The advantage of this would be

an unlimited power generation without the need for wires. The major disadvantage to this is the transfer may impede or inhibit the micro device operation.

Nikola Tesla first demonstrated this transfer technology in the macro realm in 1893, in Chicago, where he wirelessly illuminated a phosphorescent lamp. He later transmitted power over 48 km to power a lightbulb [6]. To this day, his work has still not been recreated to this distance, although a group at MIT has successfully used his technology to power a bulb at 2m [7]. Most of the work done in the wireless power transfer field has been studied in the macro realm with only a few groups worldwide working on transfer to a micro scale device. Section 5.0 will cover wireless power methods in detail.

3.0 LITERATURE REVIEW ON WIRELESS POWER TRANSFER METHODS

Wireless power transfer as discussed in earlier chapters is a very promising option to power a standalone MEMS device. This section provides a closer examination of the potentials and limitations of using this technology in the context of providing power to a wireless sensor.

Wireless power transfer is not a new concept; it began back in the late 1800's with Nikola Tesla and Heinrich Hertz. The most common method for wireless power transfer (WPT) is inductive coupling, followed by power transfer by radio frequency waves. Until recently, these two methods were the most popular, but recent technology advances have lead to wireless power via RF transmission, magnetic coupling and transfer by laser or light. There are two classes of power transfer techniques; near and far field.

Near field transfer is, as the name suggests, a transmission technique for transfers on the order of a few times the diameter of the device, or a quarter of the wavelength used. The use of near field transfer is almost always referring to induction transfer although now other methods are being utilized in the near field.

Far field transfer is the transmission of power at distances of hundreds of meters to kilometers. Far field techniques are based on radiowave and microwave techniques, although new photon based collectors for lasers and high powered lights are being developed. Far field transmission can deliver power at long ranges by matching the shape of the receiving area and the electromagnetic radiation by using high directivity antennas or well collimated lasers.

3.1 Induction

An induction based transfer technique, or inductive coupling, is one of the most commonly used near field techniques. Inductive coupling is based on mutual induction; current flow through a primary coil induces a magnetic field, which creates a current flow in a secondary coil. The main drawback of this type of system is the limited range; the secondary coil must be in close proximity to the primary coil in order for the magnetic

field to induce a current flow in the secondary coil. There are two classes of inductive coupling; magnetic induction and resonant induction.

Magnetic coupling is based on the magnetic permeability of the transfer medium and the magnetic field equation. For wireless power transfer the transfer medium is air, therefore the magnetic permeability of air will govern the transfer distance in conjunction with the magnetic field equation. The magnetic permeability coefficient, μ_r, is very low for air ($\mu_r = 1$) compared to a ferromagnetic material such as nickel-iron alloy at $\mu_r = 10{,}000$ [9]. This means the magnetic field density generated in air is 10,000 times smaller than the same field generated in a ferromagnetic alloy.

When viewing the magnetic field created by inductive coupling, the governing equation is the Biot-Savart Law. This equation relates the magnetic field density for a moving charge through a wire, to the permeability of free space and the distance from the coil.

$$\vec{\beta} = \frac{\mu_o q \bar{v} \times \hat{r}}{4\pi r^2} \qquad \text{(Equation 3.1.1)}$$

where:

$\vec{\beta}$ is the magnetic field density

μ_o is the permeability of free space

q is the electrical charge of a point charge

v is the velocity vector of the point charge, with its direction tangent to the wire

$\hat{r}$ is the unit vector directed away from the wire

r is the distance away from the wire

When observing the governing Biot-Savart law, it is easily seen in the denominator r^2 term, that as the distance from the coil is increased, the field density is decreased by a factor of two. This limits the transfer distance to a few centimeters to power any electronic device, and inside one meter to power microelectronics. So to power a micro-system using this technique would require the power source (connected to the inductive coil) to be within centimeters to under a meter of the device; once again not achievable in

most wireless micro-systems.

One way around the limited transfer distance is to implement resonant coupling. Resonant inductive coupling is similar to magnetic inductive coupling in the fact that it uses a primary coil separated by a distance from a secondary coil to produce an electric charge.

Although in this method, a capacitance plate is connected to the end of each coil, which will resonate according to:

$$\omega = \frac{1}{\sqrt{LC}} \qquad \text{(Equation 3.1.2)}$$

where:

ω = resonant frequency

L = inductance of the coil

C = capacitance of the plate

If both plates resonate at the same frequency, energy is transferred from one to the other at distances much greater than achievable with magnetic coupling. This method can provide a longer transfer distance up to a few meters (<5m) and a higher efficiency [10].

The main drawback with inductive coupling is the limited transfer distance, on the other hand, no line of sight is required making it extremely feasible for powering wireless sensors. Few groups have tried wireless power transfer for wireless sensors due to the limited research and technology. This field is in its infant stages and may in a decade or so be used to power devices, but at this stage of its development, is impractical for implementation in MEMS due to the enormous amount of hurdles that still must be overcome to produce a useable device.

3.2 Microwave Transmission

Microwave transmission is a method of transmitting power using electromagnetic waves (microwaves). A typical microwave power transmission system consists of 3 components: a microwave source, a transmitting antenna, and a rectifier antenna (rectenna). The basics behind this WPT method are to use one antenna to emit

electromagnetic wave energy (microwave energy) and use a second antenna to receive those waves and convert them into DC power. Microwave power transmission has been demonstrated over 100km with rectenna efficiency demonstrated elsewhere at over 90% [11].

There are several drawbacks of microwave transmission, including the most important for this application; line of sight is required and the microwaves will deflect off of surfaces and materials. This means that powering embedded sensors via microwave transmission is not feasible as the waves will reflect off the surface of the material, which the wireless sensors will be embedded. Another reason this method is not feasible is the large antennas required for transmitting and receiving the energy. Typical microwave rectennas are several meters in diameter to effectively "catch" the incoming microwave transmission. A large rectenna, for the case of wireless sensors, is completely unpractical due to the enormous size required compared to the micro-system.

3.3 RF Power

Radio Frequency transmission, or RF power transfer is very similar to microwave transfer with the exception of a lower transmitted frequency. A lower frequency means a longer wavelength, which means the waves can transfer through solid medium. A short wavelength will cause deflection and interference of the wave when transmitted through a solid medium. A longer wavelength allows transfer through solid medium and therefore the transfer does not require line of sight.

Power transfer by this method is a very promising technology for MEMS sensor networks. A commercially available macro-scale unit from Powercast can provide 100mW at 9 meters with a frequency of 900MHz.

Although this method can transfer the required power at a reasonable distance for wireless embedded sensors, the ability to develop this technology into a micro-system has yet to be discovered. The major problem with using this technology is the antenna required for each sensor. The RF signal must be captured by an antenna and then converted into a useable power supply. Therefore, to date, each sensor must be equipped with a macro-antenna making this method unsuitable for embedded sensors due to size and more importantly cost limitations.

4.0 PIEZO-ELECTRIC ENERGY GENERATION

4.1 Introduction to Piezo-electric Energy Generation

Piezoelectricity is a phenomenon discovered by Jacques and Pierre Curie in 1880. The etymology of the word is derived from the greek word, piezein, meaning to press or squeeze, and the English word electricity. Piezoelectricity is the creation of an electric charge in a material when subjected to an applied stress. This electric charge is a result of the crystal structure or atomic arrangement of the material. The charge is created by a slight deformation of a material when subjected to an external stress, which causes a slight variation in the bond lengths between cations and anions. Within all materials, each molecule contains regions of positive and negative charge; the cations and anions. These regions of positive and negative charges are separated symmetrically by a point called "the gravity center" [12]. Figure 4.1.1(a) shows the gravity center (grey center circle) with symmetric offsetting positive and negative charges. These charges, being symmetrically offsetting around the gravity center are mutually cancelled yielding a net overall neutral charge. However, when a force is exerted on the material, the internal structure of the material is deformed yielding a non-symmetric structure with positive and negative charges not coinciding therefore creating localized charge dipoles. Overall the material still contains a zero net charge, but locally there is a non-zero net charge, Figure 4.1.1(b). This figure shows the dipoles created which cause the material to be polarized and a charge to appear on the surface of the material. This polarization leads to the generation of an electric field and can be used to transform the mechanical deformation energy into an electric energy.

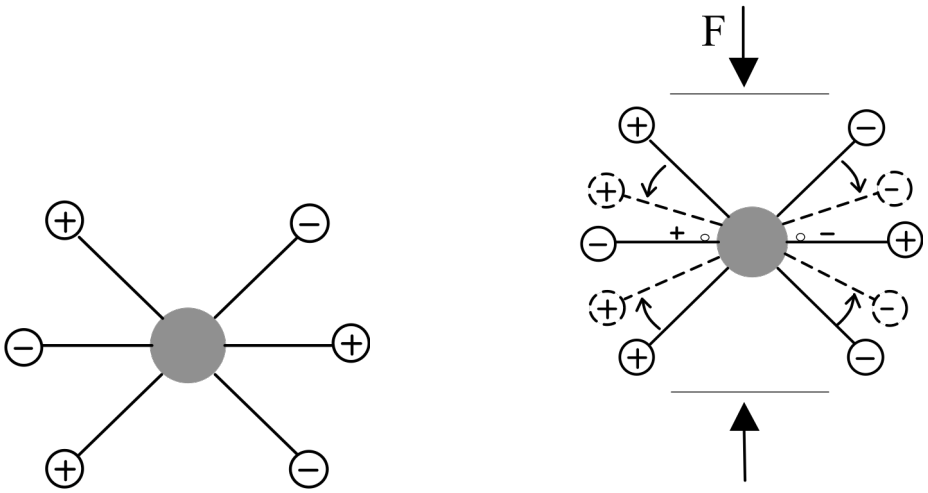

Figure 4.1.1: a) symmetrically offsetting cations and anions around a gravity center yielding a neutral net charge b) force induced deflection of charges around a gravity center creating non-symmetric charges, yielding a localized, non-zero, net electric charge.

In order for a piezoelectric material to be used as a method to generate electric energy, a few steps must be completed first. First, electrodes must be deposited on the surface of the material. Suppose that after depositing electrodes, a wire is connected to the electrodes, externally short-circuiting them. To see the effect this will have, a galvanometer can be connected to the short-circuited material. If a force is exerted on the piezoelectric material, a linked charge density appears on the surface of the material, which causes the material to become polarized. As stated earlier, this polarization causes an electric field, which will cause the excess charges present to move in the opposite direction of their charge. This flow of excess charge will be visible in the galvanometer until the pressure is removed. When the pressure is removed, the excess charge will then reverse and the material will return to its original state.

4.2 Piezoelectric Material Poling

A piezoelectric material is only useful as an energy generation device once the material has been poled. Poling is a procedure used to induce intra-molecular alignment yielding a material with enhanced piezoelectric properties.

The poling direction of a piezoelectric material is defined as the direction from the center of the crystal to the positively charged atom. Bulk piezoelectric materials have a random poling direction; meaning the pole direction is randomly distributed throughout the material (Figure 4.2.1 (a)). When using a material as a piezoelectric energy generator, the poles must be aligned in the same direction to achieve effective charge generation.

To align the poles, a material must first be heated past its Curie temperature. The Curie temperature of a material is the highest temperature it can be heated to before losing its poling direction. Each material has a specific Curie temperature; the Curie temperatures for many common piezoelectric materials can be found in Section 6.65.

After a material is heated above its Curie temperature, there are two methods to achieve a permanent change in the poling direction. The first is to apply a voltage across the material in the desired poling direction. Then, cool the material down well below its Curie temperature while still applying the voltage; removal of the voltage, once cooled, will permanently set the poling direction. The second option to pole a material is to heat it above its Curie temperature while applying a constant pressure on the material. Again, cooling the material below its Curie temperature while maintaining the pressure will cause the new poling direction to set permanently.

The poling direction is a material parameter that will significantly affect the charge output to stress input relationship.

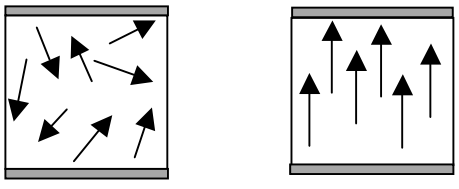

Figure 4.2.1 : a) Randomly distributed poling direction b) After poling; established poling directionality.

The poling direction is most easily understood on a molecular level by viewing polyvinylidenefluoride (PVDF). PVDF is a polymer repeat unit of CH_2-CF_2 that demonstrates a significant enhancement of piezoelectric properties when poled. Section 4.6 will cover PVDF and other piezoelectric materials more in depth.

Before poling, PVDF has a random orientation of molecules as shown in Figure 4.2.2 below. After poling, the material exhibits an ordered arrangement of molecules and increased ferroelectric and piezoelectric properties, Figure 4.2.3.

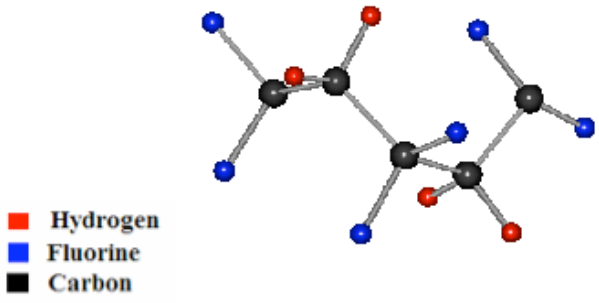

Figure 4.2.2: PVDF molecular structure before poling; random orientation. [13]

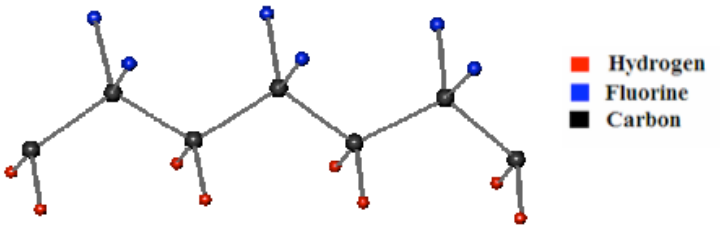

Figure 4.2.3: PVDF molecular structure after poling; ordered structure. [13]

4.3 Piezoelectric Theory

The theoretical foundation of piezoelectricity is well established and an accepted standard of describing the material behavior is prevalent in engineering. The IEEE Standard of Piezoelectricity is the accepted way of describing this behavior and relationship.

When a piezoelectric material is stressed, some of the mechanical work done is stored as elastic strain energy and some in the electric field created by the creation of a space charge. The relationship between stress and strain is described using a material's elastic properties. The relationship is simply an adaptation of Gauss's Law and Hooke's Law to account for the electro-mechanical coupling in the material.

The fully coupled, constitutive equations for an unbounded piezoelectric material are given by [48]:

$$S_{ij} = s^{E}_{ijkl} T_{kl} + d_{kijE_k} \quad \text{(Equation 4.3.1)}$$

$$D_i = d_{ijkl} T_{kl} + \varepsilon^{T}_{ik} E_k \quad \text{(Equation 4.3.2)}$$

$$S_{ij} = s^{D}_{ijkl} T_{kl} + g_{kij} D_k \quad \text{(Equation 4.3.3)}$$

$$E_i = -g_{ikl} T_{kl} + \beta^{T}_{ik} D_k \quad \text{(Equation 4.3.4)}$$

Where:

S = strain component

s = elastic compliance constant (m^2/N)

T = stress component (N/m^2)

d = piezoelectric constant (m/V or C/N)

E = electric field component (V/M)

D = electric displacement component (C/m^2)

ε = dielectric constant of the piezoelectric material (F/m)

g = piezoelectric constant for applied voltage (Vm/N or m^2/C)

β = impermittivity components (m/F)

The subscripts i, j, k, and l are the indices which take values 1,2, and 3 and show the direction within the material. The subscripts are common nomenclature in elasticity and can be converted to compressed notation following the subscript conversion rule outlined in Table 4.3.1 below. The conversion rule states that every pair, ij or kl, convert to a single subscript ranging from 1-6 as defined below.

Table 4.3.1: Compressed subscript notation conversion chart

Pair ij or kl	Single Subscript
11	1
22	2
33	3
23 or 32	4
31 or 13	5
12 or 21	6

With the above compressed notation rule, four subscripts are replaced with two subscripts and two subscripts replaced with a single subscript. As can be seen in Equations 4.3.1-4.3.4 there are a few components of these equations with three subscripts which are replaced with a set of subscripts. These triple sets of subscripts denote the surface (1st subscript) while the second two define the direction of the field; only the direction subscripts are replaced with a single pair while the surface subscript remains unchanged. This is illustrated in Figure 4.3.1, where the first subscript denotes the surface and the second the direction.

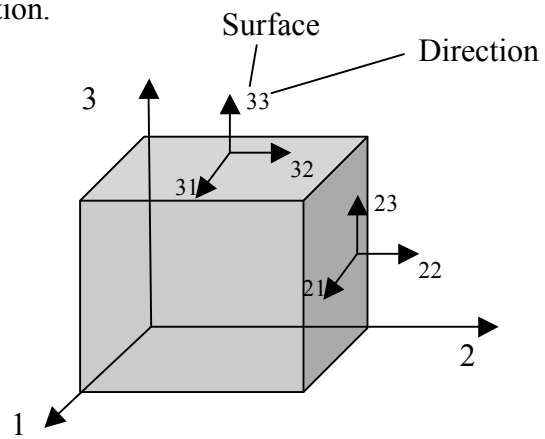

Figure 4.3.1: Subscript notation for the piezoelectric constants

When viewing the constitutive Equations 4.3.1-4.3.4, there are a total of 63 constants needed: 36 elastic constants, 18 piezoelectric constants and 9 permittivity constants. For the most common piezoelectric materials, approximately half of the constants are zero; having 6 elastic, 3 piezoelectric and 2 permittivity constants.

Therefore, a common piezoelectric material only 11 constants out of 63 are needed to describe the behavior of the material. This makes expansion and simplification of the constitutive equations much simpler.

The next relationship of importance is the energy equation. This relationship consists of two distinct halves; elastic energy and electric energy. The general energy equation for a piezoelectric material is described by [14]:

$$Energy = \frac{1}{2} * strain * stress + \frac{1}{2} * charge * electric\ field \qquad (Eq.\ 4.3.5)$$

Substituting terms from equations 4.3.1-4.3.4 yields the energy equations as defined by the constitutive equations.

When using these equations to determine the charge generated by a piezoelectric material, integration over the volume of the material must be completed because the constitutive equations are for an infinitesimally small volume.

For a compressive load, F_o, applied to a piezoelectric material, the energy generated in the material can be calculated using an expanded version of Equation 4.3.5. In this scenario, illustrated in Figure 4.3.2, there is only a compressive component of force (3 direction) which means $T_1=T_2=T_4=T_5=T_6=0$. With electrodes deposited on the top and bottom of the material, the electrodes are only in the 3 direction, therefore $E_1=E_2=0$.

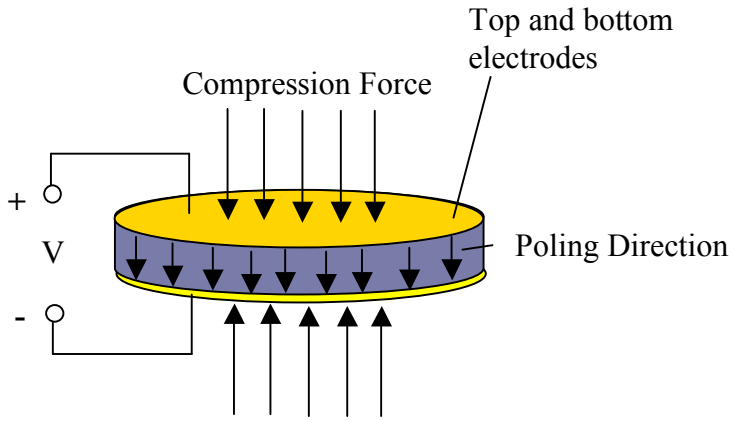

Figure 4.3.2: Illustration of a thin film piezoelectric generator with top and bottom electrodes and a compressive force.

Using conventional notation for stress and strain (σ and ε respectively) and energy as U, the equation becomes.

$$U_i = \int_{volume} \left(\frac{1}{2} \varepsilon_3 \sigma_3 + \frac{1}{2} D_3 E_3 \right) dv$$

$$= A h_p \left(\frac{1}{2} s_{33}^E \sigma_3^2 + d_{33} \sigma_3 E_3 + \frac{1}{2} \varepsilon_{33}^T {E_3}^2 \right)$$

$$U = \frac{s_{33}^E h_p}{2A} {F_o}^2 + d_{33} F_o V + \frac{A \varepsilon_{33}^T}{2 h_p} V^2 \qquad \text{(Equation 4.3.6)}$$

Where:

A= surface area

h_p= layer thickness

Electrical energy is described by charge and voltage (U=QV), therefore to calculate the total generated charge, a partial derivative of equation 4.3.6 with respect to voltage must be taken.

$$Q_{Generated} = \frac{\partial U_{total}}{\partial V} = d_{33} F_o + \frac{A \varepsilon_{33}^T}{h_p} V \qquad \text{(Equation 4.3.7)}$$

The total charge generation, as outlined in the equation above, is described in two terms, the charge due to the applied force and the charge due to an electric field. These two parameters can be viewed as boundary conditions for the equation; force and electric field. In the case of a piezoelectric energy generator, the applied voltage, V, is zero simplifying the equation to:

$$Q_{generated} = d_{33} F_o \qquad \text{(Equation 4.3.8)}$$

The charge generated by an applied force is an important value, but more important than the charge generated is the electrical energy generation. This value is the voltage that will be created on the piezoelectric material due to the applied force.

In order to calculate the electrical energy generation, we must first know the capacitance of the material. Capacitance is the relationship between voltage and charge on the material and can be seen in the partial derivative in Equation 4.3.7. This equation,

as stated earlier, has two distinct parts; force generation and voltage generation. The second portion of this equation contains a relationship between voltage and charge; the capacitance of the material.

$$C = \frac{A\varepsilon_{33}^{T}}{h_p} \qquad \text{(Equation 4.3.9)}$$

Now that the capacitance of the material is known, the voltage of the generated charge due to an applied force can be calculated:

$$V_{generated} = \frac{Q_{generated}}{C} = \frac{d_{33}h_p}{\varepsilon_{33}^{T}A}F_o \qquad \text{(Equation 4.3.10)}$$

Now, we know that generated charge is the product of multiplying the charge by the voltage (U=QV). This implies that the electrical energy generated by a force, F_o, on a piezoelectric thin film can be calculated by:

$$QV = \frac{{d_{33}}^2 h_p}{\varepsilon_{33}^{T}A}{F_o}^2 \qquad \text{(Equation 4.3.11)}$$

4.4 Architecture

Every energy harvesting system based on vibration or force-induced deflection will have a similar architecture. This architecture is based on the sub-systems that are required for production and storage of an electric charge from a piezo-electric material. Figure 4.4.1 below demonstrates the sub-systems and their interactions.

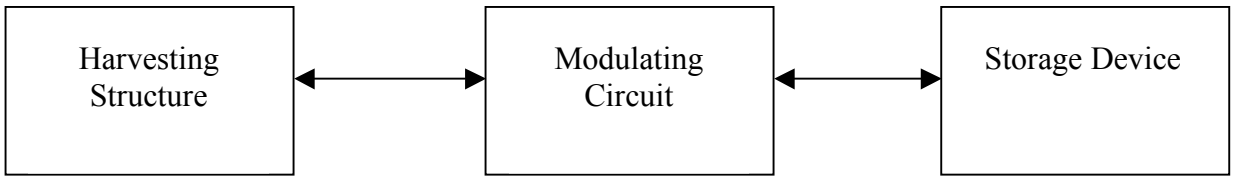

Figure 4.4.1: Energy Harvester Architecture

Within the field of energy harvesting research, there exists a plethora of combinations of the three sub-systems required. Very rarely will two energy harvesting systems utilize the exact same architecture due to the infancy of the research field demanding new combinations be tested to determine the best overall set of sub-systems. Section 4.5 will cover the range of sub-systems and current energy harvesting systems.

4.5 Energy Harvesting Configurations

Piezoelectric energy harvesting devices have many different configurations based on their intended purpose or generation mode. These devices are defined based on their poling direction as well as the applied stress direction. There are generally two modes of operation for a piezoelectric energy generator. The first mode is when a mechanical stress is applied to a piezo-material parallel to the polarization. This induces a strain in the thickness direction of the material, which in turn generates a voltage within the material that tries to return the material to its original thickness; this is known as the d_{33} mode. Alternatively, in the d_{31} mode, a stress is applied in a direction perpendicular to the polarization. This generates a strain in a direction perpendicular to the poling direction and a voltage that tries to return the material to its original length and width.

The direction modes are a very important relationship for energy harvesting; relating stress and charge. This relationship is defined as:

$$D_{ij} = d_{ijk}\sigma_{lk} \qquad \text{(Equation 4.5.1)}$$

Where:

D = charge per area

σ = applied stress

d = piezoelectric constant

The subscripts, i and j, in the above relationship are dependant upon the stresses in the material and are replaced by numbers 1-6 depending on the stress direction. For the stress component, σ, the first subscript represents the surface and the second subscript stands for the direction as defined by the general elasticity subscription rule [14].

For the piezoelectric constant, d, the first subscript describes the poling direction whereas the second subscript describes the direction of the applied force (or electric

field). The subscript of the charge per area, D, denotes the surface direction of the electrode.

Obviously, as generator systems will differ on the modes of operation and stress, the relationship will change accordingly. For example, if a longitudinal stress (parallel to polarization) is applied on the piezo-material shown in Figure 4.5.1, below; Equation 4.5.1 is rewritten as:

$$D_3 = d_{31}\sigma_{11} \qquad \text{(Equation 4.5.2)}$$

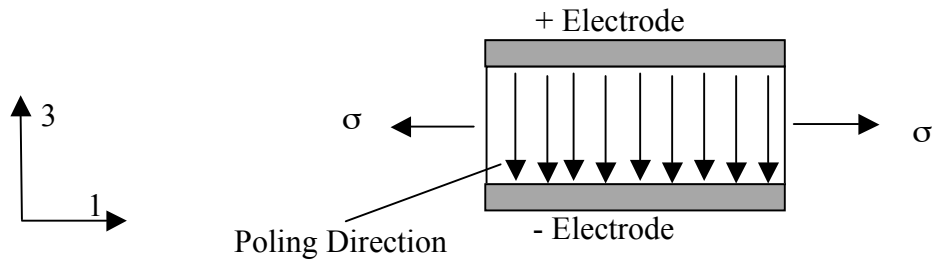

Figure 4.5.1: Piezo-material with longitudinal stress and surface electrodes, described by Equation 4.5.2.

When observing the piezoelectric constant, d_{ij} , it is obvious that in a piezoelectric energy generator the largest value will produce the highest charge per area. For class 4mm ceramics, there are only 3 pieoelectric constants, d_{13}, d_{31}, d_{33}. These range of magnitude of these three constants are $d_{13} > d_{33} > d_{31}$. Therefore, it would be an obvious choice to implement a d_{13} mode generator. In actuality, the 13 direction corresponds to shear stress and is extremely difficult to achieve in a real system.

The next obvious choice is the 33-direction, as it is the second largest in magnitude. The 33 direction is the chosen mode of operation for the current research.

4.5.1 Thin Film and Stacked Device

The thin film generator or its predecessor the stacked PEG is the most common d_{33} mode device. A bulk piezoelectric generator is a material that when compressed yields an electric charge; Figure 4.5.1.1. This bulk material can be as simple as a thin film, or a complicated stack of different or similar materials.

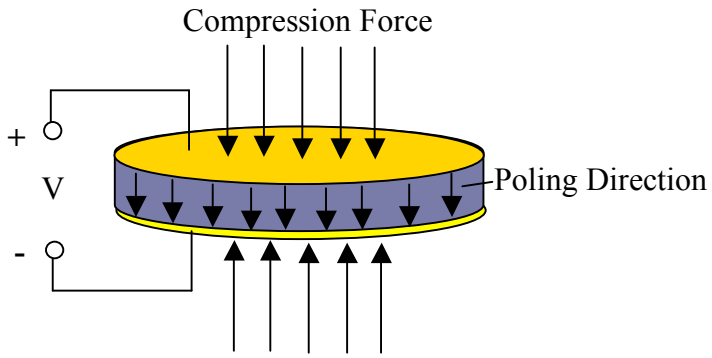

Figure 4.5.1.1: A bulk, thin film, d_{33} mode piezoelectric generator under compression.

Simple d_{33} mode piezoelectric devices are not very useful as actuators due to the extremely small displacements achievable in the thickness direction. Although using multi-layer 33 direction devices has been demonstrated to produce an acceptable range of actuation for certain applications.

The theory behind piezoelectric generation is based on straining a material, or elastic deformation. Therefore it is easy to validate the use of such a device for impact energy harvesting. Umeda et al studied the electrical generation of a thin film ceramic disk (25mm diameter) while connected to a 10kΩ resistor. The output of this device was studied under the impact of a 5.5g steel ball to determine the transformation efficiency. The results of this study were given in efficiency rather than voltage or energy. The efficiency of a piezoelectric device is defined as the amount of useable energy in closed circuit (across a capacitor or resistor) versus the amount of energy produced in an open circuit condition. Umeda found that the efficiency of this device was only around 5-9% dependant upon the height of the ball before impact. This low efficiency was due to the elastic collision of the steel ball causing a bouncing effect. In the event of an inelastic

collision the efficiency was calculated to be close to 100% , assuming a mechanical quality factor Q higher than 1000. [15]

When viewing the application of the current research, the stress conditions are high magnitude and dynamic. The use of a thin film d_{33} device was validated by Keawboonclinay in 2003, when the research conducted showed that dynamic stress produced a ten times higher voltage output than quasi-static stress. This is due to the fact that the piezoelectric capacitance has enough time to charge in the quasi-static case. The stress was defined as quasi-static when stress duration was greater than 100ms and dynamic when it was shorter than 10ms. So, for a very fast impulse, the voltage produced will be much greater than for a long impulse. This research also demonstrated that the quasi-static stress produced a bidirectional voltage whereas the dynamic stress created a unidirectional output. [16]

Mazdik et al. created a PZT transducer that was 3.1mm thick to harvest vibrational energy for aerospace applications. This research demonstrated the ability to successfully charge batteries using vibration-harvested energy. [8]

In 1998 investigation of the transformation efficiency of piezo-generators made of a single $LiNbO_3$ plate using a hammer impact was completed. The thin plate generator demonstrated an efficiency of 78% and using a multilayer generator an efficiency of 70% was achieved. Comparing this efficiency to a PZT thin plate generator with an efficiency of 65%, the difference is due to the higher Q factor of $LiNbO_3$. [17]

In 2002 Ichiki et al studied the electrical output of PZT piezoelectric disc under a 40N applied load. The peak power resulting from the load was 3 μW [18].

More recent work into polymer micro generators has been utilizing human motion and piezo-transducers embedded into clothing or shoes. Ville Kaajakari and Ding Han at Louisiana Tech design a piezoelectric polymer transducer embedded into a shoe. This microstructured polymer has a film thickness of 80 μm and is filled with microcells with an average diameter of 30 μm. The microcells were embedded into the polymer to achieve a lower Young's modulus. In this research, in order to achieve a greater transducer output, the film was rolled into a 1-cm stack of approximately 120 layers. The final transducer had dimensions of 4cm x 6 cm x 1cm with a total weight of 6.5g. The output of the transducer was measured in several different locations throughout the sole

of the shoe. Their research demonstrated that a step down converter was needed to create a voltage that was useable for portable electronics or telemetry devices. After their conversion circuit, the shoe power generator provided over 2mW of regulated power at 4.5 V [19]. This amount of power is more than sufficient to power a wireless telemetry device for wireless transmission as well as charge a storage device.

Another group in Portugal, at the University of Minho, has been extensively developing piezoelectric generators embedded into shoes. Rocha, Goncalves et al. utilized a 28μm β-PVDF (polyvinylindene fluoride) thin film to generate useable power from the energy exerted in the sole of a shoe during walking. Their piezoelectric transducer was coupled with an electrostatic generator to increase the performance and power generation. The power generated by their device ranged from tens to hundreds of milliwatts depending on the area, placement, and geometry. Their research also indicates that the voltage generated by two layers was approximately double that of a single layer; also demonstrated by Kaajakari et al. [20]. A drawing of their shoe power piezo device is shown below in Figure 4.5.1.2.

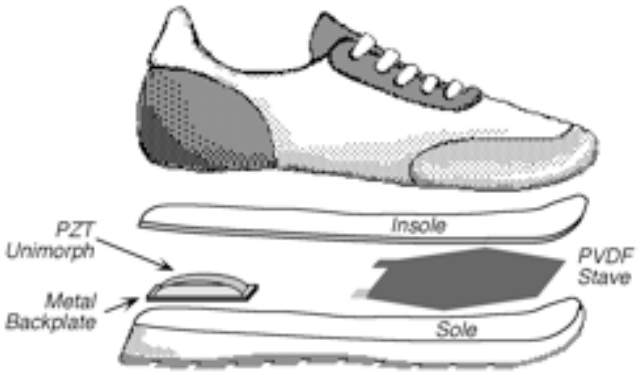

Figure 4.5.1.2: A shoe power generator with PVDF Stave and a PZT unimorph. [20]

Jonathan Granstrom et. al. devised a PVDF generator system embedded into the straps of a backpack. This system used a 52μm thick PVDF film with a length of 1m and a width of 51mm. By placing these "straps" inside the backpack straps, the results were very favorable for powering portable electronics or charging storage devices. With a 100 lb load applied to the backpack, an average useable power of 45.6mW was achieved during their tests. This test also demonstrated that due to the high impedance of PVDF

the energy output was at very high voltage but low current. To overcome this a parallel wiring scheme was implemented rather than a series. This becomes extremely useful for charging small batteries or supercapacitors [21].

Typically, these groups all demonstrate the use of ceramic-based or thin film generators under low magnitude loading. Other groups, investigating power harvesting, outside of human based scavenging, have demonstrated an increase in mechanical strength and the ability to heavily load these materials. The two most popular types of ceramic-metal composite transducers are Cymbal and Moonie transducers. These composite transducers are comprised of a piezoelectric disk with a hollow metal cap attached to the top and bottom of the disc. A Cymbal transducer is a device where the displacement is based on both flexural and rotational motion whereas a Moonie transducer is purely flexural [22]. Hyeoung Woo et al. demonstrated the use of a Cymbal transducer under a high loading force amplitude of 1kN. The generated power of this device across a 400kΩ resistor was 52mW or about 44mW/cm^3 [23].

Thin film transducers or plate generators have been demonstrated by several groups to be sufficient at generating enough useable energy to power wireless devices or charge storage devices. These transducers are typically utilized in low magnitude force applications but can be used for large force/stress applications as long as the material remains within the elastic region so as to not affect the piezoelectric response of the material. Piezoceramics and piezopolymers are both demonstrated to have a higher output in dynamic stress (less than 10ms) than in a quasi-static state (greater than 100ms). The output is also dependant on the type of material, the geometry, and conversion circuitry.

PZT is demonstrated as having a higher piezoelectric constant and a higher coupling factor compared to PVDF. On the other hand, PVDF is flexible and more durable; withstanding higher impact forces and larger mechanical forces due to PZT's brittle nature. It has also been demonstrated that PVDF can produce more useable power by implementing a "stacked type" transducer with multiple layers when compared with a single layer device. The specific application of the current research demands that the material be flexible while retaining impact strength as well as the ability to be manufactured in a thin film of any shape or size. The specific characteristics necessary for the intended research application will be further discussed in Section 9.0.

4.5.2 Cantilever

Cantilevers are a d_{31} based device, meaning that the stress is applied perpendicular to the polarization in a flexural mode. Cantilever based piezo-generators are the most popular type of generator; typically vibration harvesting based. Their popularity is based on the high magnitude of strain that can be induced in the structure as well as the high power output even under lower acceleration amplitudes. Although cantilevers demonstrate large power outputs and high strain they exhibit numerous drawbacks making them unusable in many applications. Cantilevers exhibit weak mechanical strength, a low piezoelectric coefficient, fatigue, and low maximum applied force.

There are many types of cantilever (d_{31}) piezo-based generators found in research but the most popular are a bimorph and unimorph. A bimorph cantilever can be easily described as a mutilayer cantilever beam. More specifically, a bimorph cantilever consists of a piezoelectric layer bonded to a non-piezo material on both the top and bottom of the non-piezo material. A unimorph consists of only a single layer bonded to a non-piezomaterial.

Force-based cantilevers are simply a piezo-cantilever that generates an electric field when experiencing a force on the cantilever. These types of generators are not very common as most cantilevers are utilized for vibrational energy harvesting. Force-based cantilevers are however employed as micro-actuators based on the reverse piezoelectric effect. A small voltage can induce a large tip deflection and have been proven very useful for micro and nano positioning in micro manufacturing and inside vacuum chambers of high-resolution microscopes. Although cantilevers have several negative drawbacks, they have been demonstrated as effective in generating enough useful energy to power wireless devices.

Cantilevers have been demonstrated extensively in research as being effective in harvesting vibrational energy via the piezoelectric effect. The most common method is to add a seismic mass to the end of the cantilever. When exposed to a certain frequency, this mass will vibrate causing the entire cantilever to vibrate in a flexural mode generating an electric charge. The main drawback to this method is that the device operates in the d_{31} mode which will produce less charge than the d_{33} mode by ~40-50% [24].

Roundy et al. demonstrated a PZT bimorph cantilever that generated a power density of 70μW/cm^3. In 2004 they optimized their device to generate a power density of 375μW/cm^3 from an induced vibration with a frequency of 120Hz and an acceleration amplitude of 2.5m/s^2 [25].

In late 2009, Zhu et al. published results of their experiments validating the electric output of a multi-layer vibrational energy harvesting system. This system was a bimorph cantilever with a relatively large seismic mass and was limited to a volume of approximately 1cm^3. Their prototype consisted of a brass center layer with a PZT-5H top and bottom layer coated with a thin nickel electrode, at the end of which a large tungsten mass was fixed. This device was connected to a purely resistive load and subjected to a vibration via an electromagnetic shaker. The power output of the device was found to be a maximum of 370 μW at 15.5 V subjected to a frequency of 87 Hz and an acceleration amplitude of 0.23 g, connected to a 325 kΩ resistive load. This device has since "set the bar" for cantilever based devices harvesting vibrational energy due to the extremely favorable power output for powering wireless and small electronics [26].

One rare experiment was completed by Jeon et al in 2005 demonstrating a d_{33} mode cantilever device with interdigitated electrodes. The fabrication of this device is complex and will not be covered in this report, although a SEM photograph of their device is shown below in Figure 4.5.2.1. This group demonstrated a device with three resonant modes; two bending and one torsion. The diversity of having more than one resonant mode allowed the group to harvest energy at three different frequencies (13.9, 21.9 and 48.5 kHZ). The device created consisted of a 170μm x 260μm PZT beam which was capable of generating 1 μW of continuous power to a 5.2MΩ resistive load at 2.4Vdc. This would be equivalent to 0.74 mWh/cm^2 which is comparable to lithium ion batteries [27]. This research demonstrates again the use of vibrational-based energy harvesting for low power, micro, wireless electronics.

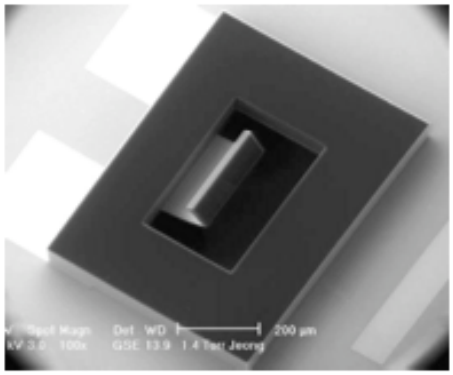

Figure 4.5.2.1: SEM of a cantilever based vibrational harvesting system. [27]

Although several research groups have demonstrated the ability to successfully harvest vibrational energy, implementation of a vibration-based device for the intended result of this research remains unknown. In-situ application of a vibrational based harvesting in asphalt or concrete would be difficult as the harvester would need to be hermetically sealed as well as subjected to an acceleration amplitude which would both be difficult to achieve. The amount of power generated through these devices makes them desirable for this application but the significant difficulties in placing them in-situ make a vibrational based or a d-31 mode device unfavorable compared to a d-33 device. Another difficulty in utilizing a vibrational device for power wireless sensors is the constant vibration source required. In order to provide a constant power supply to a wireless device, an uninterrupted vibration source must be present, which in the current research environment is not. Without a constant vibration source, the harvesting device will not be able to provide an uninterrupted power supply as it will only harvest energy when vibrations are present.

4.5.3 Diaphragm

Piezoelectric based devices that are created in a diaphragm shape are rare to find. Typically, diaphragm based devices are used as a pressure sensor. Although rare, there are a few groups utilizing a diaphragm shape, as an energy harvesting device. The rarity of diaphragm devices is due to the significant electrode effect that is present in a diaphragm. When an electrode is coated on the top and bottom of a piezoelectric

diaphragm, the edges are clamped and usually undergo different stresses in the inner and outer regions. When a force is applied to a diaphragm, the inner region expands while the outer region compresses. This stress distribution significantly decreases the energy generation of the device [14].

A research program conducted by NASA, explored the effects of temperature on energy harvesting using piezoelectric diaphragms. This research used a PZT-5A unimorph diaphragm to convert vibrational energy into electrical energy. They varied the temperature, pressure, frequency and load resistance to investigate the effects. The results demonstrated that the maximum DC voltage and power were found to be 108V and 11641μW at 20^{o}C, 275.8kPa, 2.5Hz and 2MΩ. The highest power density was evaluated at 15μWh/mm^{3}. The diaphragm used in the experiment was 66mm in diameter and .68 mm thick with a weight of 14.5 g [28].

4.5.4 Summary of Piezoelectric generators

Piezoelectric generators are designed based on their size constraints as well as the mode of operation and the required power generation. Below, in Table 4.5.4.1, is a comparison of current piezoelectric generator systems based on the mode of loading, the power density and volume of the device.

Table 4.5.4.1: Comparison of current piezoelectric generators based on mode, volume and power.

Device Mode	Volume (mm^3)	Power (μW)	Power Density (mW/cm^3)	Reference
d_{31} Cantilever	3.8	0.038	10	[44]
d_{33} Cantilever	0.027	1.01	-	[27]
d31 Cantilever	0.1992	2.16	-	[45]
d_{33} compressive loading	-	-	$12mW/cm^3$	[33]
d_{33} compressive load	500μmx90mmx70mm	2.4	0.76μW	[33]
d_{31} bimorph	-	1.3mW	-	[33]
d_{31}bimorph	-	10.2mW	1.42	[33]
d_{31} cantilever	125	2.1	16.8	[46]
d31 cantilever	1000	210	0.21μW	[25]
d31 cantilever	3.75	1.13	0.3013 μW	[47]
d33 compressive loading	-	3	-	[18]
d33 compressive loading	24000	2mW	0.08333	[19]
d33 compressive loading	-	52mW	44	[23]
d31 cantilever	1000	370	.370	[26]

4.6 Piezoelectric Material Comparison

When designing a piezoelectric energy generator, there exists a wide range of materials that exhibit piezoelectricity; the choice on which type of material to use can become overwhelming. This section compares different materials based on their piezoelectric properties, material specific properties, uses, availability and cost.

Although there are 20 crystal systems that exhibit piezoelectric properties, the most common used are single crystal, wurtzite and perovskite crystal structure. Common wurtzite crystal structure materials are aluminum nitride (AlN) and zinc oxide (ZnO). The most common perovskite structure material is lead zirconate titanate (PZT).

4.6.1 Single Crystal

Single crystal materials are a solid body in which the crystal lattice is continuous and unbroken with no grain boundaries. This is significantly important because grain boundaries affect the electrical properties of the material. Single crystals are anisotropic and can possess different properties depending on the direction the material is cut. Both ferroelectric and nonferroelectric single crystals exhibit piezoelectricity; although ferroelectrics are know to have higher piezoelectric coefficients. The most important and popular single crystal piezoelectric material is quartz, (crystalline SiO_2) followed by lithium niobate ($LiNbO_3$) and lithium tantalite ($LiTaO_3$). Single crystal piezoelectric materials have slowly been replaced by lead based materials due to the higher piezoelectric generation coefficients found in Pb based materials. As well, a single crystal material's piezoelectric properties rapidly decrease over several hundred cycles yielding a shorter lifetime than their ceramic and lead based counterparts. For an energy harvesting system, lifetime is an important quality and utilizing a material with a short lifetime, or a rapidly degrading lifetime is not an ideal choice. Developments in new classes of piezoelectric materials have made quartz and single crystal materials almost obsolete in the field of piezoelectricity.

4.6.1.1 Quartz (SiO_2)

Quartz exhibits two distinct phases separated by its Curie temperature at 573^{o}C; known as the α-phase and β-phase. α-phase quartz belongs to the triclinic crystal system and exhibits piezoelectricity whereas the β-phase is non piezoelectric. [30]

Quartz was one of the most widely used materials for piezoelectricity until recent developments in the field have yielded materials with better piezoelectric properties than quartz. Quartz single crystal has since been replaced with the use of ceramics due to the increase in piezoelectric potential of the material. Piezoceramics have a large charge coefficient; some more than two orders of magnitude higher than quartz. The fabrication of quartz is an expensive process and the low piezoelectric properties compared to alternative materials have led to a significant decline in the use for piezoelectric applications.

4.6.2 Ceramics

Piezoelectric ceramics or more commonly piezoceramics are widely used in piezoelectric actuators, sensors, transducers and power generators. Most ceramics that exhibit piezoelectricity are a perovskite crystal structure, with a generic formula ABO_3. The general formula ABO_3 demonstrates a piezoelectric ceramic made of an oxide containing corner-sharing octahedral O^{2-} ions. In the formula, A = Na, K, Rb, Ca, Sr, Ba, Pb, etc. and B=Ti, Sn, Zr, Nb, Ta or W. The ideal perovskite structure, shown in Figure 4.6.2 below, consists of a simple cubic unit cell with a cation A in the corner, a small cation B in the center and oxygens in the center of the faces [31].

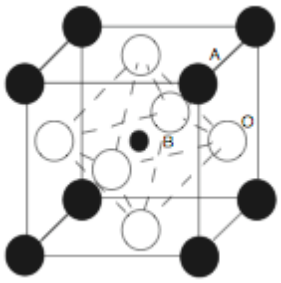

Figure 4.6.2.1: Simple cubic unit cell demonstrating perovskite structure ABO_3 [30]

Perovskite ceramics have the ability to be tailored to certain applications by the incorporation of various cations in the crystal structure; thus altering its physical and electrical properties. One of the most studied perovskite ceramics is barium titanate ($BaTiO_3$).

Ceramic materials have their definite advantages in the area of energy harvesting. But, due to their brittle nature, cannot be used for a high impact, high magnitude force application, such as the intended application. Ceramic based materials tend to have the highest application in vibration based systems as well as low magnitude force applications.

4.6.2.1 Barium Titanate ($BaTiO_3$)

Barium Titanate ($BaTiO_3$) was discovered in 1940 and was the first piezoceramics ever developed. Its use today includes applications such as microphones and transducers but is also sometimes utilized as a dielectric material in ceramic capacitors. [32]

Barium titanate has a Curie temperature between 120-130^{o}C exhibiting 3 distinct phases throughout the range of temperature. The only non-piezoelectric phase is the cubic phase where the center of positive charge (Ba^{2+} and Ti^{4+}) coincides with the center of negative charge (O^{2-}) yielding a neutral net charge. The piezoelectric coefficients are relatively high with d_{15}=270 pC/N and d_{33}=190 pC/N with a coupling coefficient of approximately 0.5 [30]. The high dielectric constant of $BaTiO_3$ makes this material widely used as a capacitor.

4.6.2.2 Lead Zirconate Titanate (PZT)

Lead Zirconate Titanate (PZT) ceramics, are becoming one of the most popular piezo-materials due to the extremely high piezoelectric properties. PZT is a binary solution of $PbZrO_3$ and $PbTiO_3$, which exhibits a perovskite structure. PZT has the ability to be doped as well as easy poling and a large enhancement of piezoelectric properties by altering its composition. There are several varieties of PZT available from suppliers worldwide depending on the type of application and the desired piezoelectric properties. PZT-4 is a “hard” ceramic and is doped with acceptor ions such as K^+ or Na^+. Doping PZT with these materials creates a ceramic that is harder to pole and de-pole resulting in lower piezoelectric properties. PZT-5 or PZT-5H is a soft ceramic, which has been doped

with La^{3+} donor ions. This creates a piezo-ceramic with significantly enhanced piezoelectric properties [31]. PZT-4 has a d_{33} value of 289 pC/N whereas PZT-5H has a d_{33} value of 593 pC/N; demonstrating the significant effect of doping and property enhancement.

Although PZT exhibits exceptional piezoelectric properties and the ability to generate a large electric field under stress, there are several drawbacks of this material when determining its suitability for a certain application. One of the main components in PZT is lead; a known toxic material and a hazard to the environment. Applications where a PZT-based device will be implemented into the environment for an extended period makes PZT an unacceptable choice due to environmental/government regulations and ethical/moral obligations. Also, an application where a high impact force occurs also restricts the use of PZT due to its brittle nature.

4.6.3 Polymers

Some piezoelectric generator designs pose strict material restrictions and have lead to the study of utilizing polymers that exhibit the piezoelectric effect. Most polymers do not, in their unaltered state, exhibit this effect, but after alteration, can exhibit the piezoelectric effect. The alteration method used to achieve this effect is poling or corona poling; this method is explained in Section 3.2.

The most popular polymer that exhibits the piezoelectric effect is polyvinylidene fluoride (PVDF) followed by a parylene polymer.

4.6.3.1 Polyvinylidene fluoride (PVDF)

PVDF is a unique polymer comprised of a repeating unit of CH_2-CF_2 that can exhibit piezoelectric properties after poling. The poling of PVDF aligns the CF_2 dipole moments along the backbone of the polymer; this is demonstrated in Section 5.2. PVDF can be altered to have a low modulus of elasticity creating a flexible polymer that is sensitive to stress yet still mechanically strong.

Semi-crystalline PVDF has two distinct phases, α and β and the separate phases are achieved by stretching and poling. The α phase is a non-polar, thermodynamically stable phase of the polymer, which demonstrates random ordering of the molecular

structure. After stretching and poling, the molecular structure is arranged in a way that aligns the dipoles, creating a piezoelectric polymer with efficient ferroelectric properties. Several research groups have demonstrated PVDF effective as an energy generator. With a piezoelectric coefficient of 30 pC/N, after coating with electrodes, a modest amount of useable electrical power can be generated.

The temperature dependance of PVDF is shown below in Figure 4.6.3.1.1.

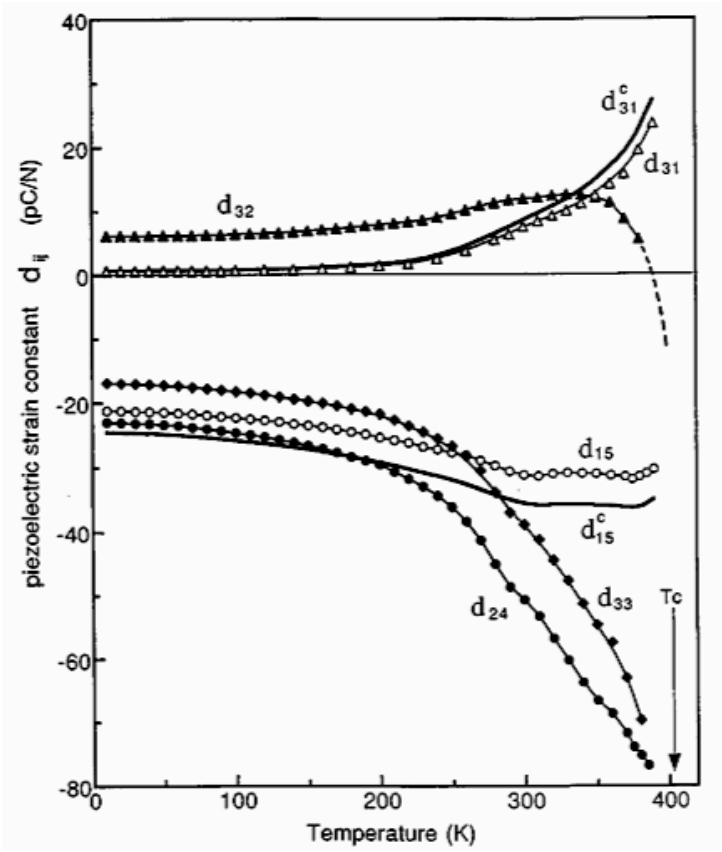

Figure 4.6.3.1.1: Temperature dependence of PVDF [156]

Shown in Figure 4.6.3.1.1 is the relationship of the piezoelectric coefficients of PVDF with varying temperature; the main coefficient of concern is the d_{33} coefficient. As seen in the Figure above, at room temperature (288 K) the d_{33} coefficient corresponds to 33 pC/N. As the temperature increases from room temperature upwards to 320 K there is a 30 % increase in the piezoelectric coefficient corresponding to a 30% increase in the charge produced by the film at that temperature. The same can be seen as the temperature decreases; at -40 ^{o} C or 233 K, the coefficient is approximately 20 pC/N. Interpolation of the above graph shows that this film will perform within the expected parameters for

electrical generation at a large range of temperatures with only a 20-30% change in generation potential. The results of this indicate that PVDF is an ideal candidate for use as a piezoelectric energy generator in varying harsh outdoor temperatures.

4.6.3.2 Parylene Electret

An electret is insulating material that demonstrates a net electrical charge or dipole moment [33]. Parylene, known chemically as poly(p-xylylene), is a unique transparent polymer that has recently been used as a power generation polymer. Parylene is created by room temperature chemical vapor deposition and corona poled to achieve a surface charge density of 3.69mC/m^2. The advantages of this polymer are that it is CMOS and MEMS compatible and easily fabricated. The use of the polymer has mainly been in biomedical coatings and microelectronics due to its chemical inertness as well as excellent barrier properties. As a vibration based harvester, a group recently achieved a power generation of 17.98 μW, obtained at 50 Hz with an external load of 80 MΩ [33]. When compared to PVDF this material is not as effective as a compressive based harvesting material nor is it as mechanically strong.

4.6.4 Thin Films

The typical structure for a piezoelectric thin film is a wurtzite crystal structure. Although many types of materials can be deposited in thin films, wurtzite structures are the most popular. The two most common thin films with a wurtzite structure are AlN (aluminum nitride) and ZnO (Zinc Oxide). Being a wurtzite structure, means the polarization (and therefore the piezoelectric response) lies in the $[0001]_{hexagonal}$ direction.

Neither AlN or ZnO exhibit ferroelectricity, as such, in order to obtain material with homogenous nucleation of grains, special processes must be used. ZnO is typically used as a bulk acoustic and SAW devices [31], whereas AlN is more suitable for sensor applications. In the case of transducers or actuators, ferroelectric films are more appropriate; especially in piezoelectric energy generators.

Thin film piezoelectric materials are gaining large amounts of interest in the energy-harvesting world. Thin films have the advantage of being applied in places where bulk ceramics cannot. Another advantage of thin films is the fact that their thickness is

under 100μm so their presence in an environment is only as noticeable as a coat of paint. In the case of wireless sensors, the thin film can also act as the interface to the environment; this can be extremely beneficial as the thin film can be large, yielding a large area of applied force.

4.6.5 Piezoelectric Properties of Common Materials

Table 4.6.5.1: Common Piezoelectric materials and their properties [21,22, 30,31,32]

Property	Quartz	PZT-5H	PZT-4	$PbTiO_3$	PVDF	$BaTiO_3$
d_{33} ($x10^{-12}$C/N)	2.3	593	289-374*	65	33	149
d_{31} ($x10^{-12}$C/N)	2.3	-274	-171	-	23	78
k_{33}	-	0.75	0.71	-	0.15	0.48
k_{31}	-	0.39	0.31-0.44*	-	0.12	0.21
ε_{33}	5	3400	1300-1700*	175	6-12*	1700
T_C(^{o}C)	-	193	328	355	-	120

* Value is dependant upon source used.

5.0 STORAGE AND MODULATION OF PIEZOELECTRICALLY GENERATED ENERGY

Energy storage and modulation is an integral component of a piezoelectric energy generator. Typically, the energy generated by a piezoelectric device cannot be directly used to power electronics because the power generated is of high voltage and low current. Also, the voltage generated is a fluctuating voltage not a regulated voltage; therefore a conversion/regulating circuit must be used. In the current research storage is necessary due to the time structure of the supply and demand of the micro system.

When investigating the use of harvested energy to power micro-electronics and telemetry circuits, it has been found in literature that, to be useful, the energy must be stored rather than used directly. The amount of useful energy generated by a piezoelectric generator is not typically sufficient to power a device and therefore must be accumulated in a storage device or used to charge a battery.

5.1 Energy Storage

Energy storage is a rapidly expanding field of research due to the high demand for efficient, high capacity, long life storage systems. A typical electrical device requires a constant supply of electrical energy so that the device can withdraw electrical energy exactly when needed. Without constant power access, such as in a harvesting system, a device must have a powerful storage device to balance the time structures of harvesting the energy (supply) and consumption by the device (demand). In storage systems, the storage device must be recharged or replaced periodically which is expensive and sometimes, in some cases of in-situ devices, not feasible. A storage device is specified in terms of the amount of energy it can store (W h), the maximum power (W), as well as size, weight, cost, and lifetime.

There are several options available for energy storage devices, the most popular being a battery.

5.1.1 Batteries

Batteries are an ideal choice for many wireless applications as the size to energy storage ratio is quite high. Batteries, for their size and weight, can store large amounts of

electrical energy with power levels suitable for electronics. The drawback to batteries is the life cycle; the life cycle of a battery is the number of times it can be charged and discharged while still retaining its storage capacity.

The two main types of standard batteries are primary (disposable) and secondary (rechargeable). These types of batteries are "off-the-shelf" batteries and used in almost every electronic device that requires a portable power source. Primary batteries are not an ideal choice as once depleted, they need to be replaced and cannot, once depleted, be recharged. Secondary batteries, on the other hand, can be recharged once depleted. This seems to be an attractive option, although, the limited technology of secondary batteries limits the cycle life. A secondary battery will lose 10% of its charge within 24 hours and continue to discharge at about 10% for every month after [33].

Newer types of batteries are being developed which have a longer cycle life and a higher energy storage capacity. Lithium-ion (Li-ion) batteries as well as thin film batteries are currently the strongest choice for battery based portable power sources.

Table 5.1.1.1 is a comparison of primary (a) and secondary (b) batteries based on their composition, energy density and nominal voltage [33].

Table 5.1.1.1: Primary and secondary battery comparison [33]

	Anode	Cathode	Electrolyte	Nominal voltage (V)	Energy density (W h l^{-1})	Specific energy (W h kg^{-1})	Shapes
Zinc/air	Zn	O_2	KOH (aqueous solution)	1.5	1270–1560	370–490	Button
Li/SO_2	Li	SO_2	Organic solvent, salt solution	2.85–3.0	313–498	160–307	Cylindrical
$Li/SOCl_2$	Li	$SOCl_2$	$SOCl_2$ w/$AlCl_4$	3.6	715–1100	380–537	Cylindrical, spirally wound, prismatic
Li/MnO_2	Li	MnO_2	Organic solvent, salt solution	3.0	371–789	129–343	Button, cylindrical, thin film and rectangular
Li/FeS_2	Li	FeS_2	Organic solvent, salt solution	1.5	487–540	247–310	Cylindrical
Li/I_2	Li	I_2 (P2VP)	Solid	2.8	820–1030	220–280	Button
Zn/Ag_2O	Zn	Ag_2O	KOH or NaOH (aqueous solution)	1.5	207–543	56–137	Button
			(b)				
Zinc/silver oxide	Zn	AgO	KOH (aqueous solution)	1.5	180	105	Prismatic
Nickel metal hydride	MH	NiOOH	KOH (aqueous solution)	1.2	53–360	41–100	Cylindrical, button, prismatic
Rechargeable primary Zn/MnO_2	Zn	MnO_2	KOH (aqueous solution)	1.5	210–458	51–150	cylindrical
Lithium ion	C	$LiCoO_2$	Organic solvent	4.0	200–450	61–200	Cylindrical and prismatic
Lithium-polymer	C	$LiFePO_4$	Organic solvent	3.2	160–217	74–91	Prismatic

A micro-battery fabrication and distribution company, Varta, markets several batteries prevalent in MEMS devices. The batteries range in size, shape and energy storage capacities. The “button” style Nickel-Metal-Hydride (NiMH) batteries are an appealing option for MEMS devices with size constraints although their nominal voltage is limited at 1.5V with capacities ranging from 16-600 milli-amp-hour (mAh). A milli-amp-hour is a measure of a batteries capacity. To illustrate this unit, if a 40 mAh battery is discharged at a 40 mA current, the battery will last 1 hr.

Their lithium polymer batteries have a nominal voltage of 3.7V with capacities ranging from 150-1880 mAh (http://www.varta-microbattery.com). Although these batteries are a desirable choice for thin micro systems with a small footprint, the lifetime of a secondary battery requires periodic replacement due to decreased storage capacity caused by cycling the device. Replacement of a battery would require de-installation of the device, replacement, and re-installation making this option far from desirable.

Recently, many designs exceed the capability of batteries due to high pulse energy requirements, or in the case of MEMS devices, size constraints. Traditionally,

capacitors were used to supply, high pulses of energy, but these devices could not supply the power required, leading to the development of high energy density capacitors (ultracapacitors or electrochemical capacitors).

5.1.2 Capacitors

A capacitor is an energy storage device which stores energy by charge separation; energy is stored in a thin layer of dielectric material that is supported by metal plates acting as terminals for the device. The metal plates on a capacitor are necessary for holding the separated charges. Ultracapacitors are a unique device developed to address the issues/drawbacks of conventional batteries. These devices have a higher power capability, as well as long shelf and cycle life. Ultracapacitors (or electrochemical capacitors) differs from a standard capacitor in its construction; an ultracapacitor is constructed much like a battery. These devices have two electrodes separated by a distance (the same as a standard capacitor) but like a battery are submerged in an electrolyte fluid. The electrodes in an ultracapacitor are different from those in a battery, or even a standard capacitor in that they are a porous material with an extremely high surface area. The surface area used in ultracapacitors is orders of magnitude higher than in batteries [34].

The method of storage in an ultracapacitor is due to the unique physical properties of the electrode materials. The porosity of an electrode material is unique in that it has pores that have a diameter on the order of nm. The charge is stored in these nm-sized pores at the solid electrode material and electrolyte interface. The benefit in this type of charge storage is the extremely short recharge times compared to batteries; an ultracapacitor can be recharged in seconds or fractions of a second. Ultracapacitors, like secondary batteries, will self-discharge over a period of time of low-voltage, but unlike secondary batteries, ultracapacitors are able to recharge to their original condition. Testing has shown that an ultracapacitor can be deep cycled (charged and discharged in seconds) 500,000-1,000,000 times with only a small change in their capacitance and resistance [35]. This means, the lifetime of an ultracapacitor is ideal for an in-situ MEMS device, as well as the discharge/recharge rate and power density matching the constraints needed for wireless MEMS devices.

Andrew Burke compiled a table of small ultracapacitors and their electrical characteristics; this is shown in Table 5.1.2.1.

Table 5.1.2.1: Small ultracapacitors and their characteristics [34]

Device	Voltage (V)	Capacity (F)	Resistance (mΩ)	RC (s)	W h/kg	(W/kg) (95% efficiency)	Weight (g)
Superfarad	1.4	114	20	2.3	2.5	324	8.5
Maxwell	3	10	100	1.0	1.75	444	6.6
PowerStor	3	2.5	40	0.1	0.57	1150	5.5
Cap xx	3	120	26	3.1	5.8	374	26
Cap xx	3	30	7.4	0.22	1.5	1368	25
Cap xx	3	10	8.1	0.08	0.74	1838	17

7.2 Voltage Conversion Circuits

The electrical energy generated by a piezoelectric device is not suitable for directly powering MEMS devices or portable electronics, as it is typically a very high voltage and low current. This is due to the extremely high impedance of piezoelectric materials. To overcome this, modulation circuits are utilized to "step-down" the high voltage to a low-voltage high current source. Several research groups have dedicated their studies to achieve efficient step down converters.

Piezoelectric generators need a voltage conversion circuit capable of converting the high voltage (>100V) produced by the piezoelectric device to a voltage suitable for electronics (3-5V). These circuits, depending on the components used can be very inefficient, especially when using a microsystem. Maxim IC, has a commercially available buck converter that has less than a 10% efficiency when operating at a high conversion ratio and 10mW power level [35].

Shenck and Paradiso developed a conversion circuit for use in their shoe mounted piezoelectrics that had an efficiency of 17.6% when converting from 200V to 4-5V [36]. These researchers demonstrated that an increase in efficiency was definitely needed in order to successfully utilize piezoelectric energy generators for powering microelectronics via energy scavenging.

There exists a number of voltage converters and buck converters in research trying to increase the efficiency but recently, a development in the field by Kajaakari and

Han has led to the new type of circuitry. Kajaakari and Han developed a high efficiency capacitive converter with a theoretical efficiency of 70% [19]. The converter operates in two phases: phase 1, there are N capacitors connected in series with the high voltage supply, V_1. The second phase has the capacitors connected in parallel to a load V_2. The theoretical efficieny as described by Han and Kajaakari is:

$$\eta = N\frac{V_2}{V_1} \qquad \text{(Equation 5.2.1)}$$

Where:

N = the number of switched capacitors

V_1 = high voltage supply

V_2 = load V_2

The operation of this converter is shown in Figure 5.2.1 below. By charging and discharging the capacitors in two different phases (series and parallel respectively) a dramatic increase in efficiency can be achieved.

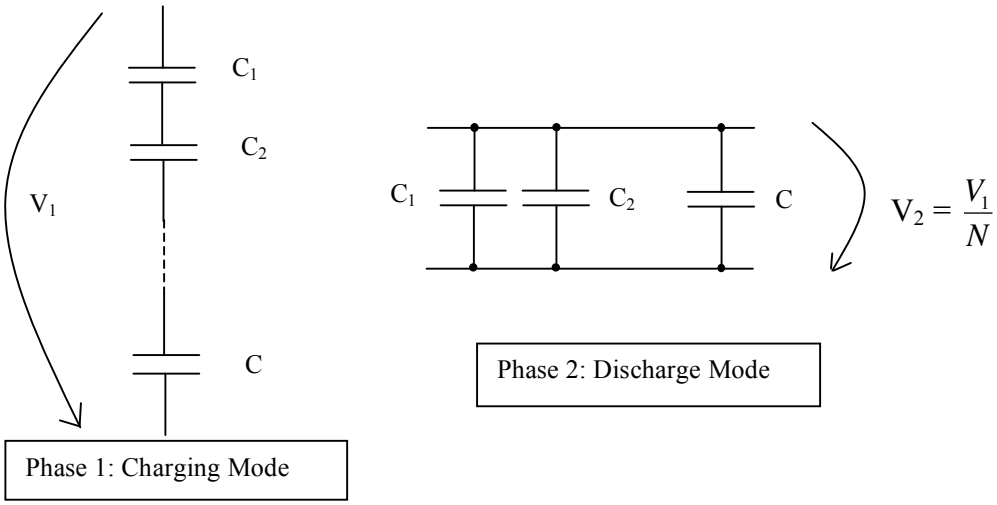

Figure 5.2.1: Schematic representation of the two phase mode of Kajaakari and Han's voltage conversion circuit.

This voltage conversion circuit is unique in that the optimal load voltage, yielding an optimum efficiency, can be tailored by adjusting the number of converter capacitors

(N). The theoretical framework, as demonstrated above, combined with control logic and voltage detection is shown below in Figure 5.2.2.

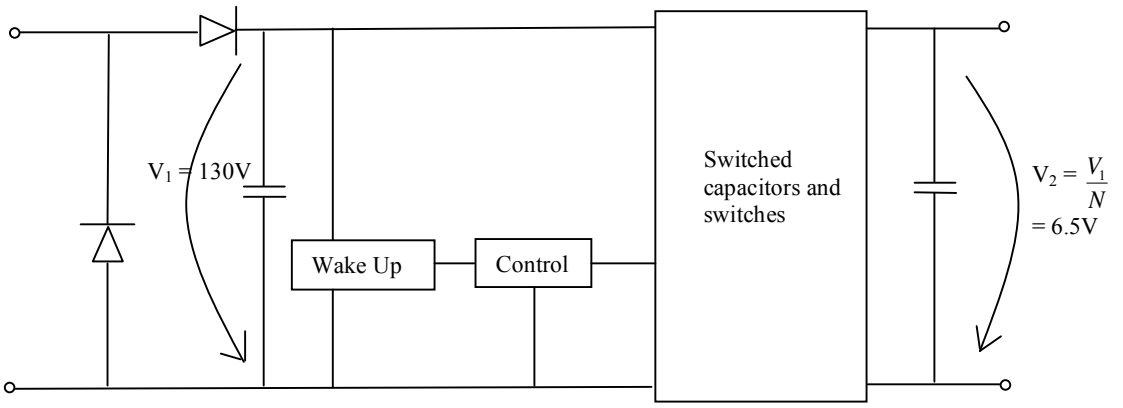

Figure 5.2.2: System level schematic of Kajaakari and Han's converter circuit

The combination of voltage detection and switches can increase the efficiency and decrease the losses from switching. The voltage detection will sense when the voltage is below 130V and switch the converter off. The wake-up detection will activate the switched capacitor converter when the transducer voltage reaches 130V. The wake-up detection circuit consumes 30nW when operated below the wake-up threshold. When the converter is operating, the control circuit power consumption is less than 01.mW combined with the wake-up circuit. This conversion circuit, with dimensions of 3cm x 3cm x 3.5mm is self-generating with no other voltage sources needed besides the transducer [19]. Although this conversion circuit has been proven for their application, in the case of this research, the voltage produced is low, and this circuit too complex for use in a simple, cost-effective system. For directly charging a capacitor or battery a complex system is not necessary.

5.2.1 Voltage Conversion for Charging a NiMH Battery

If a battery is used rather than a direct power source to the electronic system, a complex circuit is not necessary, as demonstrated by Henry Sodano [37]. Their research tested three different piezoelectric devices with the purpose of charging a nickel metal

hyrdride (NiMH) battery. Different battery sizes were used ranging from 40 to 1000 milli-amp hour (mAh).

Their results demonstrated that a PZT piezoelectric device could successfully charge a battery, with a 40mAh battery being charged in approximately an hour, while a 1000mAh battery was charged in around 22 hours. The other piezoelectric device tested, Quickpack ®, successfully charged the batteries as well. The Quickpack did not charge as fast as the PZT device, with the charge time being around double that of the PZT.

Sodano illustrates that a nickel metal hydride battery has a high charge density, and does not require a charge controller or voltage regulator, unlike their lithium-ion counterparts. To charge these batteries, a simple full wave rectifier circuit is connected to a capacitor and the battery. This is illustrated in Figure 5.2.3.

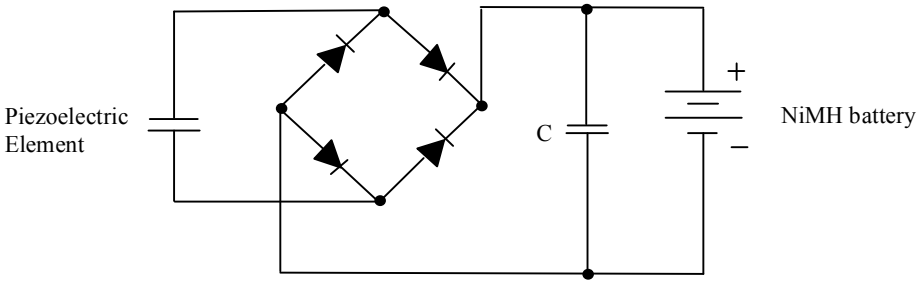

Figure 5.2.3: Sodano's schematic of the battery charging circuit [37]

The benefit of using a battery instead of a capacitor is a significantly decreased circuit complexity; this yields less power consumption by the circuit itself. The drawbacks of a battery are the size, and life cycle. The life cycle of a battery is the main drawback and reason for selecting a capacitor as the storage device for use in this research. Emerging technologies for capacitors are being brought to market everyday, yielding storage units that far exceed batteries.

5.2.2 Capacitor Chargi\ng

When utilizing a capacitor for energy storage, a voltage regulator is needed which complicates the circuitry and increases the power dissipation of the circuit itself. This is the main drawback of a capacitor, as well as being able to only supply short bursts of power. This is typically a problem in many applications, as a short burst of power during

the discharge phase is rarely long enough to power a system. The benefits are the short charge time (t<1s) and the dramatically increased life cycle of 500,000 to 1,000,000 cycles. In the current research application however, the power required for by the micro system is of short enough duration that it can be achieved by a burst discharge from a capacitor.

After an extensive literature review was completed, it was found that there are two common circuits for charging a capacitor using a piezoelectric material. The first is for very high voltage applications (V>100 volts); utilizing a transformer whose impedance matches that of the piezoelectric element. The second, for use in applications where the piezoelectric material produces lower voltages (V<100 volts) and does not require the transformer to convert the extremely high voltage to a lower voltage.

The main component in both of these circuits is a full-bridge-rectifier, also known as a diode bridge. A full bridge rectifier is one of many options available; other options are discussed in Section 7.0. A bridge rectifier provides the same polarity of output for either polarity of input. A full wave, or bridge rectifier is shown below in Figure 5.2.2.1.

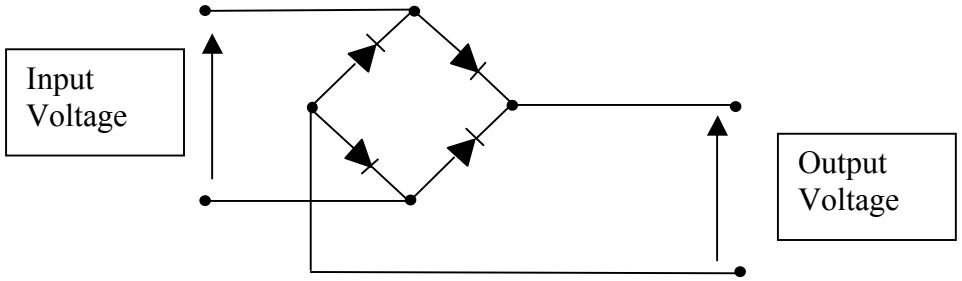

Figure 5.2.2.1: Full-bridge-wave rectifier

When utilizing a full bridge rectifier, both polarities of input are “rectified” or converted to a positive polarity and transferred to a storage capacitor, charging the capacitor in a step-wise fashion.

When modeling the circuit, the piezoelectric element is modeled as a voltage source in series with a capacitor, with a capacitance equal to the capacitance value of the

piezoelectric element. The complete, proposed circuit is shown in Figure 5.2.2.2 below; note that this circuit only contains the harvesting circuit or “front-end”. This circuit layout has been demonstrated as efficient for powering small electronics such as RF transmitters.

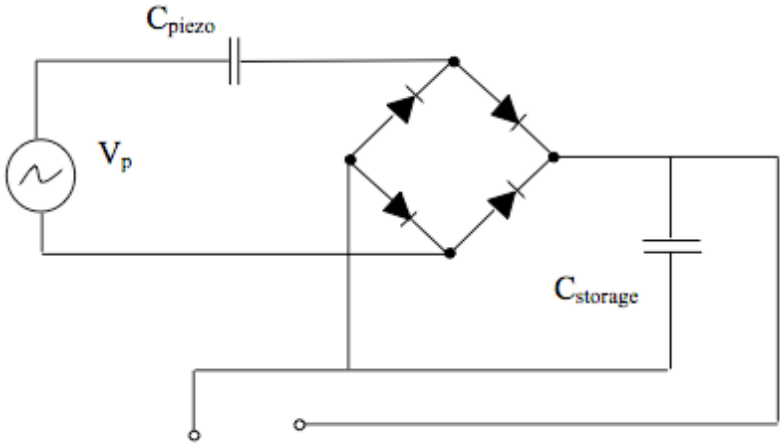

Figure 5.2.2.2: Piezoelectric Energy Harvesting Circuit

6.0 WIRELESS DATA TRANSMISSION

In an application of autonomous sensing, there needs to be a method to communicate to the outside world; wireless data transmission. For the application of an autonomous sensor, using a piezoelectric material as the sensing element (Section 4.0), harvesting energy as the power supply for the device (Section 4.5) and stored in a capacitor (Section 5.0) now needs to wirelessly transmit data obtained by the above to the outside world.

Wireless transmission of data is a rapidly expanding field of research as well as in the commercial sector. Commercially available wireless data transmitters and receivers are typically large devices with large antennas and rectenna (rectifying antenna). Data transmission can be achieved by several means although the most popular are transmission in the MHz range to the GHz range.

Several groups have demonstrated the use of SAW (surface acoustic wave) devices in transmitting data. Other groups focus on the use of RF (radio frequency devices), while others are experimenting with ultrasonic devices. All of these devices have different transmission methods and consequently different transfer distances as well as power budgets.

6.1 Current Technology

Current technology in wireless data transfer is vast and still expanding. From cell phones utilizing a 3G ® network to phone headsets utilizing Bluetooth ®. For the reliable transfer of pressure or temperature data, many groups turn to using RF, while others maintain that SAW devices are more effective.

In late 2006, Keekun Lee et al. published research results on a micro-scale surface acoustic wave, pressure-temperature sensor that operated at the 440MHz frequency. This device consumed 10mW of power which was harvested from a transmission antenna; the data readout was achieved to a distance of 1m. This device, a cavity with reflectors based on RFID tags, converted an incoming RF frequency to a surface acoustic wave. This surface acoustic wave traveled across the substrate and corresponding shifts when passing the temperature and pressure reflectors were transferred into the wave. This wave was then converted back into a radio frequency, exhibiting the corresponding shifts, and

transferred back to the base station via a transmitting antenna. The device demonstrated the feasibility of using surface acoustic waves for sensing and altering the radio frequency signal for wireless transmission of data, as their experimental results agreed with the predicted [38].

Michael Suster et al from the Case Western University in Ohio demonstrated a different approach in using a tunnel-diode-based oscillator transmitter. This LC tuned oscillator utilized a capacitive based pressure sensor with an integrated micro loop as the inductive connection. This micro loop was 2cmx2cm with 2 turns which established a wireless connection with a receiving antenna at a distance of almost 3m. [39]

Another project from Case Western demonstrated the use of a two-channel phase shift keying (PSK) and an amplitude shift keying (LSK) passive telemetry device to achieve the data transmission. This device had a wireless data transmission rate of 5Mbps and 250 kbps using the PSK and LSK respectively. The device achieved successful data transfer with a total device size of 2mm x 2mm x 1.5μm [40].

A group at the University of Massachusetts developed a novel method for data transmission that deviated from the standard transmission frequency domain (MHz-GHz). This device operated via ultrasonic waves in the kHz range due to electromagnetic shielding constraints imposed by the operating environment. This device used electrical charges generated by an energy converter to send pulse signals via an ultrasonic transmitter. These pulses were detected wirelessly and were converted to a specific pressure value by multiplying the number of pulses by the corresponding pressure threshold value. The experimental results agreed with the theoretical and predicted results [41].

6.2 Power Requirements

The power requirements for wireless transmission can vary greatly dependant upon the device as well as the transmission method and transmission environment. For the ability to harvest energy, in order to supply a transmitter with power, the power budget of several devices must first be known.

The 440MHz SAW device in [38] utilized an RF power of 10mW to power their device. This had a transfer distance of around 1m. In [39] a tunnel-diode based oscillator

was used as wireless transmission device based on a pressure to frequency converter and a micro induction loop. This device needed a DC supply voltage of 135mV to bias the diode. The device consumed an average DC current of 0.5mA and a power dissipation of 65μW. In the Case Western experiments utilizing PSK and LSK, the device used a RF to DC converter based on inductive coils operating at 50MHz. This device supplied 2.8V at 2mA which was sufficient to power the device electronics. A biomedical research group demonstrated a wireless pressure sensor surgically implanted in a rat, which wirelessly transmitted its blood pressure data, but only at very small distances (<30cm). This device had an overall power dissipation of 300μW, with their FSK transmitter having a power consumption of 120μA at 2 V. This power was supplied by their RF to DC converter with a power dissipation of 55μW [42]. Thomas van den Boom et al, demonstrated an RF transmitter used in conjunction with a pressure sensor that had reliable data telemetry up to 1 m. This device was overall size of 4.7mm x 3.2 mm x 1.5μm with a total power dissipation of 180μW.

All of these devices, although very promising research, are limited to short transfer distances. The furthest transfer distance, achieved by an LC tuned oscillator, was 3m (9.84ft). Reliable, wireless data transfer is a significant problem for wireless MEMS devices. The power dissipation of these devices is not significant and can be generated by a piezoelectric generator and stored in either a battery or an ultra-capacitor.

Table 6.2.1: Various wireless transfer methods and their operating frequency, power and distance.

Device	Transfer Method	Frequency	Power Dissipated	Distance	Reference
Surface Acoustic Wave	RF to SAW	440MHz	10mW	1m	[38]
LC-tuned oscillator	Micro Induction Loop	50MHz	65μW	3m	[39]
Strain Sensor	RF to DC	50MHz	-	-	[40]
Ultrasonic	Ultrasonic wave conversion	1130-2240kHz	-	-	[41]
Capacitive Blood Sensor	RF to DC converter	433MHz	300μW	30cm	[42]
Pressure Sensor Chip	RFID Carrier Conversion	133kHz	180μW	1m	[43]

7.0 INVESTIGATION OF PIEZO-HARVESTED ENERGY FOR POWERING AN RF MEMS DEVICE

The majority of the research completed was identifying and developing an approach to autonomous sensing. The approach was decided by extensively researching combinations of methods, materials, and systems that could lead to an autonomous sensing system. A secondary portion of research was completed to validate the decisions and conclusions drawn from the primary research objective.

The secondary portion of the research was to design a harvesting and sensing system based on the conclusions drawn from the main research objective. The proposed device is based on the conclusions drawn from an extensive literature review and constraints imposed by the application and environment the micro system is to be employed. Of all the materials studied, piezoelectric materials were objectively decided as the ideal candidate for many reasons. Piezoelectric materials have been used since 1960 as sensing elements; they have also been used as energy harvesters for the last 15 years. This leads to a unique ability to incorporate both the power source and sensing into a single element. No other material or power transfer method could lead to this combination. Harvesting energy from the environment was also chosen rather than wireless transfer due to the requirements for a rectenna and size constraints imposed by the need to conceal the device on the surface of a road.

Harvesting energy by means of a vehicle tire for the purpose of transmitting data about the vehicle meant that the material needed a thin footprint, which would ensure full contact with the incoming object. No piezoelectric material other than a thin film could achieve this. A lead free PVDF was chosen due to environmental concerns of placing a Pb based material onto roadways.

The micro-system designed to determine the feasibility of the above conclusions for the intended application is described below. The following sections were completed in addition to the research explained in Sections 1.0-6.0 to further develop the approach of an autonomous sensor.

The micro-system can be broken down into the four basic components of a miro-electrical-mechanical system: sensor, actuator, signal processing, and interface to the

environment. The idea behind this MEMS device is to integrate the sensor, actuator and interface into a single component, cutting the complexity and costs drastically. The sensor/actuator and interface to the environment will be a thin film (52 μm) sheet of polyvinylidene fluoride (PVDF) with Silver (Ag) metallized electrodes. This material, as explained in Section 4.0 is a piezoelectric polymer, which has been demonstrated as both a sensor and an actuator. By utilizing this material, the force exerted on the material can be measured and a corresponding voltage output can be used to determine the magnitude of the force (sensor). While at the same time, this voltage can be used to charge a storage device. A capacitor will be used to supply power to a micro RF transmitter for the wireless transmission of the sensor data (signal processing/interface to environment).

Since this device is used to measure several hundred kPa's, a typical micro-scale sensor cannot be employed. The area of force exertion as well as the magnitude of force result in a novel application of the thin film for sensing, actuating, and the interface to the environment. A total footprint of the interface to environment will be 0.2032m x 0.1397m x 52μm. This footprint size ensures accurate force distribution, yielding an accurate measurement via the piezoelectric effect as well as adequate electrical power generation. For future applications the film footprint will change, the size studied was an "off-the-shelf" product supplied by MSI Technologies ®.

The following sections describe the theoretical foundation of the device as well as the technical aspects of the harvesting circuitry and explanations of how the device was designed.

7.1 Theoretical Calculation of Electrical Generation

Although a typical MEMS device is only on the order of micrometers, this device will be contain a macro-scale interface to the environment in addition to the micro-portions of the device. This macro-scale portion is necessary to facilitate and ensure a smooth contact with the incoming object needed to be measured. The experimental device is to have a footprint of 20.32 cm (8") long and a width of 13.97 cm (5.5") purely for proof of concept.

The material selected for implementation in the device is a piezoelectric, metallized sheet of PVDF with Silver electrodes supplied by Measurement Specialties

Inc ®. The data sheet is found in Table 7.1.1 and the technical manual for the film can be obtained from MSI ®. The sheet thickness is 52 μm with a total size of 20.32 cm x 13.97cm. The sheet will have leads attached to the electrodes as outlined in the technical manual and explained in Section 7.2.1. The physical and electrical properties are summarized in Table 7.1.1 below.

Table 7.1.1: Datasheet for PVDF Metalized Sheet from MSI ®

Symbol	Parameter		PVDF	Units
t	Thickness		9, 28, 52, 110	μm (micron, 10^{-6})
d_{31}	Piezo Strain Constant		23	10^{-12} $\frac{m/m}{V/m}$ or $\frac{C/m^2}{N/m^2}$
d_{33}			-33	
g_{31}	Piezo Stress constant		216	10^{-3} $\frac{V/m}{N/m^2}$ or $\frac{m/m}{C/m^2}$
g_{33}			-330	
k_{31}	Electromechanical Coupling Factor		12%	
k_t			14%	
C	Capacitance		380 for 28μm	pF/cm^2 @ 1KHz
Y	Young's Modulus		2-4	10^9 N/m^2
V_0	Speed of Sound	stretch:	1.5	10^3 m/s
		thickness:	2.2	
p	Pyroelectric Coefficient		30	10^{-6} C/m^2 °K
ε	Permittivity		106-113	10^{-12} F/m
$\varepsilon/\varepsilon_0$	Relative Permittivity		12-13	
ρ_m	Mass Density		1.78	10^3kg/m
ρ_v	Volume Resistivity		>10^{13}	Ohm meters
$R_\square$	Surface Metallization Resistivity		<3.0	Ohms/square for NiCu
$R_\square$			0.1	Ohms/square for Ag Ink
tan δ_e	Loss Tangent		0.02	@ 1KHz
	Yield Strength		45-55	10^8 N/m^2 (stretch axis)
	Temperature Range		-40 to 80...100	°C
	Water Absorption		<0.02	% H_2O
	Maximum Operating Voltage		750 (30)	V/mil(V/μm), DC, @ 25°C
	Breakdown Voltage		2000 (80)	V/mil(V/μm), DC, @ 25°C

The first step in estimating the electrical generation due to an applied force is a calculation of the force. The force, F_o, is calculated by a contact pressure of 400 kPa evenly applied across the entire area of film. The 400kPa force is the lowest pressure the film will be subjected to; this will be used to determine the amount of useable energy generated in a "worst case" scenario.

Assume:

- force is equal across entire sheet; contact area is equal to sheet size

Area = L x W

Area = .1397m (.2032m)

$$\text{Area} = 0.02839\ m^2$$

Therefore, the force experienced across the sheet,

$$F = A_{sheet} * \text{Pressure}$$

$$F = 0.02839\ m^2\ (400kPa)$$

$$F = 11.35\ kN$$

Now that the force, F_o is known, the generated charge can be calculated according to Equation 4.3.8:

$$Q_{gen} = d_{33} F_o$$

$$Q_{gen} = (33 \times 10^{-12}\ C/N)(11.35k\ N)$$

$$Q_{gen} = 3.75 \times 10^{-7}\ C$$

In order to calculate the voltage this generated charge will produce, the capacitance of the material must be known. The capacitance of the material is a function of its electrical permittivity, the thickness of the film, and the area of the film; related by equation 4.3.9:

$$C = \frac{A\varepsilon_{33}^{T}}{h_p}$$

ε_{33} is the total electrical permittivity related by the relative permittivity and the permittivity of free space as defined in the relationship:

$$\varepsilon_{33}^{T} = \varepsilon_r \varepsilon_o$$

Where:

ε_{33}= electrical permittivity (F/m)

ε_r = relative permittivity, PVDF =12 (unitless)

ε_o = permittivity of free space (8.854 x 10^{-12} F/m)

$$\varepsilon_{33}^{T} = 8.854 \times 10^{-12} \text{F/m (12)}$$

$$\varepsilon_{33}^{T} = 0.106 \times 10^{-9} \text{ F/m}$$

The capacitance is now calculated with the electrical permittivity:

$$C = \frac{A\varepsilon_{33}^{T}}{h_p}$$

$$C = \frac{(0.02839 m^2)(.109 x 10^{-9} F/m)}{52 x 10^{-6} m}$$

$$C = 5.95 \times 10^{-8} \text{ F}$$

The generated voltage can now be calculated using the charge generation divided by the capacitance of the sheet using equation 6.3.10:

$$V_{generated} = \frac{Q_{generated}}{C}$$

$$V_{generated} = \frac{3.75 x 10^{-7} C}{5.95 x 10^{-8} F}$$

$$V_{generated} = 6.30 \text{ V}$$

This value represents the open circuit voltage produced from the lowest load applied. The lowest value load was chosen as the “worst case” scenario. If the lowest value can provide the required energy, then all other larger magnitude loads will provide ample energy. A load of 400 kPa on the film is the smallest magnitude load; the highest value is 900kPa. Table 7.1.2 below shows a range of loads and corresponding theoretical open circuit voltages produced.

Table 7.1.2: Load and Theoretical Open Circuit Voltage Produced for PVDF film

Area (m^2)	Pressure(kPa)	Force (N)	Q gen (C)	Capacitance,Piezo (F)	Voltage
0.02838704	400	11354.82	3.75E-07	5.95E-08	6.30
0.02838704	450	12774.17	4.22E-07	5.95E-08	7.08
0.02838704	500	14193.52	4.68E-07	5.95E-08	7.87
0.02838704	550	15612.87	5.15E-07	5.95E-08	8.66
0.02838704	**600**	**17032.22**	**5.62E-07**	**5.95E-08**	**9.45**
0.02838704	650	18451.58	6.09E-07	5.95E-08	10.23
0.02838704	700	19870.93	6.56E-07	5.95E-08	11.02
0.02838704	750	21290.28	7.03E-07	5.95E-08	11.81
0.02838704	800	22709.63	7.49E-07	5.95E-08	12.60
0.02838704	850	24128.98	7.96E-07	5.95E-08	13.38
0.02838704	900	25548.34	8.43E-07	5.95E-08	14.17

As shown by the bolded section above, corresponding to 600kPa, the expected open circuit voltage is 9.45V. This is the theoretical open circuit voltage expected from an axle impulse by a Ford ® F-150 truck.

The table above represents open circuit voltages produced, which will differ from the voltages produced across a capacitor due to additional losses in the circuitry. The above values are the best possible approximation, as the losses associated with the circuit cannot be accurately estimated. The voltage across a capacitor is a measured value and the losses from the open circuit voltage are dependant upon the circuitry. In the case of the harvesting circuit, the losses associated with the full-wave diode bridge are unknown and cannot accurately be estimated. The energy stored in the capacitor must therefore be measured experimentally.

In order to calculate the actual energy harvested, the energy stored in a capacitor is found by measuring the voltage across it.

The energy stored in a capacitor is defined as:

$$E = \frac{1}{2}CV^2$$

Once the voltages are measured through testing, the energy produced can be calculated.

7.2 Energy Harvesting Device

The overall energy-harvesting device was designed under specific environmental and application constraints. The device, as explained in Section 7.0 utilizes a PVDF thin film connected to an energy harvesting circuit. The PVDF thin film is the piezoelectric element responsible for generating a voltage to be harvested into a useable energy. The energy harvesting circuit, as described in Section 7.2.2 is responsible for converting the piezoelectric voltage input generated by the PVDF film into a useable energy.

7.2.1 PVDF Metallization and Wire Attachment

In order for a charge separation and corresponding voltage to be generated by a piezoelectric element, the material must first be coated with electrodes on opposite sides, perpendicular to the poling direction. These metallized electrodes allow the generated charge to be stored on the surface; similar to how a capacitor stores a charge.

For the PVDF, Silver (Ag) electrodes were deposited by MSI ® through screen-printing. MSI ® can deposit a range of metallized electrodes including; silver, nickel, gold, and copper. In order to deposit nickel, gold or copper electrodes, a sputter deposition is used while with the silver, a screen-printing technique is used.

Sputtered electrodes are a brittle electrode and are used when there are high signal to noise ratio requirements. By using a thin sputtered electrode, there is less mass loading caused by the addition of the sputtered film.

The Silver electrodes are used in situations where high mechanical stress is applied. The screen-printing technique allows for a flexible electrode that can be customized for wire attachments. For the case of the current research, a high mechanical stress is applied and therefore the silver electrodes were deposited to allow flexibility and to gain an increase in mechanical strength of the film. Once deposited, the electrodes need a method to connect to the harvesting circuitry.

28 American Wire Gauge (AWG) wires were affixed to the film as outlined in MSI's ® technical manual. The method is described as using 3M's ® Conductive Copper

Tape to affix wires to the film. The copper tape provides a means to affix wires to the film without damaging the film through the soldering process. Since both the film and electrodes are thin, the heat experienced during soldering directly to the film could destroy both.

This method was first tested on a piece of copper to ensure the connection had negligible loss and good connectivity; the results showed negligible loss and great conductivity.

The wires were soldered to a small piece of copper adhesive tape (1cm x 1 cm), which was, after soldering, adhered to both electrodes of the PVDF film. The wires were soldered to the tape before adhering them to the film to ensure the heat experienced by soldering did not affect the thin silver electrodes. Figure 7.2.1.1 below shows the PVDF film with soldered lead wires.

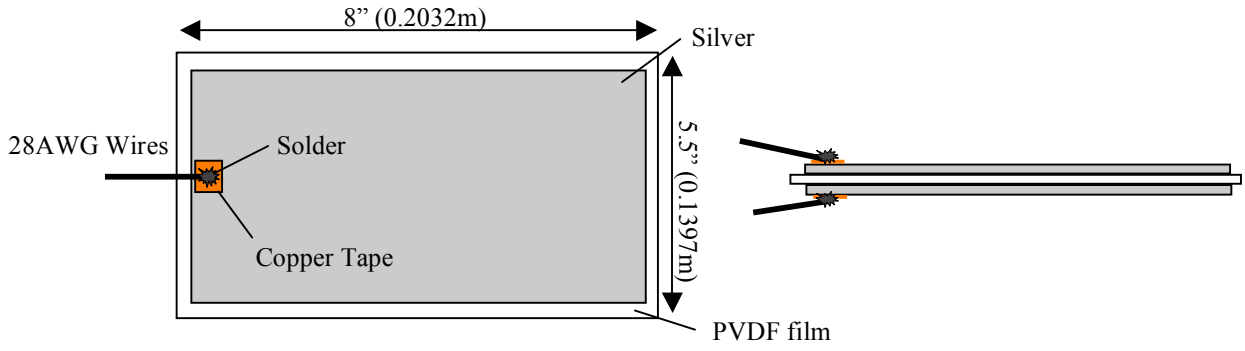

Figure 7.2.1.1: Bonding technique used for the PVDF film wires

7.2.2 Harvesting Circuit

The harvesting circuit is used to convert and store the piezoelectric input from the PVDF film when experiencing a force or stress. A piezoelectric material, as explained in Section 4.0, generates a voltage with alternating polarity. In order to make use of both the positive and negative polarity, the circuit must rectify both polarities into a positive output; this is achieved through a full bridge rectifier.

The full bridge wave rectifier uses simple, glass diodes arranged in a full-bridge. The diodes are used to rectify the positive and negative inputs into a positive output. The diodes are placed in series with a capacitor to store the generated energy. A schematic of the entire energy-harvesting device is shown in Figure 7.2.2.1.

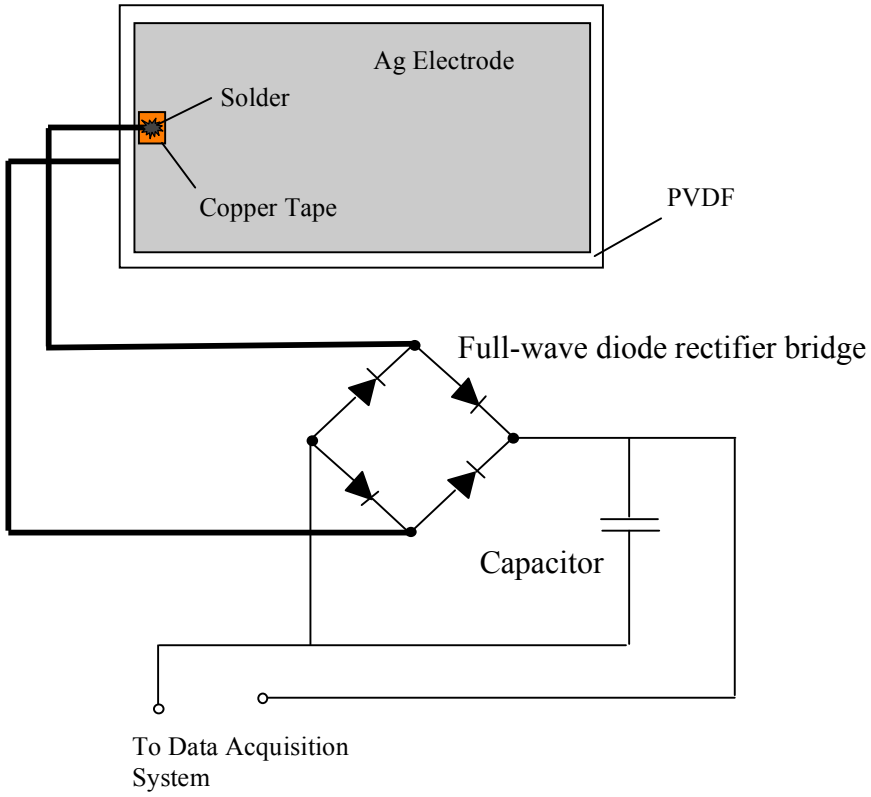

Figure 7.2.2.1: Schematic of Energy Harvesting System

In order to evaluate the circuit, two prototypes were made with different sizes of capacitors. The first circuit uses a 2.2 μF, simple, glass capacitor and the second uses a larger 0.1mF polyester film capacitor.

The two prototypes built are shown below in Figures 7.2.2.2 and 7.2.2.3. Note that the size of these prototypes is magnitudes larger than that which can be achieved using micro-fabrication. A commercially available micro-harvesting circuit from Linear Technologies ® with similar components is shown in Figure 7.2.2.4 to demonstrate the size achievable for the harvesting circuit. A Canadian quarter has been included in the

photographs for size reference. Lastly, in Figure 7.2.2.5 all three energy harvesting circuits are demonstrated for size reference.

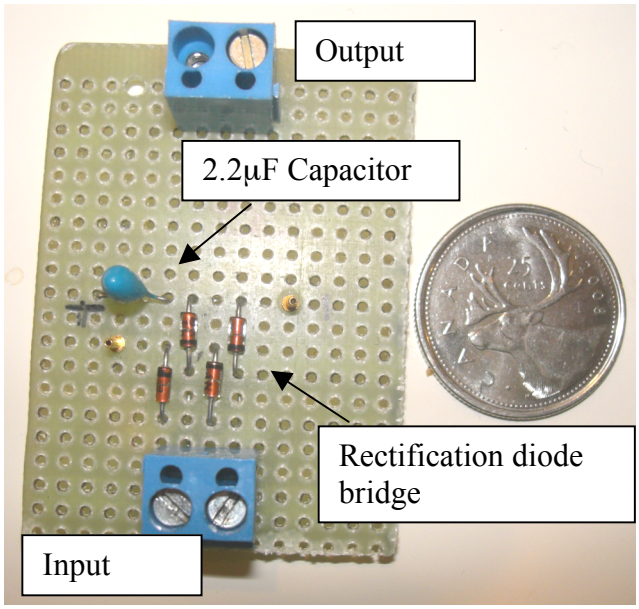

Figure 7.2.2.2: Prototype # 1 Energy Harvesting Circuit (Quarter as size reference)

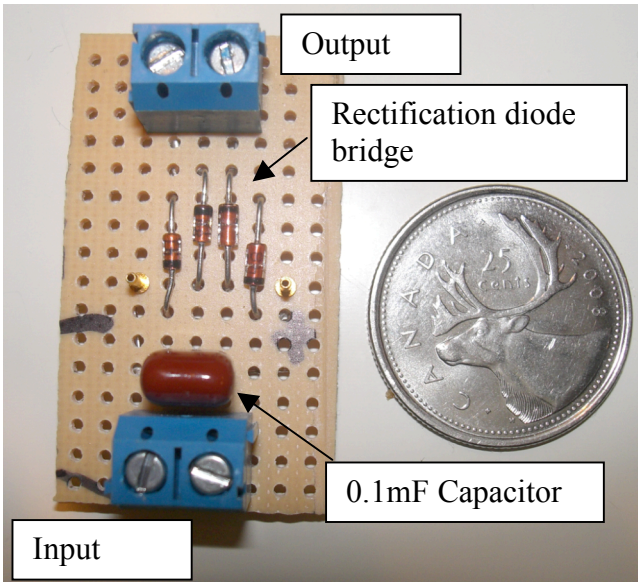

Figure 7.2.2.3: Prototype #2 Energy Harvesting Circuit (Quarter as size reference)

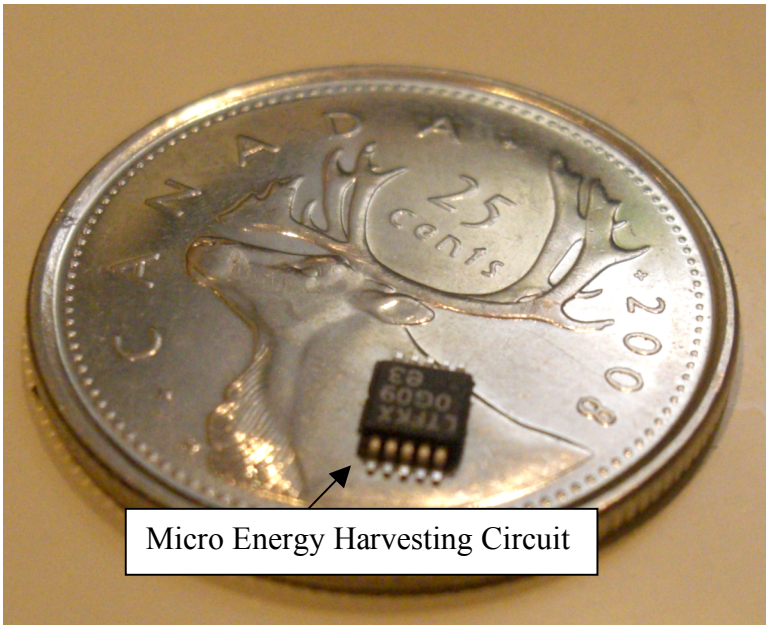

Figure 7.2.2.4: Linear Technology ® Micro Energy Harvesting Circuit

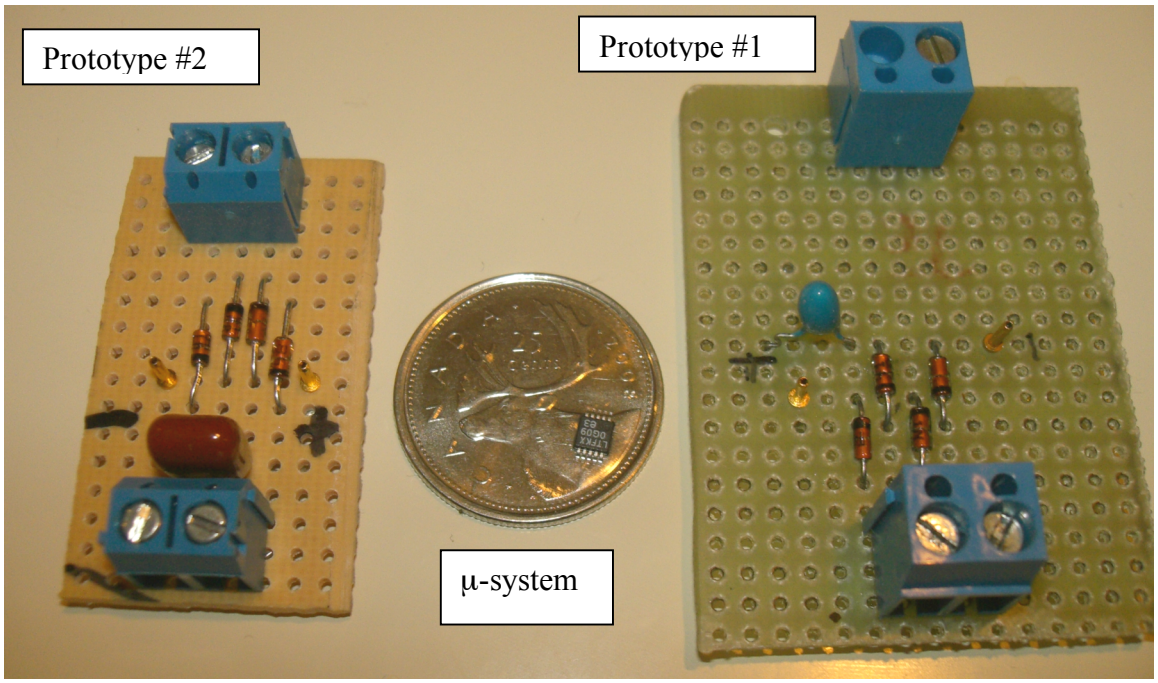

Figure 7.2.2.5: All three energy harvesting circuits shown for size reference

7.2.3 Radio Frequency Transmission Device

In order to demonstrate the feasibility of harvesting energy with the intention of powering a wireless telemetry device, an RF unit was selected to establish power requirements.

The selected radio frequency device, or RF device, is a micro scale RF transmitter that is commercially available from several suppliers worldwide; it is known as the RFM HX1003. This device operates at 418MHz and consumes 7.5mW of power with a transmission distance up to 100 ft (30.48m). This specific transmitter sends packets with 8 bits of ID and 4 bits of data; research demonstrates that 4 successful receipts of 12 bit packets must be achieved for the receiving station to log the data. In order to have a successful transmission, the voltage must first be encoded so the RF transmitter and receiver know what data it is transmitting/receiving. This portion of the transmission is completed by a digital encoder; the HT12E digital encoder produces a repeating 12 bit serial ID code for transmission. The drawback to the requirement of a digital encoder is the need for a voltage regulator to provide a regulated power supply to the encoder and the RF device; this voltage regulation is completed by a MAX666 low drop-out linear regulator.

Joe Paradiso et. al. demonstrated that the required time for successful transmission is 20ms. Therefore, at a power consumption of 7.5 mW for 20ms the total energy required is 150μJ. This energy consumption is based on constant operation, although the standby and transmission modes have different power consumptions. The total transmission time of 20ms is comprised of 10 seconds of transmission and 10 seconds of stand-by operation. The current draw of the RF unit during transmission is 8mA and in standby 0.1μA; this yields a power consumption of 2.64mW in transmission and 0.33μW in standby [49]. For one transmission, this yields a total energy requirement of 26.4 μJ for one 12bit transmission. For successful receipt we need four packets to be sent, therefore, the total energy requirements for a successful data transmission is 105.6μJ [50].

7.3 Methodology

The experimental method for this research is separated into 3 distinct phases; open circuit response to determine the sensor response to a given signal, proof of harvesting circuit to test the energy supply component of the system, and full scale testing in order to determine its feasibility for the intended application. In order to ensure full scale testing using a vehicle was a worthwhile venture, proof of concept of the film and harvesting circuit needed to be completed first.

7.3.1 Phase I: Open Circuit Response

The proof of concept testing of the film to produce an open circuit voltage was carried out by impact loading of the film by means of a rubber mallet. The film was connected to an oscilloscope to measure the corresponding voltage when impacted with a rubber mallet. The voltages were measured using an HP 54602B – 150 MHz oscilloscope with an Agilent Technology's 10 MΩ probe. This experimental portion was not meant to be accurately repeatable, as the magnitude of each rubber mallet impact would vary strike to strike. This portion of the experiment was a proof of concept to prove that the film, once metallized, would produce an open circuit voltage.

7.3.2 Phase II: Proof of Concept-Energy Harvesting Circuit

After an open circuit voltage was achieved through impact loading, the next step in the proof of concept phase was to test both energy-harvesting circuits to determine if a voltage could be stored on the capacitor.

The voltage across the capacitor was measured directly by connecting the oscilloscope probe to either side of the capacitor and loading as per Phase I. Again this Phase was a proof of concept test to determine if the circuitry would rectify the double polarity voltage, as well as to determine if a voltage could be seen across the capacitor using an oscilloscope.

7.3.3 Phase III: Full Scale Testing

After proving that the film would produce an open circuit voltage, as well, that the harvesting circuit would produce a voltage across a capacitor, the film needed to be tested using a vehicle tire as the stimulus. The next phase of testing was to demonstrate the feasibility of utilizing a 52μm thick piece of PVDF film for harvesting energy from a vehicle driving over the film. This phase of testing was to evaluate the open circuit response of the film as well as to evaluate and compare two energy-harvesting circuits. The test setup was conducted at the University of Saskatchewan, Hardy Lab, with a concrete floor, at 15 ^{o}C. The vehicle used was a 2004 Ford F-150 5.4L V8 truck, with a gross vehicle weight (GVW) of 3265 kg. The tire footprint was measured as approximately 0.3048m (12") by 0.1524m (6"). The full scale testing was setup as shown in the schematic in Figure 7.3.3.1.

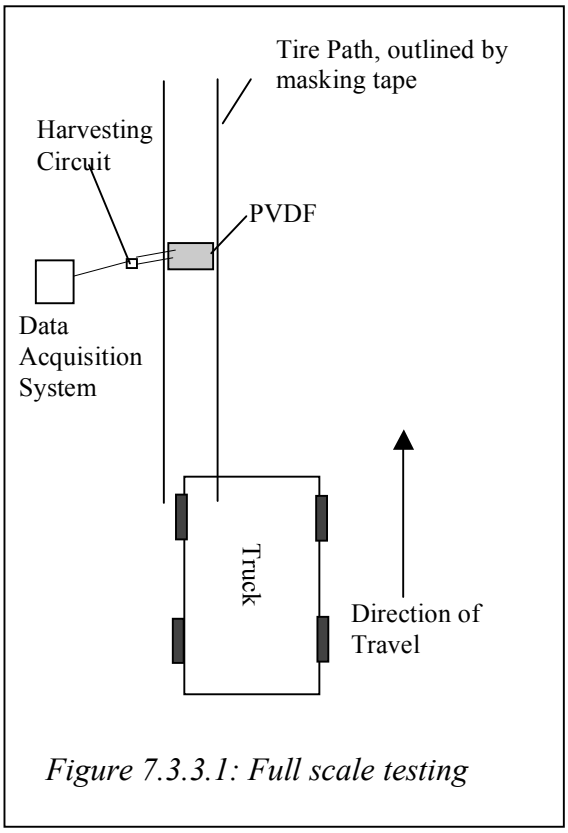

Figure 7.3.3.1: Full scale testing

The full scale-testing phase consisted of a three different sub-phases; open circuit response, harvesting circuit response, and protective film effect.

The first sub-phase of full scale testing was designed to demonstrate that a vehicle driving over the film produced an open circuit voltage as expected by theoretical calculations. The PVDF thin film was affixed to the concrete floor of the Hardy lab and connected via 28 G wires to an oscilloscope. A Ford F-150 truck was then driven over the film between 5 and 20 km/hr and the resulting waveforms were recorded.

After the open circuit voltages were recorded, full scale testing utilizing the energy harvesting circuits was completed; the second sub-phase. Two energy-harvesting circuits were utilized one with a 2.2μF simple glass capacitor and the second a 0.1mF

polyester film capacitor. The voltages across the capacitors were measured using the oscilloscope as the vehicle passed over the films.

The last portion of the full scale testing was to determine the effect of a protective coating over the film to improve its lifetime under harsh roadside environment conditions. To investigate this, two different coating "simulations" were used. The first was a piece of thin cardboard taped over top of the film, the second was a Zip-lock ® bag. The two coatings were visually investigated for wear as well as wear on the PVDF thin film underneath. In addition to wear, the effect the coating had on the voltage produced was investigated through the waveforms recorded on the oscilloscope.

7.4 Results

7.4.1 Open Circuit Response- Proof of Concept

The main purpose of this phase was to demonstrate the film could produce a voltage when subjected to an incoming force.

Shown in Figure 7.4.1.1 is a typical open circuit voltage response of the film to a mallet strike. In this figure, the response shows an initial impulse over 1ms raising from 0 to 4.55 V followed by a rapid decay to a negative polarity over 2 ms. At 3 ms after the impulse, the voltage stays in the negative polarity for the remaining 6 ms shown on the figure. The film will eventually re-zero (10-100ms depending on voltage magnitude); this is due to the slow relaxation time of the polymer. This is the main reason why a full-wave rectifier was chosen for the harvesting circuitry, to make use of this negative polarity voltage swing. The waveform response shown in Figure 7.4.1.1 shows the vibrations experienced by the film as well. The mallet strike produced vibrations in the table the film was affixed to. These vibrations are demonstrated in the constant small oscillations of the waveform.

Figure 7.4.1.1: Typical open circuit response of the PVDF film when impulsed with a rubber mallet (Note: white axes added for time clarification)

For the open circuit response phase, 50 trials were completed using the rubber mallet impulse. The open circuit voltages measured from an impact were found to range from 2-20 Volts depending on the magnitude of the impact experienced by the film.

Variations in response times were evident when different speeds of impact were used. A faster, harder impact resulted in a larger peak voltage and a faster rise/decay time of the waveform and vice versa. A faster strike also produced a larger negative polarity voltage than a slower strike; this phenomenon is explained in detail in Section 7.5.

7.4.2 Harvesting Circuit- Proof of Concept

After an open circuit voltage was achieved through impact loading, the next step in the proof of concept was to test the energy harvesting circuit. The testing completed for this phase was identical to Phase I, with the exception that the PVDF film was connected to the harvesting circuit. The voltage across the capacitor was measured

directly by connecting the oscilloscope probe to either side of the capacitor and impacting the PVDF film with a rubber mallet.

The voltage across the capacitor was, once again, a function of the magnitude of the force experienced. Figure 7.4.2.1 shows the voltage across the 2.2μF capacitor for a mallet impulse, raising the voltage across the capacitor by 1.0625 V.

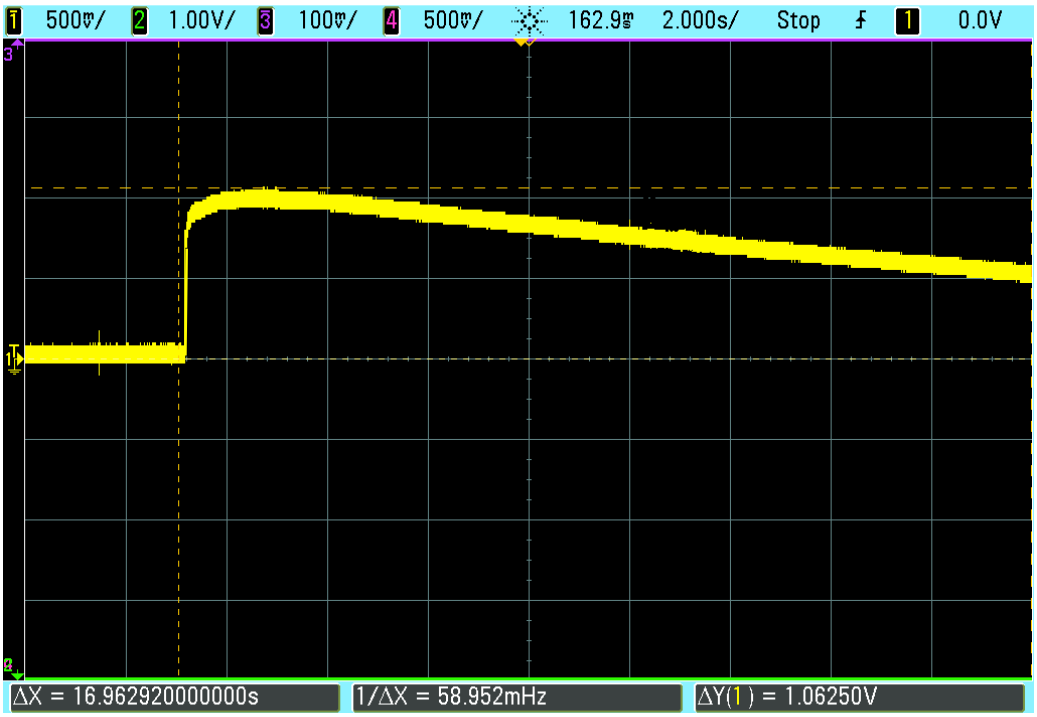

Figure 7.4.2.1: Voltage across 2.2μF capacitor when PVDF subject to a mallet strike

From the figure above, it can be seen that even when the film is subjected to a loading such as a mallet strike, the voltage across the capacitor is significant. Not evident in the above oscilloscope screenshot, is the rectification from the full wave diode bridge. Shown in Figure 7.4.2.2 is another simple impulse of the PVDF when connected to the energy harvesting circuit clearly demonstrating rectification. A different timescale was used to demonstrate the rectification.

Figure 7.4.2.2: Close-up of voltage across 2.2μF capacitor demonstrating rectification of double polarity voltage produced by the PVDF film when subjected to a mallet strike

From Figure 7.4.2.2 it can clearly be seen that the full-wave diode bridge was performing as expected. The double polarity input from the PVDF is rectified into a positive output in a stepwise fashion. The first voltage step is produced by the mallet strike on the PVDF film, after which the film swings to a negative polarity to "self-adjust" the voltage across its electrodes. This negative polarity voltage is rectified by the diode bridge into the second voltage step yielding a positive overall charge of 900mV across the capacitor.

It can be clearly noted that the voltage produced across the capacitor is significantly lower than the open circuit voltage produced by the same impulse. This is due to the large loss experienced in the diodes as well as across the capacitor; this will be explained in depth in Section 7.5. The capacitor discharge seen in the Figures above is discussed in detail in Section 7.5.

After 50 trials using a rubber mallet, the proof of concept of the harvesting circuit was complete. The lowest voltage experienced across the capacitor was 690mV while the largest was 1.23 V. The success of both the film and the harvest circuit demonstrated that

the combination was very feasible as an on-road energy harvesting system using a vehicle tire as the stimulus.

7.4.3 Full Scale Testing Results

Full scale testing was completed to demonstrate the feasibility of utilizing the PVDF film and energy harvesting circuit as an on-road energy harvesting system to harness the energy of a vehicle driving over the film to power a wireless device. In order to demonstrate this, first the open circuit response was recorded and analyzed, second the capacitor voltage was recorded and used to evaluate the harvesting circuit response. Lastly, due to the film's frangible nature, the wear experienced by the film was visually inspected after each pass of the vehicle. In response to the slight degradation of the film after several passes, a few "coatings" were evaluated for performance and effect on voltage production.

7.4.3.1 Full Scale Open Circuit Response

The first stage of full scale testing was to measure the open circuit voltage produced by the film and the piezoelectric response of the film when subject to a vehicle driving over it at approximately 5 km/hr. Shown in Figure 7.4.3.1.1 is a typical open circuit response of the PVDF film from a single pass (both axles).

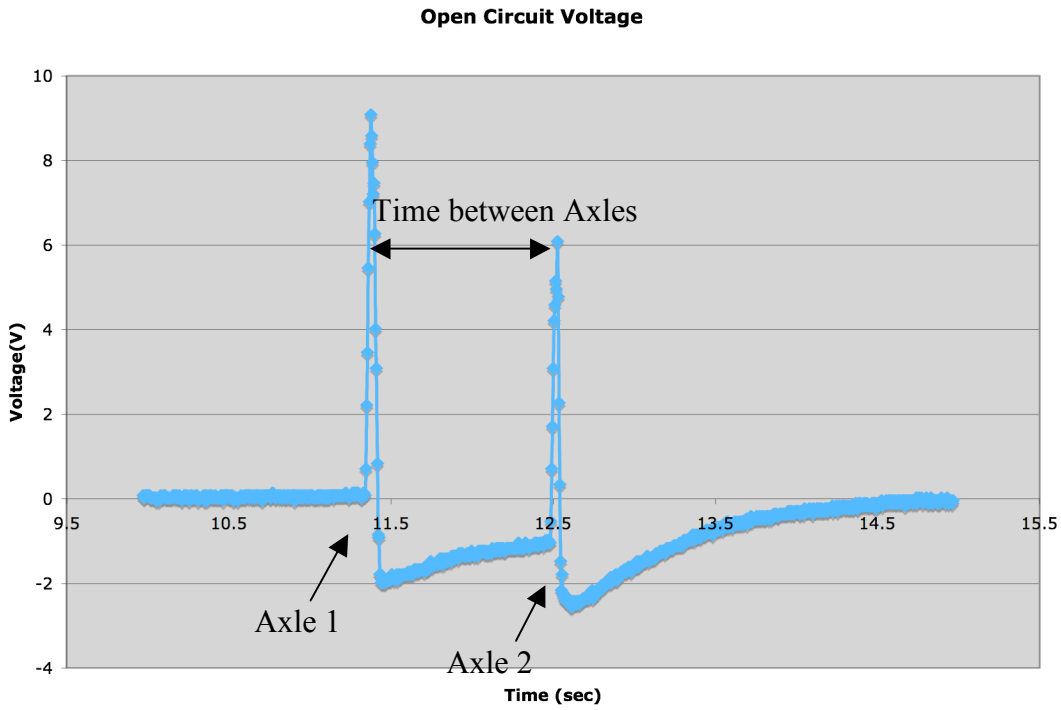

Figure 7.4.3.1.1: Typical Open Circuit Response of PVDF Film during full scale testing

When observing the waveform of Figure 7.4.3.1.1, it is easily seen that each axle event corresponds to a voltage spike. The magnitude of the voltage is a linear function of the force exerted on the material according to piezoelectric theory. The waveform response of the material is exactly as expected; the undershoot of the voltage to a negative polarity is a clear indication that rectification would be advantageous for an energy harvesting circuit.

After initial open circuit testing of a bare PVDF film, slight degradation of the silver electrodes was evident as rocks and dirt on the vehicle tires had caused scratches in the film. After 25 trials, it was conclusive that a thin, protective coating would be necessary in an industrial application.

7.4.3.2 Energy Harvesting Prototype 1 (2.2μF) Response-Full Scale Testing

The first prototype harvesting circuit consisted of a 2.2μF capacitor with a full-wave rectification bridge as outlined in Section 7.2.2. The prototype circuit behaved exactly as expected; the voltage was rectified and a voltage potential was observed across

the capacitor. A large drop occurred in the diodes, resulting in a low voltage across the ineffective capacitor. The capacitor used was a very inexpensive, simple, glass capacitor and the voltage experienced across it was only 600-800mV.

The parameters for this experiment were identical to the open circuit, full scale testing with the exception that the PVDF film was connected to the energy harvesting circuit. The oscilloscope probe was connected across the capacitor to measure the voltage and observe the waveform produced by the film in response to a vehicle driving over the film. Twenty-five passes were completed to ensure the results (waveform and voltage across capacitor) were repeatable within experimental error. Results were as expected based on observations from the open circuit experiments. A typical waveform and voltage produced across the capacitor from a single pass are shown in Figure 7.4.3.2.1.

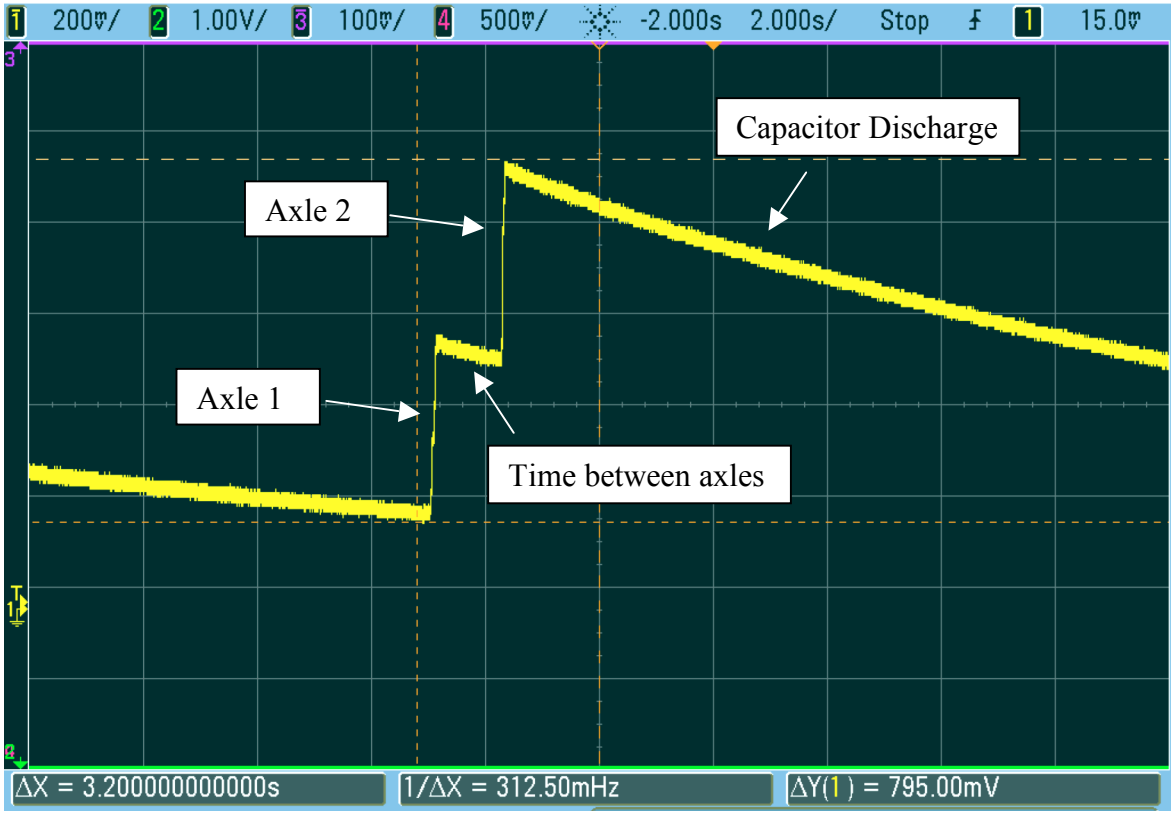

Figure 7.4.3.2.1: Waveform and voltage across a 2.2 μF capacitor from a single pass of a vehicle

The figure above demonstrates a waveform exactly as expected; a voltage spike corresponding to each axle as the vehicle passes over the film. This voltage spike is the

voltage across the capacitor, with a peak-to-peak magnitude of 795 mV. Note that a negative voltage is not present due to the full bridge wave rectifier producing a positive output for both a negative and positive input. The small flat section in between the two peaks is the time between axles of the vehicle as it passed over the film. After the peaks, the decay of the capacitor can be seen. This figure is a good indication of the overall response of the capacitor including its charging and decay time, but to demonstrate the rectification, a much faster timescale is needed.

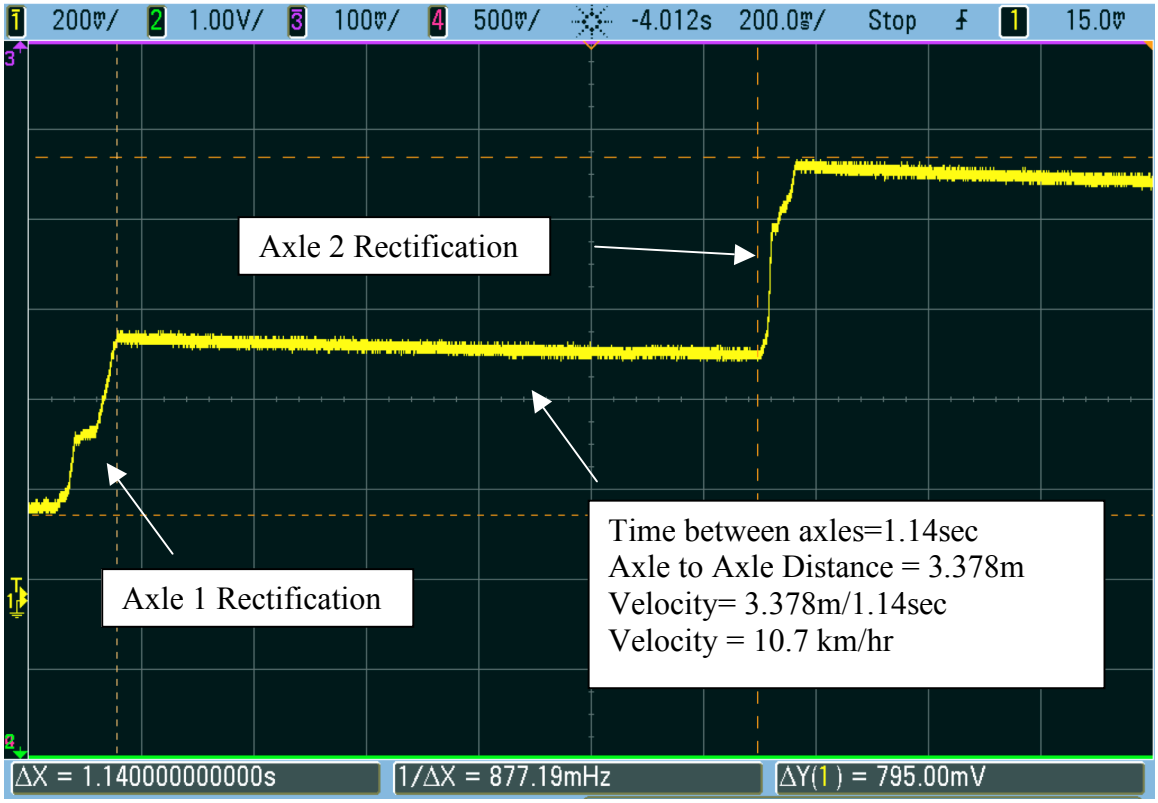

Figure 7.4.3.2.2: Voltage across capacitor showing rectified input, both axle events as well as time between axle events. Note: Same test as Figure 7.4.3.2.1 but on a different timescale.

From Figure 7.4.3.2.2 above, the 795 mV rise across the capacitor is easier to observe. This figure is the exact same pass/result as Figure 7.3.3.2.1 but on a faster timescale. The figure clearly demonstrates both axle events; also evident is the rectification. Close observation of the first voltage spike shows two distinct raises in the voltage. This corresponds to the positive and negative spikes produced by the film. The

rectifier transforms both polarity of input voltages into a positive output. Also seen in this image is the time between axle events, the flat yellow section between voltage rises. Since the time between axle events is known, also the axle-to-axle distance of the vehicle is known, the velocity of the vehicle can easily be calculated.

7.4.3.3 Energy Harvesting Prototype 2 (0.1mF) Full Scale Response

As shown in Figure 7.4.3.3.1, the voltage across the 0.1mF capacitor was substantially higher than that experienced by the 2.2µF capacitor. This is due to the performance and storage of the 0.1mF capacitor far exceeding the 2.2µF capacitor. The polyester film capacitor allowed for a higher voltage to be stored as well as, due to the higher capacity, easier biasing of the diodes.

With the increase in performance comes an increase in energy stored, but a significantly faster decay time; the reason for this is explained in Section 7.5.

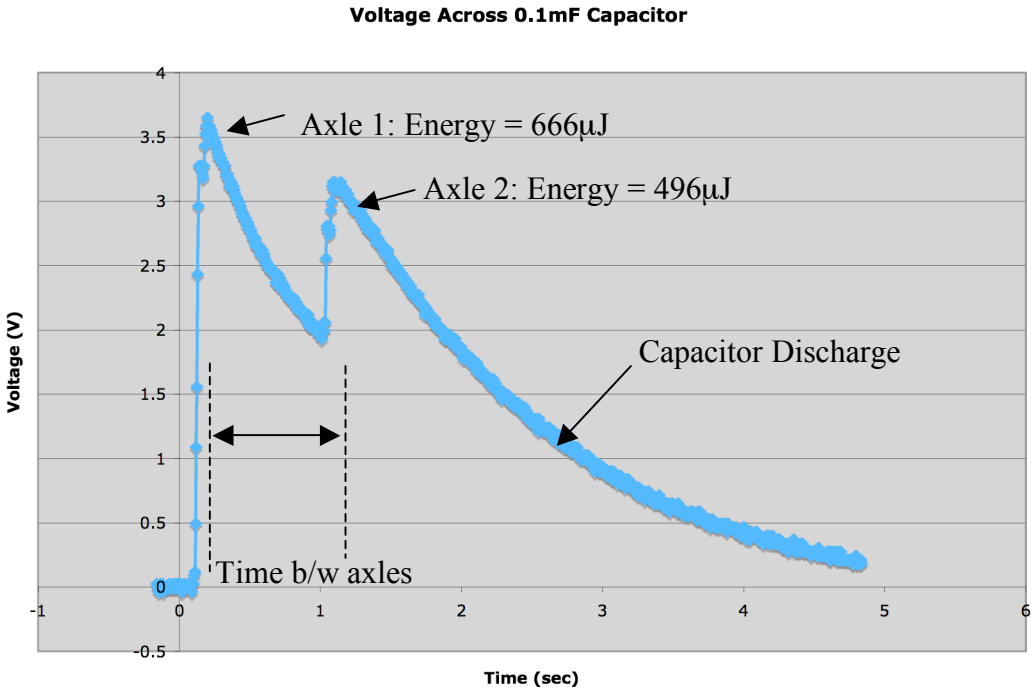

Figure 7.4.3.3.1: Typical voltage response, across the 0.1mF capacitor in energy harvesting prototype 2, when subjected to a vehicle driving over the PVDF film

7.5 Discussion and Analysis of Results

The results from the three phases of testing all conclusively demonstrate energy harvesting via the piezoelectric effect utilizing a lead free, PVDF, piezoelectric polymer and a vehicle tire as the stimulus. The experiments, although demonstrating a feasible application of energy harvesting did have some drawbacks as well as the energy harvesting circuit itself. The following section will discuss the results obtained during full-scale testing including an analysis of the experimental method, circuit drawbacks, and prototype 1 and 2 performance.

7.5.1 Full Scale Testing- Open Circuit Voltage

During the full-scale testing Phase I, the open circuit voltage produced by the film was measured for 25 trials to obtain an average voltage produced and to determine the distribution of the different passes from the average. This experimental portion was not to be a measure of repeatability but only to serve as a baseline for expected experimental voltage.

Below in Figure 7.5.1.1, a bar graph representation of 25 trials demonstrates the distribution from average. Each bar represents the voltage produced by the front axle for a single trial. The black horizontal line indicates the average voltage produced. Observing the figure, a large distribution can be seen over the 25 trials. The largest voltage produced was 10.59V with the smallest being 7.025V. The average voltage produced from 25 trials is 9.053V, which is very close to the expected theoretical voltage. The distribution across the trials is due to the variation in vehicle speed, as well as the tire footprint area in contact with the PVDF film varying each trial. This will be explained in depth in the experimental method analysis.

The same distribution pattern can be seen in Figure 7.5.1.2 which is the same bar graph demonstrating the variance in open circuit voltage produced but for the 2nd axle of the vehicle. It can be noticed that the voltage produced by the 2nd axle event is much lower than that achieved by the 1st axle. There are several reasons the voltage produced by the second impulse is lower than the 1st. Firstly, the vehicle used as a stimulus was a Ford ® F-150 ½ ton truck, this vehicle has a far heavier front axle than the back due to the placement of the motor being over the front axle. A lower weight produces a lower

force, which in turn, produces a lower voltage; according to theoretical expectations the voltage produced should be around 1V lower. However, the voltage produced was on average 3.7 V lower (using the average from 25 passes for both axles).

The reason for this is the "self correction" of the PVDF film when experiencing an incoming force. Refer back to Figure 7.3.4.1.1, the typical open circuit response of the film. The voltage spike corresponding to the 1st axle event is followed by an undershoot of the voltage to a negative polarity to "offset" the large magnitude positive voltage produced; i.e. "a self-correction". If the voltage is measured from the zero point, it is not a true reading of the voltage produced as the peak voltage started from a negative polarity. In Figure 7.3.4.1.1, the first undershoot following the 1st axle voltage spike, drops to -2.1V meaning the 2nd axle event must first produce the 2.1V to bring the number to the positive polarity and then the magnitude becomes positive. In order to obtain a more accurate voltage the undershoot magnitude was added to the voltage spike produced by the second axle. This can be viewed as an absolute value magnitude.

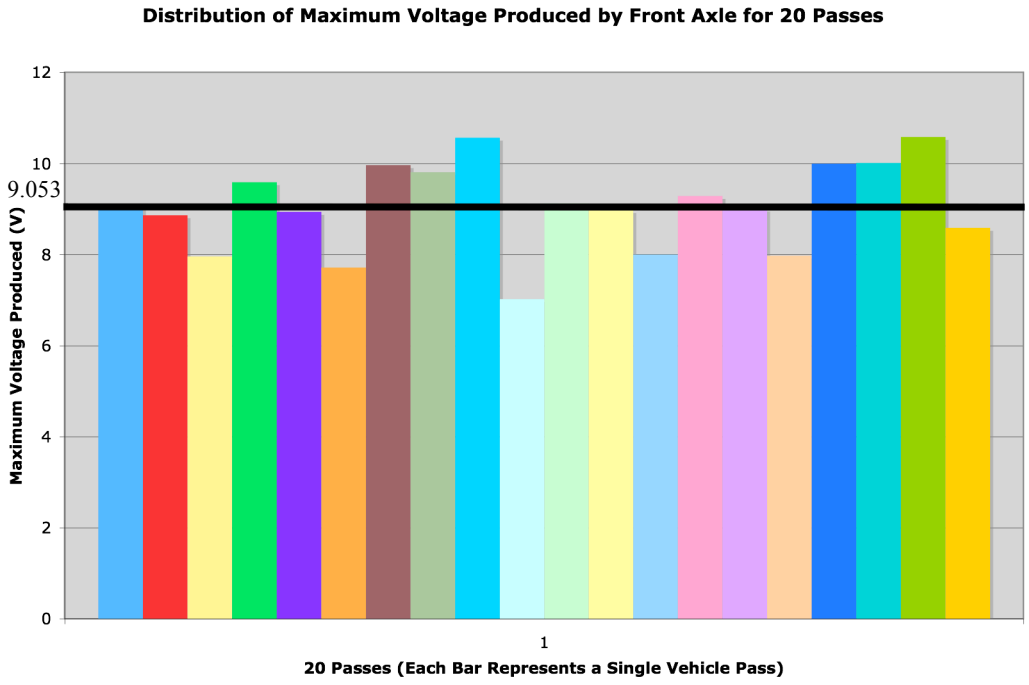

Figure 7.5.1.1: Bar graph showing distribution from median voltage (black line) for 20 passes

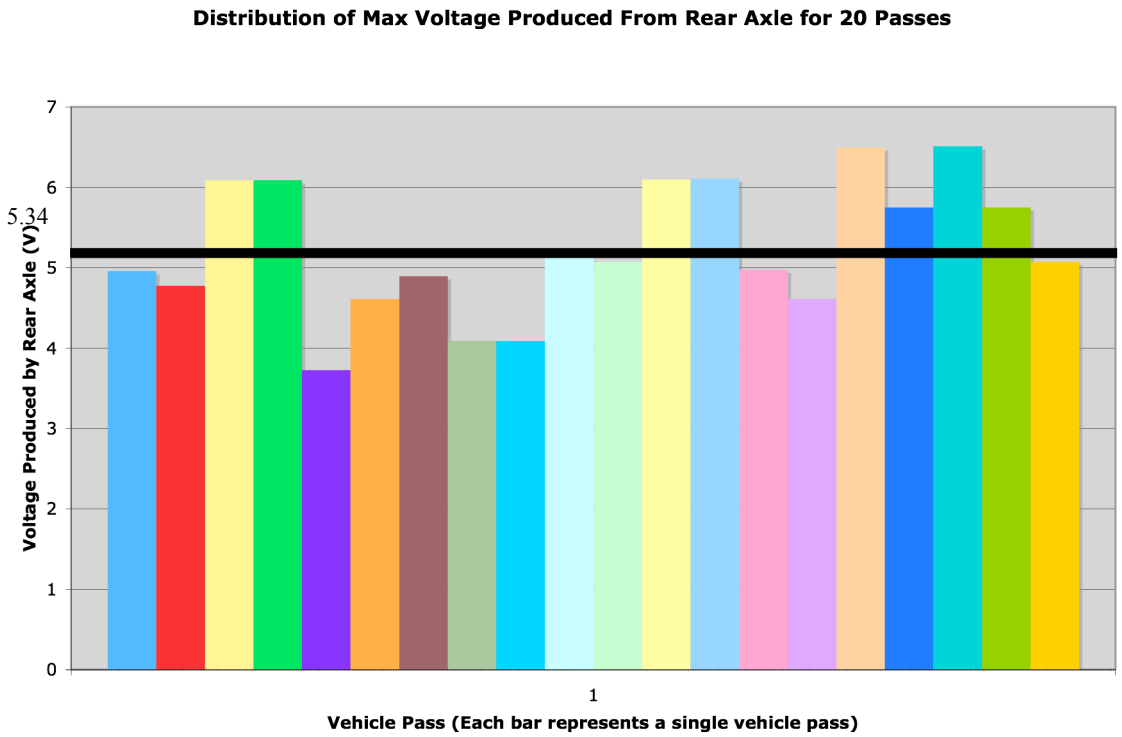

Figure 7.5.1.2: Bar graph showing distribution from median voltage (black line) for 20 passes

After initial observation of the distribution of voltages produced, it can be seen that the variance from trial to trial is high. Although, when comparing the average voltage produced to the theoretical expected voltage, an error of only 4.1% is seen. Below in Figure 7.5.1.3, the theoretical voltage is compared to the experimental voltages for 20 passes. Also plotted are the median experimental and average experimental voltages. The figure does exhibit a large distribution from trial to trial as was demonstrated earlier. Again, this was due mainly to experimental error; mainly variation in tire contact area on the PVDF film from trial to trial.

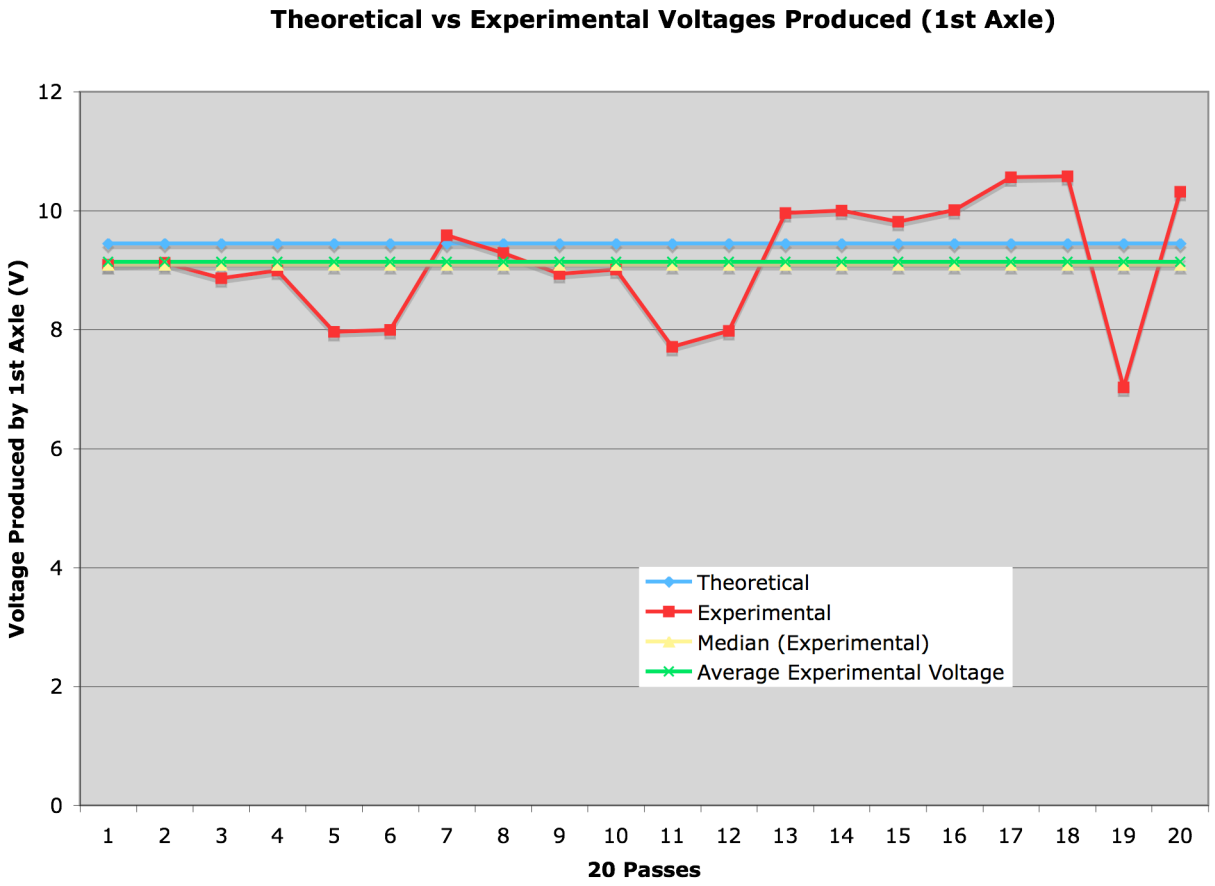

Figure 7.5.1.3: Theoretical Vs Experimental Voltage Produced (1st Axle) for 20 Trials

The theoretical vs. experimental voltage produced by the 2nd axle is shown in Figure 7.5.1.4. At first glance this appears to be very similar to the 1st axle event; this is because the figure depicts the "absolute value magnitude" of the voltage produced. Meaning that the voltage magnitude is a combination of the negative undershoot as well as the positive voltage peak. This yields a more accurate value of the voltage produced by the 2nd axle event. A similar variance from trial to trial is seen as was shown in the 1st axle figure; this again is due mainly to experimental error. The average voltage produced across 20 trials was 7.58 V and the theoretical expected voltage was 7.87 V; this yields a percent error of only 3.7% when comparing the average voltage to the theoretical voltage.

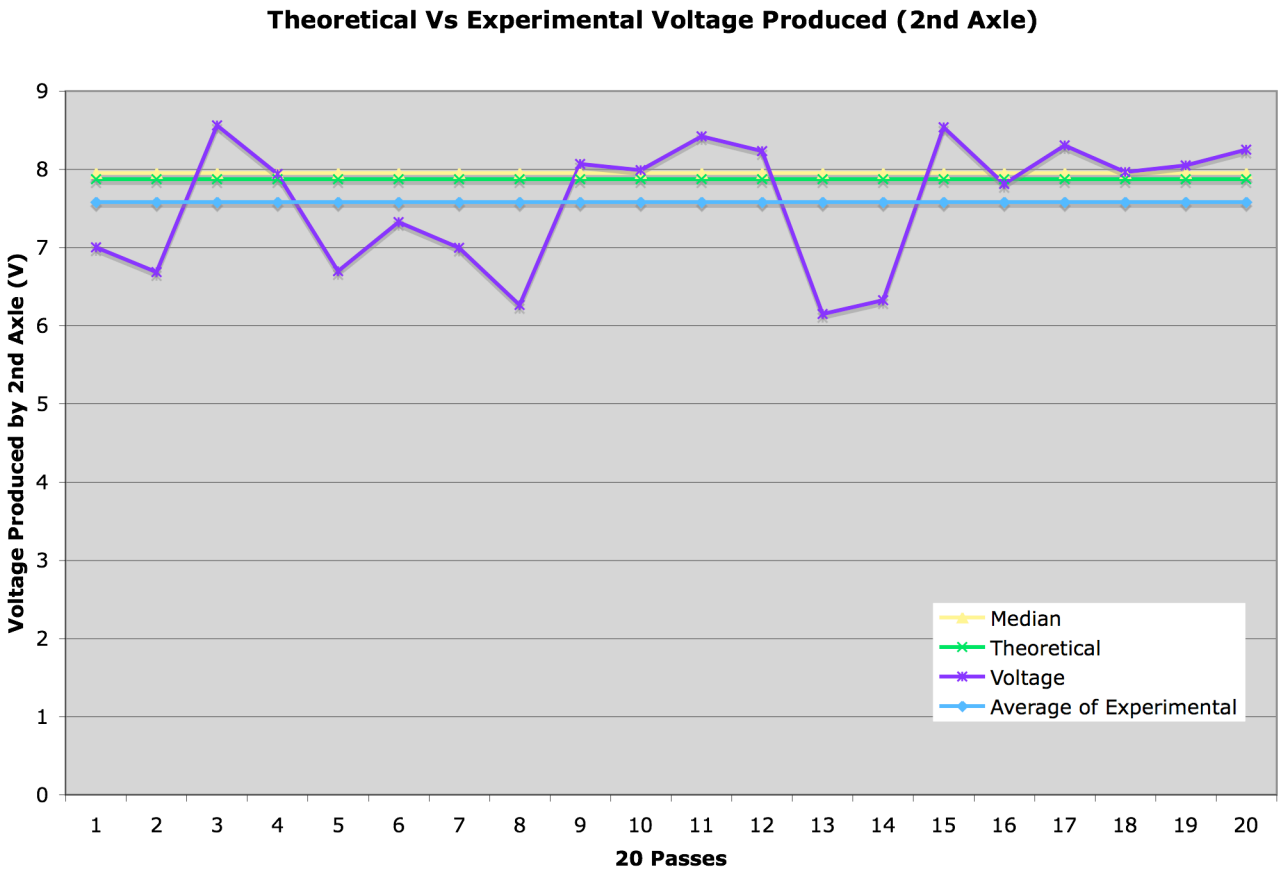

Figure 7.5.1.4: Theoretical Vs Experimental Voltage Produced (2nd Axle) for 20 Trials

7.5.2 Full Scale Testing- Energy Harvesting Circuit Performance

The energy harvesting circuits performed relatively well in harvesting energy from the voltage produced by the PVDF film but there were some definite drawbacks of the initial designs. The following section will discuss the drawbacks and benefits of the overall circuit design as well as the overall performance of both prototypes.

7.5.2.1 Prototype 1 Performance

The initial prototype energy harvesting circuit (Prototype 1) used a small, simple glass 2.2μF capacitor in series with a full-wave diode rectification bridge. Although the capacitor did store the harvested energy from the film, the size of the capacitor was too small to allow for an effective diode biasing. In order to bias the diodes of the

rectification bridge, a large electric potential difference must exist across the diodes. Using the small 2.2μF capacitor, this large electric potential difference does not exist, yielding a large loss in the diodes.

In order to compare differing combinations of piezoelectric devices, a leading research group has developed a value for comparison. Ding Han and Ville Kaajakari along with Paradiso have developed an "efficiency", defined as the voltage across the capacitor in closed circuit condition divided by the open circuit voltage of the device. Although not an efficiency in a physical sense, this value is adopted as common practice to allows energy harvesting groups worldwide to compare their devices on common ground. [19, 36,37]

When comparing the average open circuit voltage produced (9.05 V) to the average voltage produced across the capacitor (724mV), a massive loss in voltage is noticed. This loss, although very large, is common in voltage conversion circuits.

The loss in voltage for the harvesting circuit is 92%, or only an 8% efficiency in converting and storing the charge. This is due to the losses occurring in the biasing of the diodes as well as the ineffective storage of the charge across the capacitor. Although this value seems unreasonable, the efficiency value is actually quite comparable to other voltage conversion circuits demonstrated by energy harvesting groups worldwide. A simple buck converter commonly used has an efficiency of ~8-12% whereas other groups have demonstrated efficiencies of 10-20%. Voltage conversion circuits, or energy harvesting circuits are an enormous area of research and this specific circuit was chosen for simplicity and cost/size reduction.

Shown in Figure 7.5.2.1.1, the variation in voltage across the capacitor is demonstrated for 25 trials. This is compared to the average voltage produced as the theoretical voltage could not be calculated due to the unknown performance of the diode bridge. Some variance from trial to trial is seen over 25 trials; again due to the experimental error. The voltage rise demonstrated in the figure below is the total peak voltage across the capacitor from both axle events.

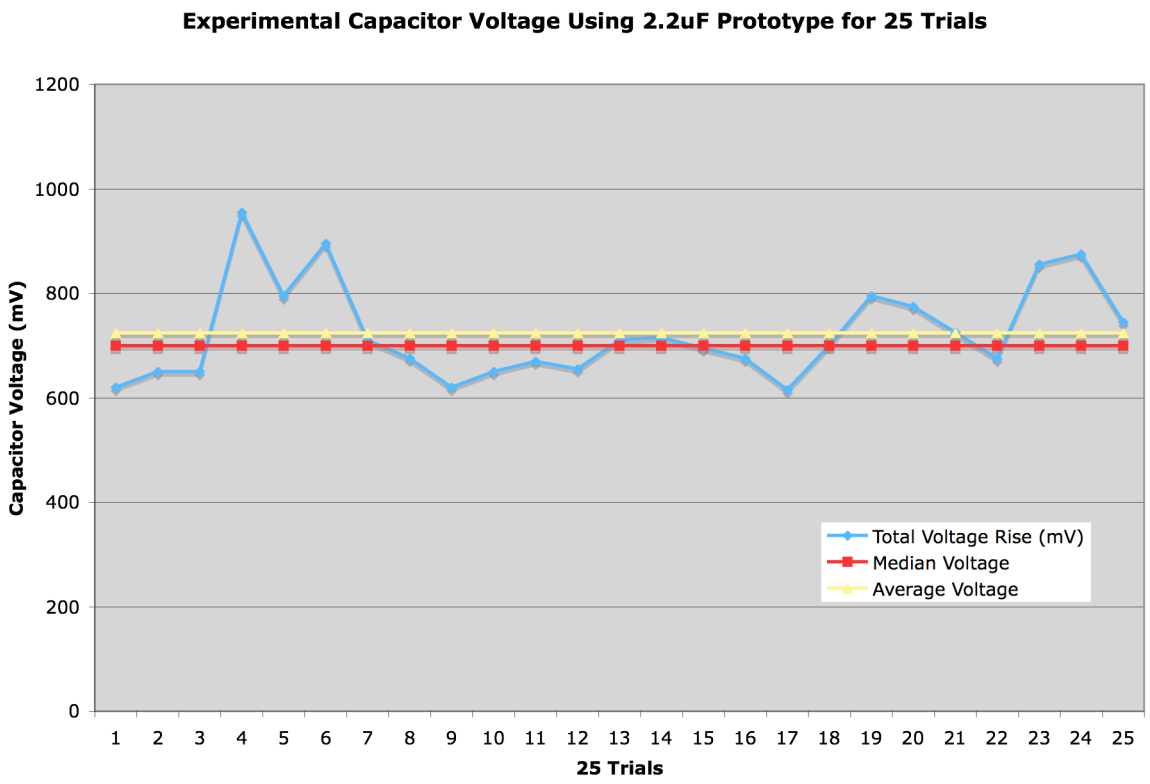

Figure 7.5.2.1.1: Experimental Voltage Produced Across 2.2μF Capacitor for 25 Trials

7.5.2.2 Prototype 2 Performance

After the 1st Prototype testing, it was realized that a much larger capacitor was needed for both the storage of the voltage as well as the ability to more effectively bias the diode bridge. Prototype 2 used a polyester film, 0.1mF capacitor instead of a small glass capacitor. A larger capacitor would create a larger voltage potential across the diodes, yielding a lower loss and a more effective storage of the voltage input.

When comparing the average open circuit voltage (9.05 V) to the average voltage across the 0.1mF capacitor in prototype 2 (3.8V), a dramatic increase in efficiency can be seen. This corresponds to a loss of 58% of the input voltage or an conversion and storage efficiency of 42%. This dramatic increase is due to the larger voltage potential allowing for a more effective diode bias yielding a lower loss in the diode bridge itself. Also, it has been demonstrated by others that a polyester film capacitor is more effective at storing a piezoelectric input than a glass capacitor. This larger capacitor, although increasing the

efficiency dramatically, did have some major drawbacks, which will be outlined in Section 7.5.4.

Shown in Figures 7.5.2.2.1 and 7.5.2.2.2 below are the voltage across the capacitor produced by the 1st and 2nd axles respectively. The first axle produced an average voltage of 3.8V and the 2nd axle produced an average of 3.4V. Again, a variance over 25 trials is noticed.

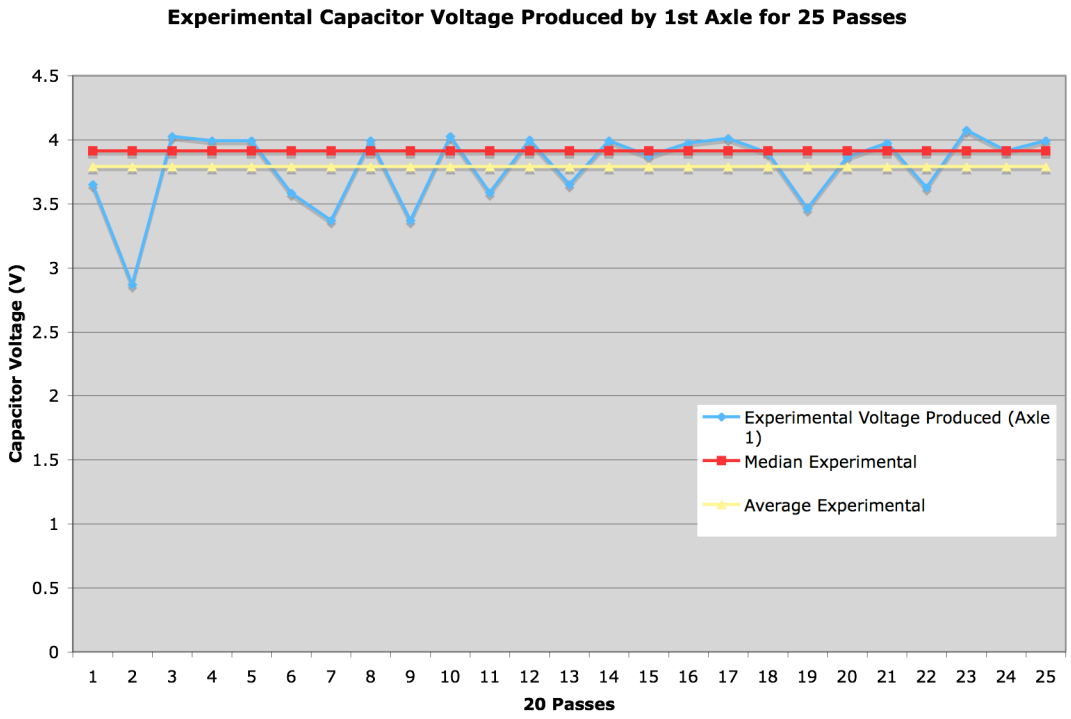

Figure 7.5.2.2.1: Experimental Capacitor Voltage Produced by 1st Axle for 25 Trials

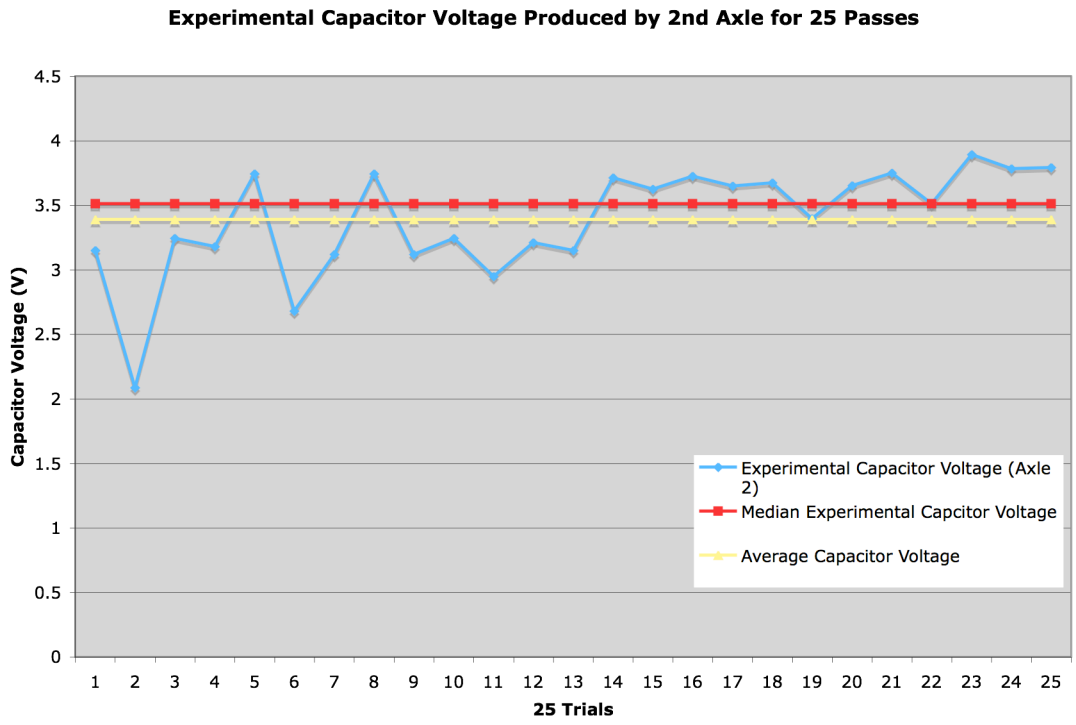

Figure 7.5.2.2.2: Experimental Capacitor Voltage Produced by 2nd Axle for 25 Trials

7.5.3.1 Energy Harvested- 2.2µF Capacitor

The voltages produced across the capacitor, as outlined in Section 7.5.2, can be used to calculate the energy stored in a capacitor. Recall from Section 7.1, the energy stored in a capacitor is equal to one half the capacitance (F) multiplied by the voltage squared: $E = 0.5\ C*V^2$. The energy harvested by Prototype 1, using the 2.2µF capacitor for 25 trials is outlined in Figure 7.5.3.1.1. A large variance is noticed in the energy produced, larger than that observed in the voltage across the capacitor in Section 7.5.2 due to the fact that the voltage is squared. When observing the energy generated it ranges from .4µJ -1µJ. This amount of energy is insufficient to power any wireless device for data transmission.

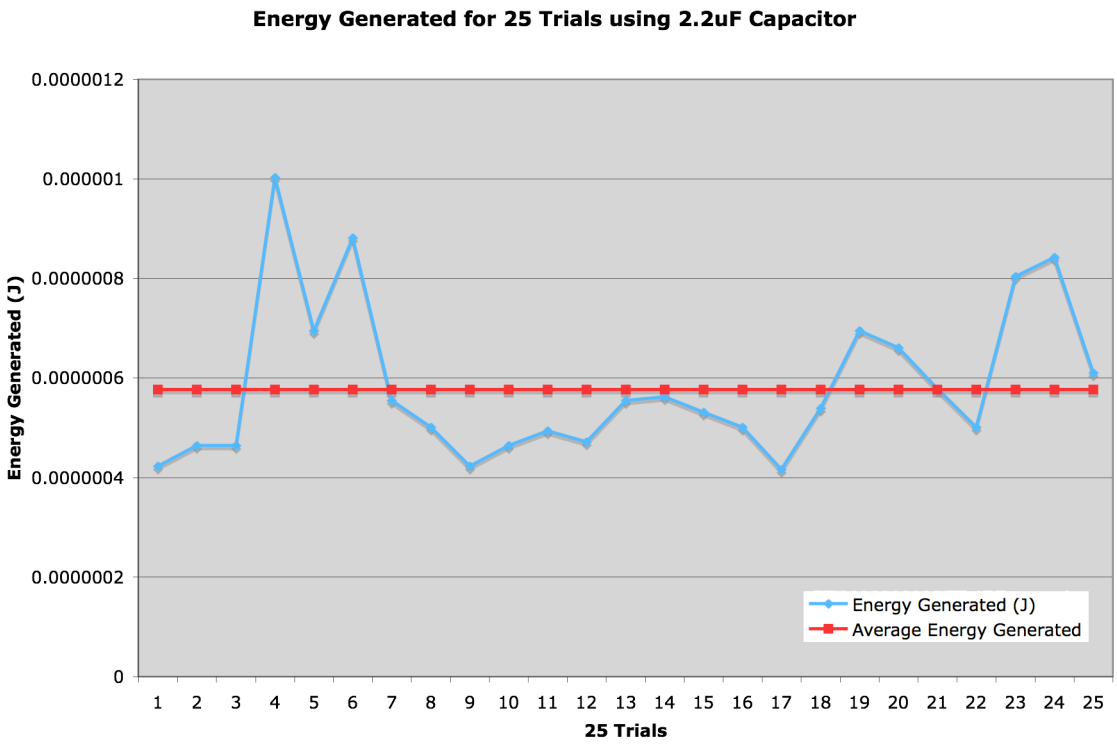

Figure 7.5.3.1.1: Energy Generated using 2.2μF Capacitor for 25 Trials

Although very small, the benefit of using the smaller capacitor is that the voltage stored on the capacitor was not enough to re-bias the diode bridge allowing for a return path the voltage could take through the bridge, discharging the capacitor back through the bridge. The lack of a re-bias resulted in the voltage being stored on the capacitor for a very long time. This is the ideal case as far as a timeframe the voltage is stored on the capacitor, but not for the magnitude of the voltage. In this case, the full-wave rectification was an ideal candidate as the voltage produced was low and the rectification, as shown in Section 7.4.3, added a large component to the final voltage stored on the capacitor.

The average voltage stored on the 2.2μF capacitor for 25 trials was 0.576μJ, which was several orders of magnitude below the 105 μJ required to power the RF transmitter. A dramatic increase was needed in order to power a wireless device.

7.5.3.2 Energy Harvested- 0.1mF Capacitor

The energy harvested by prototype 2 using the 0.1mF polyester film capacitor was far greater than that achieved by the 2.2μF glass capacitor. The energy harvested by both axles for 25 trials is shown in Figure 7.5.3.2.1. This figure demonstrates the energy required (yellow line), the energy produced by the 1st and 2nd axles for 25 trials (blue and red lines respectively), as well as the average energy produced over 25 trials for both the front and rear axle (green and purple lines respectively).

It can be clearly seen that the energy required is far less than that supplied by each axle. There is again a large variance in the actual energy produced from trial to trial, but the overall average energy produced by each axle is 6-8 times that which is required. The front axle produced an average energy of 723μJ while the second axle produced an average energy of 584μJ.

A large variance in energy produced from trial to trial can be seen in the figure indicating that the vehicle tire did not pass directly over the film creating larger and smaller voltages produced. The largest energy produced for the front axle was 830μJ indicating a good tire-film contact while the lowest energy produced was 411μJ indicating the tire only contacted approximately half of the film. The rear axle produced a low of 217μJ and a high of 757μJ indicating a near miss of the film with the tire and a relatively good contact for the low and high respectively.

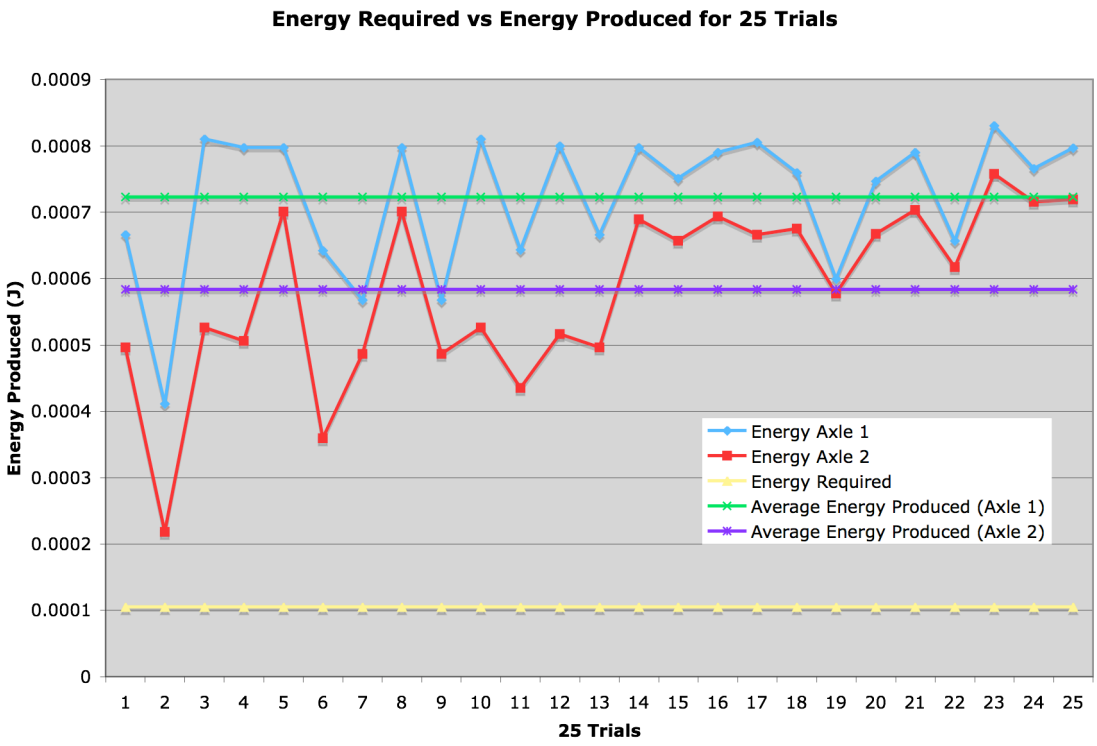

Figure 7.5.3.2.1: Energy Generated using Prototype 2 for 25 Passes

Although the 0.1mF capacitor did harvest more than 5 times the required energy there were some drawbacks evident with the dramatic increase in voltage stored on the capacitor. The main drawback can be seen when comparing the waveforms of the 0.1mF capacitor to the 2.2µF capacitor. In the latter, the voltage, although low, remained stored on the capacitor for a long period of time. Whereas with the 0.1mF capacitor, the capacitor discharge was very quick indicated in Figure 7.4.3.3.1. This is due to the diode bridge being re-biased by the large voltage stored on the capacitor. This allowed a return path for the voltage on the capacitor to flow back through the circuit, creating a rapid discharge of the capacitor. This did not occur in the 2.2µF capacitor, as the voltage stored was not high enough to re-bias the diode bridge thus "trapping" the voltage on the capacitor.

This is the major drawback of the full-wave bridge in prototype 2. In the first prototype, the full-wave rectification was needed to supplement the low voltage produced to "scavenge" as much energy as possible. In the second prototype, the voltage produced

was 5-8 times that required so a full-wave rectification was not necessary. If instead, a half-wave bridge was used in prototype 2, the voltage would not have a return path to travel, thus storing the voltage on the capacitor for a long time. The voltage stored would be lower as a half-wave bridge would only store a positive polarity voltage and "cut-off" any negative input. Even with the negative polarity voltage removed, the energy produced would be greater than the energy required.

7.5.4 Energy Produced Vs. Energy Required

The overall purpose of the energy harvesting system was to provide a power source to a micro-RF wireless data transmitter. The RF unit selected as a baseline for an energy budget, as outline in Section 7.2.3, was selected from work done by Paradiso et al.

The micro transmission device selected was the RFM HX1003 418MHz transmitter and the HT12E digital encoder. From the study it was found that the RF unit has a total energy requirement of 26.4 μJ for one 12bit transmission. For successful transmission, receipt of four packets of 12 bits is needed, therefore, the total energy requirements for a successful data transmission is 105.6μJ (Paradiso et. al.).

So, for a successful transmission we need 105 μJ and per axle, using Prototype 2, we produce from 500-800 μJ; there is enough energy generated per axle to transmit 4-8 data transmissions or 192-384 bits of data.

The drawback of using a piezoelectric supply as a power source is the alternating/fluctuating voltage output. Using a diode rectification bridge and a storage capacitor can combat this fluctuation in input, although still, the storage capacitor has an AC output. To overcome this, there are two common methods, one is to use the storage capacitor in series with a second discharge capacitor; effectively making the storage capacitor a "smoothing" capacitor. By using two capacitors in series, the first capacitor discharges into the second yielding a smoother overall output. The second option is to use a linear regulator, as was the case studied by Paradiso et al. This option uses a regulator to provide a continuous, steady supply of power at a certain, pre-defined voltage. The drawback of this is the constant power draw of the regulator regardless of the power usage. These concepts will be discussed further in the Future Works Section.

7.5.5 Protective Coating Effect and Film Degradation

After initial testing of the film for voltage generation using a vehicle as a stimulus, it was noted that a slight degradation of the silver electrodes occurred due to rocks, dirt, and the movement of the vehicle tire over the film. After 25 passes using a vehicle, the top (surface) electrode had noticeable scratches and wear. From this it was clear that a hard, protective coating would be necessary for an industrial application.

In order to establish the type of coating that would be best suited two coating thickness were tested in order to evaluate the protection they would give as well as the effect on voltage generation.

The first coating "simulation" was a piece of hard cardboard taped over the film. This "coating" provided adequate protection from rocks, dirt and debris. On the other hand, the added cardboard layer decreased the voltage generation from an average of 9.06 V, without the added layer, to an average of 2.5 V over 25 trials.

This significant decrease in voltage generation is due to the compressibility of the cardboard as well as the area the cardboard covered. The piece of cardboard dampened the force experienced by the film itself. The cardboard size was larger than the film thus distributing the force into the concrete around the film rather than directly into the film. This demonstrated that a coating material with a high solidity ratio is needed, meaning the material must be incompressible, as the cardboard caused a drop in voltage generated of 72%.

Since the cardboard affected performance due to its compressibility, a thinner incompressible coating "simulation" was used. This coating was a simple Zip-lock ® bag that fit the film perfectly. The film was placed inside the bag and the bag/film was taped to the floor. The "coating" provided excellent protection from water, debris, and rocks by not allowing direct contact, thus reducing the scratching of the surface electrode. There was no evident effect on voltage generation with average voltage produced of 9 V over 25 runs. This coating provided a great estimation of the thickness/compressibility required for an industrial protective layer. This will be discussed further in the Future Works section.

7.5.6 Experimental Method Analysis

The experimental method employed in this study did produce favorable results, although there were several downfalls of the experiment. The purpose of the experiments was to provide a proof of concept for utilizing a piezoelectric polymer film as an on-road energy harvesting system. Therefore, the repeatability of the experiments was low, but repeatability and/or optimization were not the purpose of the study.

The open circuit voltages produced by the film as a vehicle passed over it were as expected by the theoretical calculation of open circuit voltage based on the vehicle weight (refer to Table 7.1.2). Some variances in the voltages produced were evident due to experimental error. This error is due to the variance in contact area between the tire and film during different passes. This is due to the fact that to perfectly pass both axles evenly over the film every pass was not possible. Due to the size of the film being smaller than the tire footprint (for experimental testing) the alignment of the vehicle over the film each pass was difficult to regulate. This is demonstrated by Figure 7.5.5.1 below.

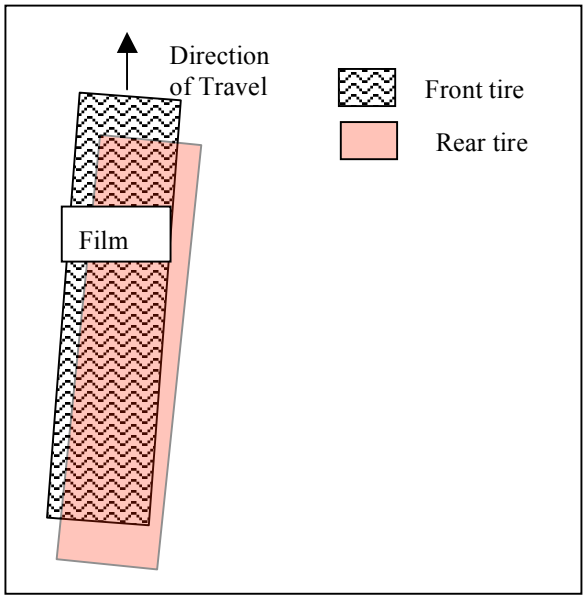

Figure 7.5.5.1: Variance in voltage generated due to the difference in tire-film contact area

Although this caused a large variance across the trials, this effect will not be present in an industrial setting due to the width of the film crossing the entire road, rather

than being only 8” wide. The small size of film used for testing was chosen due to availability. This will be discussed further in Section 8: Future Work.

8.0 FUTURE WORK

The initial phases of testing outlined in the preceding chapters of this thesis are the starting point for development and commercialization of an on-road energy-harvesting device. The research completed was initially an intensive literature review to determine and design a prototype and then to test the validity and performance of a piezoelectric thin film polymer through full scale testing. The work completed can be viewed as a feasibility study and initial prototype development. This research answered numerous questions surrounding the concept while at the same time, opened the floodgates with a plethora of new questions and areas of research; common in the development of novel technologies. The following section will briefly discuss further areas of research needed to provide a commercialized, on-road, self-powered, wireless data transfer device using piezoelectric energy harvesting as the power source.

8.1 Harvesting Circuitry and Front-end Interface

The analysis of the harvesting circuit used demonstrated good rectification and storage of the piezoelectric input. While performing as expected, there were some downfalls of this specific circuit, as outlined in Section 7. Further study of harvesting circuit structure should be completed to obtain both an increase in energy stored as well as a smoother capacitor output. Also needed is implementation of new super-capacitors or ultra-capacitors and a study to determine their added performance.

In order for the piezoelectric output to be used to power a wireless RF device, a capacitor or storage device must be used to ensure adequate energy stored (supply). Shown in the previous research is a constant power supply, but this was an AC output. In order to ensure the RF device performs as expected, a linear regulator should be used in series with the output capacitor. A study should be done to determine the effect this has on the overall circuit performance. Paradiso et al. completed a similar study and found favorable results using a PZT impulse to power a wireless device; results should agree when using PVDF.

The main area of the harvesting circuitry that needs further attention is the front-end and harvesting interface. Since this device is desired to be self powered (which has been demonstrated), but also be able to wirelessly transfer the piezoelectric data, the

components and inter-connection performance should be investigated. A recommended overall device set-up is shown and discussed in Section 10.4.

8.2 Microsystem Development

Although the development of the harvesting device is the first major hurdle in implementing such a device in an industry setting, a second hurdle is implementing micro-fabrication technologies to reduce the size of the device. The reduction in size of the harvesting circuitry will yield a device, which is not as intrusive to the road.

Using micro-fabrication technology, a dramatic reduction in size can be obtained. The easiest way to view the drastic size reduction is to refer back to Section 7.2.2; specifically Figure 7.2.2.2-7.2.2.4. This micro system, fabricated in Singapore, by Linear Technologies Inc ® demonstrates clearly the size reduction possible. The micro-system shown contains the same components as the two prototypes tested in this research with a few added components.

After a harvesting circuit has been decided on, the device needs to be fabricated by a combination of photolithography and screen-printing techniques. The overall layout of the device needs to be decided and the masks required for the lithography need to be designed. The development of the system into a micro-scale device is a large undertaking that requires specialized knowledge as well as a specialty fabrication facility. There are however, a few companies worldwide who design and build micro-systems as well as a large number of academic based facilities at Universities worldwide.

8.3 Wireless Data Transfer

A main component of the wireless portion of the device is the encoding, transfer, and decoding of the sensor data desired to be transmitted. An added bonus of utilizing a piezoelectric material for the power supply is the significant use of piezoelectric materials as sensors. To use the piezoelectric signal as a sensor, it must be routed to a digital encoder in series with an RF transmitter. Another added benefit of a piezoelectric signal input is the extensive use of wireless devices to transfer piezoelectric signal inputs. Piezoelectric sensors are widely available and are even used as on-road sensors, therefore, the signal processing should not be a difficult task. The encoding of a

piezoelectric signal is also used widely in industry, in cell-phones, microphones, and speakers.

The research that needs to be completed is testing of a combined piezoelectric input, encoder, and transmission device for distance, power consumption, varying transfer medium, and noise/interference. This should be first completed using a constant power source to ensure encoding/transfer/decoding is achieved as desired, and then a final prototype built and tested as outlined in Section 10.4.

8.3 Fatigue and Lifetime Testing

After the research demonstrated that the PVDF film could be used as an on-road energy harvesting system, a long-term lifetime study of the film must be completed. The film needs to be subjected to repeated loading with a vehicle tire. The voltage generated for each impulse should be recorded and a lifetime analysis completed. This can be done on-road, although there are many factors affecting the voltage (vehicle size, speed, temperature etc). In order to control the factors affecting the voltage output and to obtain a reliable/consistent loading, a controlled experiment needs to be completed. There are a few test sites worldwide that could be utilized for such an experiment; the first is the California Department of Transportation (Caltrans) Heavy Vehicle Simulator test site near Palmdale, California. The second is an in-door piezoelectric road sensor test facility in Japan to determine lifetimes of piezoelectric sensors. This facility uses a vehicle tire that can be hydraulically loaded as required, on a radial arm pinned at the center. This radial arm can then be rotated at varying speeds over the sensor. This simulates a vehicle driving over the sensor hundreds of thousands of times and is a great method for deducing the average lifetime of the sensor.

The overall lifetime and performance characteristics of a fatiguing PVDF film are a definite necessity if the sensor is to be employed in a commercial setting. The lifetime of the PVDF should exceed 3 years to be functionally applicable as an on-road device.

Also needed for lifetime/fatigue testing is the proposed 3M ® epoxy coating as a protective layer over the film. In order to protect the PVDF film and the silver electrodes a proposed epoxy layer over the film is needed. This protective layer is a method to extend the lifetime of the film and a study needs to be completed to determine the

extension of lifetime of the PVDF by using the film and the lifetime of the protective layer itself.

8.4 α-Phase Prototype

After the prototype that was obtained in the preceding research, a second more refined prototype must be fabricated. The next stage in the design process is to fabricate and test an Alpha Phase prototype. An alpha phase prototype's purpose is to evaluate the integrated system performance as well as further product development. It can be viewed as the final product, which is to be tested for production. This is not entirely the case as an alpha prototype is further refined into a beta phase prototype used for commercial testing in the field. In this case, the alpha prototype should be built and designed to be tested in the laboratory and then the field.

The α-prototype should be constructed using components as outlined in the preceding report, and any alterations needed as a result of research explained in Sections 8.1-8.3. The use of a large piece of PVDF rather than the 5.5"x8" should be used. This piece of film will span an entire lane or road to ensure an effective tire-film contact area is achieved.

8.7 β-Phase Prototype

A β phase prototype is also known as a preproduction prototype or PPP. This prototype is a finalized refinement of the α prototype after extensive laboratory and field experiments. The PPP is used to qualify the device for customer use and production prior to its release for commercialization.

The PPP for this device will be a finalized device based on the results of all other testing completed. The beta-phase prototype (PPP) should be shipped to a select group of customers (or used internally at a select number of sites) and tested for its final purpose at various locations around the world under differing conditions.

After the PPP is deemed as an appropriate device for its intended function, it should be marketed and commercialized to customers worldwide. This device has the potential to be implemented on every road/highway worldwide to enforce weight limits,

count/analyze vehicle traffic, classify vehicles, used in toll stations, automatic gates, parking garages, bridges and overpasses, and traffic lights.

9.0 CONCLUSIONS

The preceding thesis summarizes the research carried out in order to identify and develop a sensing and energy harvesting approach for autonomous sensors. The approach was decided by extensively researching combinations of sensing methods, materials, power supplies and micro systems that could lead to an autonomous sensing unit. Secondly, after the primary research indicated a suitable system, a proof-of-concept demonstrator was tested to validate the conclusions and decisions drawn from the primary research. This was achieved by investigating the feasibility using a piezoelectric polymer thin film affixed to a road as both a sensor and a power supply for a wireless RF transmitter through two prototypes.

The secondary portion of the research was to design a harvesting and sensing system based on the conclusions drawn from the main research objective. The proposed device is based on the conclusions drawn from an extensive literature review and constraints imposed by the application and environment the micro system is to be employed. Of all the materials studied, piezoelectric materials were objectively decided as the ideal candidate for many reasons. Piezoelectric materials have been used since 1960 as sensing elements; they have also been used as energy harvesters for the last 15 years. This leads to a unique ability to incorporate both the power source and sensing aspects of the system into a single element. No other material or power transfer method could lead to this combination. Harvesting energy from the environment was also chosen rather than wireless transfer due to the requirements for a rectenna and size constraints imposed by the need to conceal the device on the surface of a road.

Harvesting energy by means of a vehicle tire for the purpose of transmitting data about the vehicle meant that the material needed a thin footprint, which would ensure full contact with the incoming object while not intruding on the roadway. No piezoelectric material other than a thin film could achieve this. A lead free PVDF was chosen due to environmental concerns of placing a Pb based material onto roadways.

In order to validate the decisions formed in the primary research objective, testing the film in a real-world application using a vehicle as a stimulus was carried out. The PVDF thin film was adhered to the road and a vehicle was driven over the film at 5-20 km/hr and the resulting open circuit voltages were recorded using an oscilloscope. Open

circuit voltages ranged from 7-10.5 V over 20 trials showing a slight deviation from theoretical. This deviation is due to experimental error; more specifically it is due to the tire-film contact area differing with each pass. When viewing the average voltage produced over 20 trials for the front and back axle, an error of only 3.1% and 4.0% from theoretical was found. This concludes that although each individual trial had error associated with experimental error, the average overall voltage produced had an acceptable error when compared to theoretical.

The second portion of testing was to produce a prototype. This involved connecting the PVDF film to an energy harvesting circuit consisting of a full-wave rectifier bridge and a storage capacitor. Two prototypes were built and tested; one containing a simple, inexpensive 2.2μF glass capacitor, and the second a larger, better performing 0.1mF polyester film capacitor.

The first prototype using the 2.2μF capacitor showed excellent rectification of the input voltage produced by the PVDF film when subjected to a vehicle tire stimulus. Although the prototype did harvest energy from the film, the low storage capacity could not effectively bias the diodes in the full-wave rectification bridge leading to a large loss across the diodes. This is due to the lack of voltage potential across the bridge yielding a conversion efficiency of 8%. With an average input voltage of 9.05 V an average voltage across the capacitor was found to be 724mV. This seems very poor but is comparable to conventional buck converters with an efficiency of 10-12 %. A benefit of using this small capacitor was the ability for the charge to be stored on the capacitor for a large period of time. The voltage stored on the capacitor was not large enough to be able to re-bias the diodes, thus “trapping” the energy on the capacitor.

The second prototype clearly demonstrated energy harvesting using a piezoelectric polymer affixed to a road; harvesting energy from a vehicle tire as it passed over the film. The conversion performance of the circuit was significantly higher than prototype 1 at 42% efficiency. With an average input voltage of 9.05V, the average voltage stored across the capacitor for the front and rear axle was 3.8V and 3.4V respectively. A large variance across the 25 trials was noted and it is attributed to the tire-film contact area which, in a commercialized product would not be present due to a large area of film used rather than a small piece.

The amount of energy harvested by the second prototype ranged from 400-800μJ per axle. The average energy harvested by the front and rear axles were 723μJ and 584μJ respectively. The front axle produced a maximum energy of 839μJ with a minimum of 411μJ demonstrating a near perfect tire-film contact area (max) and a poor tire-film contact area (min). The second axle maximum and minimum were 757μJ and 217μJ indicating the same.

The power requirements of the selected RFM HX1003 418MHz transmitter and HT12E digital encoder is 105.6μJ for successful transmission of 4 packets of 12 bits of data. This corresponded to the possibility to power the 418MHz device for 4-8 successful data transmissions per axle. With 4-8 successful data transmissions per axle this yields a transfer of 192-384 bits of data per axle event.

Secondary conclusions were drawn from wear exhibited by the film after approximately 20 passes. After approximately 20 passes, dirt and water from the tire had caused wear of the silver electrodes, evidence a protective coating was necessary. Two "coating simulations" were tested. The results demonstrated the need for an incompressible material to be used as the coating so as to not impede the functionality of the system. The coatings to be used should be a thin film with a high solidity ratio (incompressible), with chemical and thermal stability and ease of manufacturing and processing. There are several commercially available products that suit this criteria.

Although this prototype produced a novel concept for autonomous sensing, the future work to provide a commercialized product is still a large area of research. The film and protective coating need to be tested for lifetime and failure. The energy harvesting circuit needs to be manufactured as a micro-system, as well, the actual encoding and transfer of the data needs to be completed. After this has been done, alpha and beta phase testing can follow and a commercialized product result.

In conclusion, the research completed has investigated combinations of materials, power sources and components to reveal a possible approach to autonomous sensing. The conclusions drawn from the primary research were validated by testing two prototype units.

10.0 REFERENCES

[1] International Road Dynamics, Technical Brief, “Weigh In Motion Technology Comparison”, January 2001

[2] George S. Nolas, Jeffrey Sharp, H. J. Goldsmid, “Thermoelectrics: basic principles and new materials developments” Volume 45 of Springer series in materials science , Springer, 2001.

[3] Ziff, Davis. “ Battery Technology: History, Present and Future Technology”, ExtremeTech, 2007

[4] Buchmann, Isidor. “Non-Correctable Battery Problems”, Battery University, February 2009.

[5] Ohta, T., “Energy technology: sources, systems, and frontier conversion”, 1st ED, PERGAMON, 1994

[6] Barrett, John Patrick. “Electricity at the Columbian Exposition”. 1894

[7] Reidy, Chris. Johnson, Carolyn. "MIT team lights it up - without wires", Boston Globe, June 8th 2007.

[8] Mazdik, Shawn. “Self-Induced Power Generation for Wireless MEMS Devices” University of California State, Department of Electrical Engineering. January 2009.

[9] E. W. Lee, Magnetism: An Introductory Survey, New York: Dover Publications, 1970.

[10] Jonathan Fildes, "Physics Promises Wireless Power," BBC News, Nov. 2006.

[11] Brown, W. C., “Experimental Airborne Microwave Supported Platform”, Raytheon Company, Spencer Labs. April 1965.

[12] Arnau, Antonio, Soares, David. “Piezoelectric Transducers and Applications”, Springer. 2008

[13] Minerly, Kathleen. “ Polymer Nanomaterials for Applications in Sound and Pressure Sensing”, University of Binghamton, New York, 2005.

[14] Kim, Sunghwan, “Low Power Energy Harvesting with Piezeoelectric Generators”. University of Pittsburg, 2002.

[15] M. Umeda, K. Nakamura, and S. Ueha, "Analysis of the transformation of mechanical impact energy to electric energy using piezoelectric vibrator," Japanese Journal of Applied Physics, vol. 35, pp. 3267-3273, 1996.

[16] C. Keawboonchuay, "Maximum Power Generation in a Piezoelectric Pulse Generator," IEEE Transactions on Plasma Science, vol. V. 31, No. 1, 2003.

[17] T. Funasaka, M. Furuhata, Y. Hashimoto, and K. Nakamura, "Piezoelectric generator using a LiNbO3 plate with an inverted domain," Proceedings of the IEEE Ultrasonics Symposium, vol. 1, pp. 959-962, 1998.

[18] M. Ichiki, K. Ashida, and T. Kitahara, "Characterization of piezoelectric lead zirconate titanate from the viewpoint of transducer and power generator properties," Japanese Journal of Applied Physics, vol. 41, pp. 7080-7083, 2002.

[19] Han, Ding. Kaajakari, Ville. “Microstructured Polymer For Shoe Power Generation”, IEEE Tranducers, Denver Colorado. 2009.

[20] Roch, J.G. , Goncalves, L.M, Rocha, P.F, Silva, M.P., Lanceros-Mendez S. “Energy Harvesting From Piezoelectric Materials Fully Integrated in Footwear”, IEEE Transactions on Industrial Electronics, Vol 57. No.3 March 2010.

[21] Jonathan Granstrom, Joel Feenstra, Henry A Sodano, Kevin Farinholt. “Energy harvesting from a backpack instrumented with piezoelectric shoulder straps”. Smart Materials and Structures, Vol 16. Pgs 1810-1820. 2007

[22] Shen, Dongna. “ Piezoelectric Energy Harvesting Devices for Low Frequency Vibration Applications.” University of Auburn, Alabama. 2009.

[23] H. W. Kim, A. Batra, S. Priya, K. Uchino, D. Markley, R. E. Newnham, and H. F. Hofmann, "Energy harvesting using a piezoelectric "cymbal" transducer in dynamic environment," Japanese Journal of Applied Physics, vol. 43, pp. 6178-6183, 2004.

[24] Reilly, Elizabeth. “Modeling and Fabrication of a Thin Piezoelectric Microscale Energy Scavenging Device.” Department of Mechanical Engineering. University of California, Berkley. 2007

[25] S. Roundy and P. K. Wright, "A piezoelectric vibration based generator for wireless electronics," Smart Materials and Structures, vol. 13, pp. 1131-1142, 2004.

[26] Meiling Zhu, Emma Worthington, “Design and Testing of Piezoelectric Energy Harvesting Devices for Generation of Higher Electric Power for Wireless Sensor Networks. IEEE Sensors 2009, Pg 699-702. 2009

[27] Jeon, Y., Sood, R. , Jeong J, Kim S. “ MEMS Power Generator with Transverse Mode Thin Film PZT” Sensors and Actuators, Vol 122 (2005).

[28] Mane, Mossi, Green, Bryant. “ Studing the effects of temperature on energy harvesting using pre-stressed piezoelectric diaphragms.” Behavior and Mechanics of MultiFunctional and Composite Materials, 2007.

[30] Kholkin, Kiselev, Kholkine, Safari. “Piezoelectric and Electrostrictive Ceramics Transducers and Actuators.” Taylor and Fracis Group LLC. 2008

[31] Kholkin, Pertsev, Goltsev. “Piezoelectricity and Crystal Symmetry.” 2008

[32] Wadhawan, Vinod. “Introduction to Ferroic Materials” Gordon and Breach, Amsterdam, 2000.

[33] Cook-Chennault, Thambi, Sastry, “Powering MEMS portable devices—a review of non-regenerative and regenerative power supply systems with special emphasis on piezoelectric energy harvesting systems.” Smart Materials and Structures, Volume 17, 2008.

[34] Burke, Andrew. “ Ultracapacitors: Why, How and Where is the Technology.” Institute of Transportation Studies, University of California. December, 2000.

[35] “MAX 5033, 500mA, 76V, High-Efficiency, MAXPower Step-Down DC-DC Converter” Datasheet, Maxim IC, 2007.

[36] Shenck, Paradiso. “ Energy scavenging with shoe-mounted piezoelectrics”, IEEE Micro, Volume 21, Pgs 30-42, 2001.

[37] Sodano, Henry. “ Comparison of Piezoelectric Energy Harvesting Devices for Recharging Batteries.” Journal of Intelligent Material Systems and Structures, Volume 16. Pg 799. 2005.

[38] Keekeun Lee, Wen Wang, Taehyun Kim and Sangsik Yang, “A novel 440 MHz wireless SAW microsensor integrated with pressure–temperature sensors and ID tag” Journal of Micromechanics and Microengineering. Volume 17, pgs 515-523, 2007.

[39] Michael Suster, Darrin J. Young, Wen H. KO , “Micro-Power Wireless Transmitter for MEMS Sensing and Communication Applications” Department of EECS, Case Western Reserve University, Cleveland, Ohio. 2004

[40] Darrin J. Young, Wen K. Ho. “ Wireless Strain Sensing Microsystem”, Department of EECS, Case Western Reserve University, Cleveland, Ohio. 2005.

[41] Li Zhang, Charles B Theurer, Robert X Gao, David O Kazmer, “Design Of Ultrasonic Transmitters With Defined Frequency Characteristics For Wireless Pressure Sensing In Injection Molding” IEEE Transactions on Ultrasonics, 2004.

[42] Peng Cong, Nattapon Chaimanonart, Wen H Ko, “A Wireless and Batteryless 10-Bit Implantable Blood Pressure Sensing Microsystem With Adaptive RF Powering for Real-Time Laboratory Mice Monitoring”, IEEE Journal of Solid State Circuits, Volume 44, No. 12, 2009.

[43] Thomas van den Boom, Dirk Teßmann, Renee Lerc, “Remote CMOS Pressure Sensor Chip with Wireless Power and Data Transmission” IEEE Solid State Circuits Conference, Session 11, 2000.

[44] M. Marzencki, B. Charlot, S. Basrour, M. Colin, and L. Valbin, "Design and Fabrication of Piezoelectric Micro Power Generators for Autonomous Microsystems," Symposium on Design Testing Integration and Packaging of MEMS, Switzerland, 2005, pp. 299-302.

[45] H.-B. Fang, J.-Q. Liu, Z.-Y. Xu, L. Dong, L. Wang, D. Chen, B.-C. Cai, and Y. Liu, "Fabrication and performance of MEMS-based piezoelectric power generator for vibration energy harvesting," Microelectronics Journal, vol. 37, pp. 1280-1284, 2006.

[46] P. Glunne-Jones, S.P. Beeby, and N.M. White, “Towards a piezoelectric vibration powered micro-generator”, IEE Proc.-Sci. Meas. Technol. Vol 148, Pg 68-72, 2001.

[47] H. Kim, V. Bedekar, R. Islam, W. Lee, D. Leo, and S. Priya, “Laser micro-machined piezoelectric cantilevers for mechanical energy harvesting” IEEE Ultrasonic Frequencies and Ferroelectrics, 2008.

[48] IEEE standard 176, IEEE Standards on Piezoelectricity, The Institute of Electrical and Electronics Engineers, 1978

[49] YK Tan, KY Hoe, “Energy Harvesting Using Piezoelectric Igniter for Self-Powered Radio Frequency Wireless Sensors”, IEEE, June 2007.

[50] Paradiso, J., Felmeier, M. “A Compact Wireless Self-Powered Pushbutton Controller”, MIT Media Laboratory, 2001.

[51] J. K. Ajitsaria, "Modelling and Analysis of PZT MicroPower Generator," 2008, pp. 1-159.

[52] C. Anderson, "414-09 ACI Harvestor III.sh.qxd," 2009, pp. 1-2.

[53] S. P. beeby, et al., "Energy Harvesting Vibration Sources for Microsystems Applications," 2006, pp. 1-22.

[54] S. Bhardwaj, "Simplified Loss Analysis and Comparison of Full-bridge, fullrange-ZVS DC-DC Converters," 2008, pp. 1-24.

[55] R. Brown, "AtoChem-Energy Generation using Piezo Film," 1999, pp. 1-9.

[56] R. Brown, "Energy Generation in A Tire Using PVDF," in Confidential, 2004, pp. 1-7.

[57] R. Brown, "Energy Generation Using MSI's PVDF," 1999, pp. 1-4.

[58] R. Brown, "Energy Generation using Piezo Film By Thermal Destruction," 2010, pp. 1-1.

[59] R. Brown, "Piezoelectric Energy Generation Using PVDF," 2010, pp. 1-24.

[60] R. Brown, "Power Generation Using PVDF on a Credit-Card," in Confidential, 2002, pp. 1-3.

[61] B. Calhoun, "Design Conideration for Ultra-Low Energy Wireless MicroSensor Nodes," 2005, pp. 1-14.

[62] A. V. Carazo, "Piezoelectric Converters for DC/DC and AC/DC Applications," 2005, pp. 1-7.

[63] C. Electronics, "Single Phase Passivated Bridge Rectifier," 2004, pp. 1-3.

[64] N. Electronics, "Silicon Bridge Rectifier," 2001, pp. 1-2.

[65] N. Elvin and A. Elvin, "A General Equivalent Circuit Model for Piezoelectric Generators," in Journal of Intelligent Material Systems and Structures vol. 20, 2008, pp. 3-9.

[66] K. Fairholt, et al., "RF Energy Transmission for a Low-Power Impedance Sensor Node," 2009, pp. 1-8.

[67] A. Fernandes and J. Pouget, "Accurate Modelling of Piezoelectric Plates: Single Layer Plate," 2001, pp. 1-16.

[68] A. Fernandes and J. Pouget, "Two-dimensional modelling of laminated piezoelectric composites: analysis and numerical results," 2000, pp. 1-20.

[69] J. Fernandes and M. Martins, "An Energy Harvesting Circuit for Self-Powered Sensors," 2010, pp. 1-4.

[70] N. Gayathri, "Design and Implementation of FPGA-based Phase modulation control for series resonant inverters," 2008, pp. 1-18.

[71] M. J. guan and W. H. Liao, "On the Efficiencies of Piezoelectric Energy Harvesting Circuits towards storage device voltages," 2007, pp. 1-9.

[72] N. Guilar, "A Flexible Power Management System for Interfacing with Energy Harvesting Transducers," 2009, pp. 1-159.

[73] L. Guo, et al., "Intelligent Traffic Management System Base on WSN and RFID," 2010, pp. 1-4.

[74] D. Han and V. Kaajakari, "Microstructured Polymer for Shoe Power Generation," 2009, pp. 1-4.

[75] S. Harte, et al., "Design and Implementation of a Miniaturised, Low Power Wireless Sensor Node," 2007, pp. 1-4.

[76] J. Harvey, "Performance of Two Overlay Strategies Under Heavy Vehicle Simulator Trafficking," 2001, pp. 1-11.

[77] C. A. Howells, "Piezoelectric energy harvesting," in Energy Conversion and Management vol. 50, 2009, pp. 1847-1850.

[78] T. Hu, "Development of MIcro Built-in Calibration Pressure Sensors with Piezoelectric Energy Harvesters," 2010, pp. 1-117.

[79] X. Hu and L. SUn, "Laboratory Measurement of Actual Tire-Pavement Contact Pressure Using a Static Test Device," 2009, pp. 1-13.

[80] V. Ivanov, "Evaluation of Tire Contact Properties Using Nondestructie Testing," 2008, pp. 1-7.

[81] C. Keawboonchuay, "Maximum Power Generation in a Piezoelectric Pulse Generator," 2001, pp. 1-6.

[82] C. Keawboonchuay and T. Engel, "Scaling Relationships and Maximum Peak Power Generation in a Piezoelectric Pulse Generator," 2004, pp. 1-7.

[83] S. Kim, "Low Power Energy Harvesting With Piezoelectric Generators," 2002, pp. 1-150.

[84] N. Kong and T. Cochran, "A Self-Powered Power Management Circuit for Energy Harvested by a Piezoelectric Cantilever," 2009, pp. 1-7.

[85] J. Kymissis and C. Kendall, "Parasitic Power Harvesting In Shoes," 1998, pp. 1-8.

[86] N. Lakshminarasama, "A New Family of Soft Transition Converters: Design and Dynamic Model," 2008, pp. 1-21.

[87] T. Le, "Efficient Power Conversion Interface Circuits for Energy Harvesting Applications," 2008, pp. 1-223.

[88] T. T. Le, "Efficient Power Conversion Interface Circuits for Energy Harvesting Applications," 2008, pp. 1-223.

[89] E. Lefeuvre, et al., "A comparison between several vibration powered piezoelectric generators for standalone systems," 2006, pp. 1-12.

[90] B. Lin, "Power and Energy Transduction in Piezoelectric Wafer Active Sensors for Structural Health Monitoring: Modeling and Applications," 2010, pp. 1-391.

[91] B. Liu, "A Finite Element Study of Piezoelectric Thin Films on Substrates," 2008, pp. 1-107.

[92] J. Liu, et al., "A MEMS-based piezoelectric Power Generator Array for Vibration Energy Harvesting," 2008, pp. 1-5.

[93] C. Luo, "Active Energy Harvesting for Piezoelectric Dynamic Systems," in Dissertation, 2010, pp. 1-133.

[94] R. Luo, "Effect of Measured Three-Dimensional Tire–Pavement Contact Stress on Pavement Response at Asphalt Surface," 2008, pp. 1-13.

[95] R. Machemehi, "Analytical Study of Effects of Truck Tire Pressure on Pavements with Measured Tire-Pavement Contact Stress Data," 2006, pp. 1-10.

[96] S. Mandzik, "Self-Induced Power Generation for Wireless MEMS Devices," 2009, pp. 1-55.

[97] M. Marzencki, et al., "Integrated Power Harvesting System Including a MEMS Generator and Power Management Circuit," 2007, pp. 1-4.

[98] L. Miller, et al., "Integration of a low frequency, tunable MEMS piezoelectric energy harvester and a thick film micro capacitor as a power supply system for wireless sensor nodes," 2009, pp. 1-8.

[99] G. Minjie, "Characteristics of Piezoelectric Energy Harvesting Circuits and Storage Devices," 2010, pp. 1-143.

[100] N. N. Guilar, et al., "A full-wave rectifier circuit for interfacing with multi-phase piezoelectric Energy Harvesters," 2007, pp. 1-16.

[101] Nelsonk, " Metallized_Piezo_Film_Sheets.doc," 2009, pp. 1-2.

[102] E. Ng, et al., "Road Traffic Monitoring Using a Wireless Vehicle Sensor Network," 2009, pp. 1-4.

[103] T. H. NG and W. H. Liao, "Sensitivity Analysis and Energy Harvesting for a Self-powered Piezoelectric Sensor," 2005, pp. 1-14.

[104] G. Ottman, "Optimized Piezoelectric Energy harvesting Circuit Using Step-Down Converter in Discontinuous Mode," 2004, pp. 1-7.

[105] G. Ottman and H. Hofmann, "Adaptive Piezoelectric Energy Harvesting Circuit for Wireless Remote Power Supply," 2001, pp. 1-8.

[106] G. Ottman, et al., "Adaptive Piezoelectric Energy Harvesting Circuit for Wireless Remote Power Supply," 2001, pp. 1-8.

[107] G. Ottman, et al., "Optimized Piezoelectric Energy Harvesting Circuit Using Step-Down Converter in Discontinuous Conduction Mode," 2001, pp. 1-8.

[108] J. Pandey, et al., "Toward an Active Contact Lens: Integration of a Wireless Power Harvesting IC," 2009, pp. 1-4.

[109] C. Park and P. H. Chou, "AmbiMax: Autonomous Energy Harvesting Platform for Multi-Supply Wireless Sensor Nodes," 2006, pp. 1-10.

[110] J. Park, "Development of MEMS Piezoelectric Energy Harvesters," 2010, pp. 1-175.

[111] M. Pasha, et al., "Toward Ultra Low Power Hardware Specialization of a Wireless Sensor Network Node," 2009, pp. 1-6.

[112] M. Penella and M. Gasulla, "Runtime Extension of Low-Power Wireless Sensor Nodes Using Hybrid-Storage Units," 2010, pp. 1-9.

[113] C. S. Pinkston, "An Investigation and Characterization of A High Energy Piezoelectric Pulse Generator," 2005, pp. 1-84.

[114] N. Pletcher, et al., "A 52 microW Wake-Up Reciever with -72dBm Sensitivity Using an Uncertain-IF Architecture," 2008, pp. 1-12.

[115] J. Rabaey, et al., "PicoRadio Supports Ad Hoc Ultra Low Power Wireless Networking," 2000, pp. 1-7.

[116] J. Rabaey, et al., "Challenges and Opportunities in Broadband and Wireless Communication Designs," 2004, pp. 1-7.

[117] A. Rajasekaran, "Buck-Boost Converter Based Power Conditioning Circuit for Low Excitation Vibrational Energy Harvesting," 2008, pp. 1-4.

[118] I. Rectifier, "Hyperfast Miniature Rectifier," 2001, pp. 1-8.

[119] E. Reilly, "Modeling and Fabrication of a Thin Film Piezoelectric Microscale Energy Scavenging Device," 2007, pp. 1-189.

[120] Z. Salam, "AC to DC Conversion- Rectifier," 2002, pp. 1-33.

[121] T. Sasilatha and J. Raja, "A 1 V, 2.4 GHz low power CMOS Reciever front end for Wireless Micro Sensor Nodes," 2009, pp. 1-6.

[122] SEMIKRON, "Rectifier-SKB_25_07238680," 2010, pp. 1-3.

[123] Y. ShaoPu, "Dynamics of Vehicle-Pavement coupled System Based on a revised flexible roller contact tire model," 2009, pp. 1-10.

[124] D. Shen, "Piezoelectric Energy Harvesting Devices for Low Frequency Vibration Applications," 2008, pp. 1-196.

[125] N. Shenck and J. Paradiso, "Energy Scavenging with Shoe Mounted Piezoelectrics," 2001, pp. 1-13.

[126] H. Sodano, et al., "Comparison of Piezoelectric Energy Harvesting Devices for Recharging Batteries," 2005, pp. 1-10.

[127] H. Sodano, et al., "Estimation of Electric Charge Output for Piezoelectric Energy Harvesting," 2004, pp. 1-11.

[128] H. Sodano, et al., "Generation and Storage of Electricity from Power Harvesting Devices," 2004, pp. 1-10.

[129] U. Sonmez, "WIM Studies Using Strip Type Sensors: Preliminary Results," 2008, pp. 1-26.

[130] Sparkler, "Sparkler Piezoceramics," 2005, pp. 1-13.

[131] M. Suster and D. Young, "Micro-Power Wireless Transmitter for MEMS Sensing and Communication Applications," 2004, pp. 1-4.

[132] A. Talib, et al., "Simulation of a MEMS Piezoelectric Energy Harvester," 2010, pp. 1-5.

[133] C. Townsend and S. Arms, "Thin Film Battery Recharging from Micropower Energy Harvesting Sources," 2008, pp. 1-1.

[134] J. Twiefel, et al., "Power Output Estimation and Experimental validation for Piezoelectric Energy Harvesting Systems," 2008, pp. 1-6.

[135] A. Willig and R. Shah, "Altruists in the PicoRadio Sensor Network," 2004, pp. 1-10.

[136] WJEC, "Rectification," 2010, pp. 1-13.

[137] R. Xia, et al., "Self-Powered Wireless Sensor System Using MEMS Piezoelectric Micro Power Generator," 2007, pp. 1-4.

[138] F. Yildiz, "Low Power Energy Harvesting, Conversion and Storage Circuits," 2009, pp. 1-6.

[139] F. Yildiz, "Low Power Energy Havesting and Storage Techniques from Ambient Human Powered Energy Sources," 2009, pp. 1-258.

[140] Yiming, "Active Energy Harvesting," 2006, pp. 1-143.

[141] Yiming, "Microsoft Word - ThesisMaster.doc," 2006, pp. 1-143.

[142] M. Zhu and E. Worthington, "Design and Testing of Piezoelectric Energy Harvesting Devices for Generation of Higher Electric Power for Wireless Sensor Networks," 2009, pp. 1-4.

[143] M. Zhu, et al., "Analyses of Power Output of Piezoelectric Energy-Harvesting Devices Directly Connected to a Load Resistor Using a Coupled Piezoelectric-Circuit Finite Element Method," 2009, pp. 1-10.

[144] K. Omote, " Temperature dependance of elastic, dielectric and piezoelectric properties of single crystalline films of vinylidene fluoride." Department of Materials Science and Engineering, Yamagata University, Jonan 4-3-16, Yonezawa 992, Japan